Geochimica et Cosmochimica Acta

Pore-Scale Dissolution Mechanisms in Calcite-CO2-brine Systems: The Impact of Non-Linear Reaction Kinetics and Coupled Ion Transport

--Manuscript Draft--

Manuscript Number:	GCA-D-20-00014R2
Article Type:	SI: Multiscale Simulation
Keywords:	Pore-Scale Dissolution Mechanisms Calcite-CO2-brine Systems Non-Linear Reaction Kinetics Coupled Ion Transport
Corresponding Author:	Edo Sicco Boek, PhD Queen Mary University of London London, UNITED KINGDOM
First Author:	Farrel Gray, Ph.D.
Order of Authors:	Farrel Gray, Ph.D.
	Benaiah Anabaraonye, Ph.D.
	John P Crawshaw, Ph.D.
	Edo Sicco Boek, PhD
Abstract:	We simulate two sets of dissolution experiments in which CO2-saturated solutions are injected into calcite formations. We explore the impact of non-linear reaction kinetics and charge-coupled ion transport in systems representing different levels of flow and mineralogical complexity. First, we flow CO2-saturated water and brine through cylindrical channels drilled through solid calcite cores and compare directly with experimental dissolution rates. We find that simulations using a linear saturation model match experimental results much better than the batch-reactor-derived non-linear saturation model. The use of a coupled diffusion model causes only a very small increase in the overall dissolution rate compared to a single diffusion coefficient, due to the increase in transport rates of reaction products, particularly the highly charged Ca^(2+) ion. We also determine the relative importance of the two calcite dissolution pathways, with H+ and H2CO3, and conclude that the H2CO3 - calcite reaction is by far the more dominant, in contrast with common assumptions in the literature. Then, we compare to the experiments of Menke et al. (2015) in which CO2-saturated brine was injected into a microporous Ketton carbonate, and compare dissolution rates over time. We find that including non-linear saturation behaviour markedly changes the simulated dissolution rate, by up to a factor of 0.7 in the case of the experimentally derived saturation model of Anabaraonye et al. (2018), however neither case matches the experimental result which is several times slower than the simulation. Including the effects of coupled ion transport lead to virtually no change in overall dissolution rate due to the convection dominated behaviour. The model also shows differences in the trend of the dissolution rate over time observed in Menke et al, with an approximately linear relationship with time compared to the experimental square-root dependence on time. We conclude that the geochemical model may need to include other effects such as dissolution inside microporous regions.

Powered by Editorial Manager® and ProduXion Manager® from Aries Systems Corporation

31 March 2021

Dr Edo Boek PhD
Associate Professor in
Chemical Engineering & Renewable Energy
School of Engineering and Materials Science
Queen Mary University of London
Mile End Road, London E1 4NS
e-mail: e.boek@qmul.ac.uk

To: Executive Editor
Geochimica et Cosmochimica Acta

We wish to resubmit the following manuscript to Geochimica et Cosmochimica Acta:

Manuscript Number: GCA-D-20-00014R2
Title: Pore-Scale Dissolution Mechanisms in Calcite-CO2-brine Systems: The Impact of Non-Linear Reaction Kinetics and Coupled Ion Transport

Authors: F. Gray[1], B.U. Anabaraonye[1], J. P. Crawshaw[1] and E. S. Boek[2+]

[1]Qatar Carbonates and Carbon Storage Research Centre (QCCSRC),
Department of Chemical Engineering, South Kensington Campus,
Imperial College London, London SW7 2AZ, United Kingdom.

[2]Division of Chemical Engineering, School of Engineering and Materials Science,
Queen Mary University of London, Mile End Road, London E1 4NS, U.K.

[+] Corresponding author:

Dr Edo S. Boek
Associate Professor (Reader) in Chemical Engineering & Renewable Energy
Soft Matter & Porous Materials Research Group
School of Engineering and Materials Science
Queen Mary University of London
Mile End Road
London E1 4NS
+44 (0)20 7882 2964
https://www.sems.qmul.ac.uk/staff/e.boek
e.boek@qmul.ac.uk

Yours faithfully,

Dr Edo Boek

Manuscript Number: GCA-D-20-00014R2

Title: Pore-Scale Dissolution Mechanisms in Calcite-CO2-brine Systems: The Impact of Non-Linear Reaction Kinetics and Coupled Ion Transport

Response to Comments

Reviewer # 1 suggested to run the benchmark case presented in Molins et al. 2020 (Part II) for comparison and validation purposes. We are pleased to confirm that we have simulated the 2D benchmark case successfully and obtained good comparison with the results presented in Molins et al. 2020 (Part II).

In detail, we have updated our manuscript as follows:

- Line 62-62: “We include a comparison with one of their benchmark cases in the present work.” was added to the Introduction
- Line 259: A new section 2.1 was added with the title “Verification of the moving solid-liquid interface model”. Here we present the results of our benchmark study as suggested by Reviewer #1. We observe good agreement with the results presented in Molins et al. 2020 (Part II).
- Line 691: A new Figure 3 was introduced, showing the evolution of a) volume, b) surface area and c) average dissolution rate, as a function of time during the dissolution of the 2D calcite disk as described in part II of (Molins, Soulaine et al. 2020).
- Line 700: A new Figure 4 was introduced, showing the H+ ion concentration contours for the 2D dissolution of a cylindrical calcite grain.
- Line 706: A new Figure 5 was introduced, showing the evolution of calcite grain shape due to dissolution under flowing conditions after a) 15 min., b) 30 min., c) 45 min. and d) 60 min., observed from our LB-FV simulations

Manuscript Click here to view linked References

Pore-Scale Dissolution Mechanisms in Calcite-CO_2-brine Systems: The Impact of Non-Linear Reaction Kinetics and Coupled Ion Transport

F. Gray[1]*, B. U. Anabaraonye[1], J. P. Crawshaw[1] and E. S. Boek[2+]

[1]Qatar Carbonates and Carbon Storage Research Centre (QCCSRC), Department of Chemical Engineering, South Kensington Campus, Imperial College London, London SW7 2AZ, United Kingdom.

[2]Division of Chemical Engineering, School of Engineering and Materials Science, Queen Mary University of London, Mile End Road, London E1 4NS, U.K.

*farrel.gray@imperial.ac.uk [+]e.boek@qmul.ac.uk

Abstract

We simulate two sets of dissolution experiments in which CO_2-saturated solutions are injected into calcite formations. We explore the impact of non-linear reaction kinetics and charge-coupled ion transport in systems representing different levels of flow and mineralogical complexity. First, we flow CO_2-saturated water and brine through cylindrical channels drilled through solid calcite cores and compare directly with experimental dissolution rates. We find that simulations using a linear saturation model match experimental results much better than the batch-reactor-derived non-linear saturation model. The use of a coupled diffusion model causes only a very small increase in the overall dissolution rate compared to a single diffusion coefficient, due to the increase in transport rates of reaction products, particularly the highly charged Ca^{2+} ion. We also determine the relative importance of the two calcite dissolution pathways, with H^+ and H_2CO_3, and conclude that the H_2CO_3 – calcite reaction is by far the more dominant, in contrast with common assumptions in the literature. Then, we compare to the experiments of Menke et al. (2015) in which CO_2-saturated brine was injected into a microporous Ketton carbonate, and compare dissolution rates over time. We find that including non-linear saturation behaviour markedly changes the simulated dissolution rate, by up to a factor of 0.7 in the case of the experimentally derived saturation model of Anabaraonye et al. (2018), however neither case matches the experimental result which is several times slower than the simulation. Including the effects of coupled ion transport lead to virtually no change in overall dissolution rate due to the convection dominated behaviour. The model also shows differences in the trend of the dissolution rate over time observed in Menke et al, with an approximately linear relationship with time compared to the experimental square-root dependence on time. We conclude that the geochemical model may need to include other effects such as dissolution inside microporous regions.

1 Introduction

A better understanding of the detailed dissolution mechanisms in carbonate rock by CO_2 – brine systems is of great fundamental and applied interest. Applications include field scale operations in carbonate reservoirs such as CO_2 sequestration (Molins 2012), where the acid is formed by dissolution of the injected CO_2 in the brine present in the reservoir; and matrix acidizing for hydrocarbon recovery (McLeod 1984, Fredd and Fogler 1998), where the acid is injected directly into the formation to increase permeability and reservoir productivity.

Recently, a number of detailed pore scale investigations have been reported on the dissolution of carbonate rocks by acidic solutions. These include micro-CT imaging studies by Qajar and Arns (Qajar J 2012) and image based modelling studies by Nunes *et al*. (Pereira Nunes, Blunt et al. 2016). In particular, we mention the micro-CT imaging paper by Menke *et al*. (Menke, Bijeljic et al. 2015) in which CO_2-saturated brine was injected into a microporous Ketton carbonate, and full time-dependent dissolution was resolved. Dissolution of carbonate minerals is a complex process encompassing the interaction between transport and chemical reaction processes in porous media.

Indeed, accurate modelling of calcite dissolution at the pore scale, including the complex feedback between flow and surface chemistry, requires detailed verification of the modelling framework used. Before considering complex diffusion and chemical reaction mechanisms in complex 3D porous media, it is recommended to carry out detailed verifications that the code is working properly, in particular regarding moving fluid and solid boundaries. Molins *et al.* (Molins, Soulaine et al. 2020) reviewed and proposed a benchmark problem set of test cases for the simulation of mineral dissolution at the pore scale with evolving fluid-solid interfaces. In a previous paper (Gray, Cen et al. 2016), we carried out a detailed verification study of our modelling framework, including diffusion, mesh convergence and concentration fields in flow past a single sphere in a channel. In addition, we introduced and verified the surface rescaling method used in our current manuscript. These verifications are similar to some of the test cases proposed by (Molins, Soulaine et al. 2020). We include a comparison with one of their benchmark cases in the present work. As further validation, we simulated the geochemical system of (Molins, Trebotich et al. 2014) using their micro-CT data set. Our model gave close agreement to their simulated dissolution rates. Results will be discussed in more detail in future work.

Furthermore, the experimental framework has to be verified before considering the full complexity of diffusion and chemical reaction mechanisms in complex 3D porous media. As an example verification we note the microfluidic experiments of a calcite crystal dissolving in a microchannel (Soulaine, Roman et al. 2017). Inspired by this study, in a previous paper we carried out a validation study to examine dissolution in a 1 mm diameter cylindrical channel drilled through a solid calcite crystal, using a combination of micro-fluidic experiments and simulations (Gray, Anabaraonye et al. 2018). In addition, very recently calcite cylinder

dissolution experiments similar to our current work (see section 4.1) were reported by (Agrawal, Raoof et al. 2020). Regarding reaction kinetics, (Noiriel, Steefel et al. 2012) studied calcite precipitation rates in porous media and found nearly linear dependence of the rates on supersaturation, which could not be attributed to a diffusion control..

In our previous paper (Gray, Anabaraonye et al. 2018), we also discussed the chemical mechanisms of dissolution of calcite by HCl in porous media, using a combination of computer simulations and experiments. Here we extend these studies to CO_2-brine systems.

The main aims of this paper are to examine the influence of the following effects on the dissolution process: a) charge coupled diffusion, b) non-linear reaction kinetics and c) the controlling dissolution reaction pathway. We will discuss each of these aims in the following sections.

As discussed in our earlier paper (Gray, Anabaraonye et al. 2018), the diffusion of charged species in electrolytes is controlled by the Nernst-Planck-Arrhenius equations (Vinograd and McBain 1941). This has led to the development of multi-component diffusion models, including charge-coupling effects on ion diffusion rates (Steefel and Maher 2009), which have been used to interpret multi-component diffusion effects in bulk solutions (Maher, Steefel et al. 2006) and porous media (Giambalvo, Steefel et al. 2002) (Appelo and Wersin 2007). To the best of our knowledge, only a few papers in the literature have extended this effect to reactive flow models. In the majority of research papers on this topic, a single diffusion coefficient is used for all species (Yoon, Valocchi et al. 2012, Yoon, Kang et al. 2015, Gao, Xing et al. 2017, Liu and Mostaghimi 2017, Liu and Mostaghimi 2018). This maintains electro-neutrality, but does not capture electrochemical migration effects. In a few cases, however, multicomponent diffusion effects have been included alongside chemical reactions. In particular, Muniruzzaman and Rolle (Muniruzzaman and Rolle 2016) used a multicomponent ionic transport model coupled to a geochemical reaction network to investigate dispersion in 2D systems at the core-scale. Recently, Sprocati et al. (Sprocati 2019) extended this to core-scale modelling of electrokinetic reactive transport processes in saturated porous media. They emphasized the importance of Coulombic interactions in electrokinetic applications using a variety of benchmark tests. Their reactive transport model was compared with PHREEQC (Steefel, Appelo et al. 2015) simulation data, including surface complexation reactions, but not directly with reactive transport experiments. In the case of pore-scale simulation studies in the literature, Ovaysi and Piri (Ovaysi and Piri 2014) included a multicomponent diffusion term in their particle-based reaction model, as did Li *et al*. (Li 2008) in their study of flow past a dissolving calcite surface. In our earlier paper (Gray, Anabaraonye et al. 2018) we observed that, for dissolution of calcite by HCl, it was important to include the effect of charge coupled diffusion. Here we will investigate if the same is true for dissolution of calcite by CO_2-water/brine solution, using a direct comparison of new experimental data and our reactive transport model including charge-coupling effects.

Regarding the effect of reaction kinetics on dissolution mechanisms, the majority of papers in the literature use simple linear saturation models. For example, Ovaysi and Piri (Ovaysi and Piri 2014) simulated a reactive flow experiment in a microfluidic channel performed by Li *et al*. (Li 2008) and found good agreement for the Ca^{2+} concentration as a function of flow rate.

Recent batch reactor studies, however, suggest that reaction kinetics close to equilibrium may become non-linear due to a switch in dissolution mechanism related to the surface properties of the underlying crystal. In particular, Anabaraonye *et al*. (Anabaraonye 2017) found dissolution kinetics of calcite to be highly non-linear in batch reactor studies, where a single calcite crystal surface was exposed to dissolution. As shown in Figure 1, they observed a substantially faster reduction in reaction rate with increasing saturation state for the non-linear model compared to the linear model. In our previous paper on dissolution of calcite by HCl (Gray, Anabaraonye et al. 2018), the saturation term was unimportant as the reactions were far from equilibrium. In the current work on CO_2 -saturated solutions however, the chemical conditions are closer to equilibrium and therefore we expect the saturation term to have a strong influence on the overall dissolution rate.

Finally, we explore the details of the controlling reaction pathway for dissolution. The dissolution of calcite by carbonic acidic solutions is usually described in terms of two main reaction pathways:

$$CaCO_3 + H^+ \leftrightarrows Ca^{2+} + HCO_3^- \quad (1)$$

$$CaCO_3 + H_2CO_3 \leftrightarrows Ca^{2+} + 2HCO_3^- \quad (2)$$

Many papers in the literature on this topic assume reaction (1) to be dominant, and state that the overall dissolution can be expressed solely by this pathway (Pereira Nunes, Blunt et al. 2016, Gao, Xing et al. 2017, Tian and Wang 2018). Here we examine this assumption and hypothesize that the H^+ concentration near the reactive surface may well be substantially lower than in the inlet solution, causing reaction (2) to make an important contribution. In the below, we directly compute the relative influence of the two pathways using the concentration fields of the relevant chemical species. This allows us to establish which of the two reaction pathways (1) and (2) is most important. To the best of our knowledge, this has not yet been reported in the literature.

Then we consider recent micro-CT imaging experiments, in which CO_2-saturated brine was injected into a micro-porous Ketton carbonate (Menke, Bijeljic et al. 2015), as an example of a more complex porous medium. We use these imaging data to calculate the experimental amount of calcite dissolved as a function of time. This is compared directly, using the same time lapse image series, with our dissolution simulations. The model used here only considers dissolution at the grain surfaces. In a recent experimental study of micro-porous carbonate limestone dissolution by Singh *et al.*(Singh, Anabaraonye et al. 2018), evidence is presented that dissolution reactions are mainly occurring in the micro-pores, not at the surface of the carbonate rock samples. Such dissolution processes involving micro-porosity are not yet fully

understood, and modelling efforts may need to take into account these micro-pore effects too.

1.1 Geochemical Model

We consider the dissolution of calcite by carbonic acidic solutions as described by the two main reaction pathways, defined in reactions (1) and (2) above. The total dissolution rate is generally described by a linear reaction model in far-from-equilibrium conditions given by: $R = -A\alpha_{H^+}k_1 - A\alpha_{H_2CO_3}k_2$, where R is the dissolution rate in mol s^{-1}, A is the surface area in m^2, α_x is the activity of given species x, and $k_1 = 2.5 \times 10^{-4}\mathrm{ms}^{-1}$ and $k_2 = 5.5 \times 10^{-7}\mathrm{ms}^{-1}$ are the reaction rate constants of the reactions (1) and (2) respectively at 50C (Peng, Crawshaw et al. 2015).

The dissolution kinetics of calcite has been found to be highly non-linear in batch reactor studies, where a single calcite crystal surface was exposed to dissolution (Molins 2012, Peng, Crawshaw et al. 2015). According to the model of Anabaraonye et al. (Anabaraonye 2017), the non-linear behaviour can be described by a single fitted exponent of the form

$$R = -(A\alpha_{H^+}k_1 + A\alpha_{H_2CO_3}k_2)\left[1 - \frac{Q}{K}\right]^p \tag{3}$$

Here, Q is the solubility product, defined in terms of the ratio of products to reactants

$$Q = \frac{\alpha_{Ca^{2+}} \cdot \alpha_{HCO_3^-}}{\alpha_{H^+}} \tag{4}$$

$K = 27.07$ is the equilibrium constant and the exponent $p = 7.76$ (Anabaraonye 2017). Q/K is the saturation index and $[1 - Q/K]^p$ is the saturation term. The behaviour of this non-linear saturation model is shown in Figure 1, and shows a substantially greater reduction in the saturation term, and therefore in reaction rate, with increasing saturation state compared to the linear model.

During the formation of carbonic acid, CO_2 quickly dissolves into solution to produce aqueous H_2CO_3. This then produces the acid species H^+ through the equilibrium reactions:

$$H_2CO_3 \leftrightarrows H^+ + HCO_3^- \tag{5}$$

$$HCO_3^- \leftrightarrows H^+ + CO_3^{2-} \tag{6}$$

The additional contribution through the dissociation of water $H_2O \leftrightarrows H^+ + OH^-$ can be ignored at low enough pH, such as are considered here.

2 Simulation Model

The systems considered are investigated using a high resolution pore-scale reactive flow model (Gray, Anabaraonye et al. 2018). The flow-field inside the domain is computed using the multi-relaxation-time lattice Boltzmann model (Gray and Boek 2016) and chemical

transport is performed using an explicit second order flux-limiter scheme (Gray, Cen et al. 2016). Fluid chemical equilibrium reactions were computed to steady-state at each time-step using a Newton-Raphson solver, and heterogeneous reactions at mineral surfaces were performed using a 4th order accurate numerical integration step (Gray, Anabaraonye et al. 2018). Surface area was determined for heterogeneous reactions from the Cartesian grid surface by locally interpolating parabolic surface elements. The projection of the grid block surface onto the smooth element is then used to estimate the true area represented by the exposed grid surface (Gray, Cen et al. 2016).

The effects of charge coupling on ion diffusion rates was included by incorporating an extra electrochemical term into the diffusive flux (Steefel and Maher 2009).

$$J_j = -D_j \frac{\partial C_j}{\partial x} + \frac{z_j D_j C_j}{\sum_k z_k^2 D_k C_k} \sum_k z_k D_k \frac{\partial C_k}{\partial x} \tag{7}$$

where J_j is the diffusive flux for each species j, C_j is the species concentration, z_j the ionic charge and D_j are the self-diffusion coefficients.

To demonstrate the effect of this term, a system of Ca^{2+} and HCO_3^- ions in a 1 : 2 ratio was simulated. The mixture was initialised as a point source at the origin with initial concentrations of 1 x 10^{-4} [mol L^{-1}] and 2 x 10^{-4} [mol L^{-1}] respectively, and allowed to diffuse for 1.03 s. The resulting distributions are shown in Figure 2a (solid lines). The literature values for the self-diffusion coefficients of these ions were found to be 1.406 x 10^{-9} m^2s^{-1} [6] and 2.104 x 10^{-9} m^2s^{-1} [7] respectively. However, due to the charge coupling effect, we observe that both ions actually diffuse at the same rate, as is required to conserve electroneutrality in the solution. In this case, the distributions of both ions are Gaussian and their effective diffusion coefficient is 1.805 x 10^{-9} m^2s^{-1}. This was computed as half the rate of change of the variance σ_i^2 in the concentration distributions for each species i, namely

$$D_i^{Eff} = \frac{1}{2}\frac{d\sigma_i^2}{dt} \tag{8}$$

A second calculation is also shown in Figure 2a (dashed lines) in which the same point source of ions was allowed to diffuse in a background mixture of 0.855 M NaCl brine. In this case, electrochemical migration effects are observed. The ions now diffuse at different rates, which are in fact equal to (or indistinguishable from at the resolution of simulation) their self-diffusion coefficients. The reason for this is that the Na^+ and Cl^- ions in the background brine can also migrate, as shown in Figure 2b where small perturbations from the initial 0.855 mol. dm^{-3} solution concentration are apparent. Li *et al.* (Li 2008) performed similar experiments but found rates that were considerably lower for water without NaCl. They noted that an explanation might have been a slower rate of diffusion from the pore wall to the center of the pore caused by smaller gradient in chemical potential in pure water compared to a 10 mM NaCl solution. In the saturated CO_2-brine systems used in this work, the activity coefficients for the chemical species will be almost entirely determined by the background

NaCl concentration, and therefore gradients in chemical activities are unlikely to be significant.

With more complex mixtures of ions, individual species can diffuse at different rates, whilst still maintaining electroneutrality, and their behaviour is not necessarily Gaussian. An example of this is shown in Figure 2c, which consists of an initial mixture of H^+ (0.0167 mol.dm^{-3}), Cl^-(0.05 mol.dm^{-3}) and Ca^{2+} (0.0167 mol.dm^{-3}) ions. Such a system is applicable to the case of 0.05 mol.dm^{-3} HCl being injected into a calcite ($CaCO_3$) system, for example the calcite cylinder validation example in Gray et al. (Gray, Anabaraonye et al. 2018). Here we assume that 1/3 of the initial H^+ has reacted with calcite to produce corresponding amounts of Ca^{2+} and HCO_3^- ions. Then, due to the equilibrium reaction (5), almost all of the HCO_3^- has then reacted with remaining H^+ to produce H_2CO_3. Since HCO_3^- now exists only in trace amounts, and H_2CO_3 is uncharged and thus unaffected by (7), these components are neglected. Once again, the mixture was initialised as a point source and allowed to diffuse for 1.03 s. The ions in this case once again diffuse at different rates, whilst maintaining electroneutrality, however it is clear from Figure 2c that the distribution of H^+ is highly non-Gaussian. The effective dispersivity was again computed using (8), and gave $D_{H^+}^{Eff}$ = 8.415 x 10^{-9} m^{2}s^{-1}, $D_{Ca^{2+}}^{Eff}$ = 1.705 x 10^{-9} m^{2}s^{-1} and $D_{Cl^-}^{Eff}$ = 3.942 x 10^{-9} m^{2}s^{-1}. By comparison, if equal amounts of H^+ and Cl^- diffuse together without any Ca^{2+} ions, they maintain a Gaussian distribution with an effective diffusion coefficient of 5.922 x 10^{-9} m^{2}s^{-1}. It is therefore interesting to note how the addition of product ions from the surface reactions allows the H^+ ion to diffuse much faster than in the initial HCl solution. This would explain why using a constant diffusion coefficient in the cylinder example in Gray et al. (Gray, Anabaraonye et al. 2018) lead to a considerably slower overall dissolution rate than when the coupled diffusion model was used. With the coupled model, the transport rate of H^+ ions to the reactive surface was increased further down the system as product ions built up from surface reactions. We would like to point out that the value of the HCl diffusion coefficient used in Gray et al. (Gray, Anabaraonye et al. 2018) of 5.6 x 10^{-9} m^{2}s^{-1} was obtained using the value from Lobo et al. (Lobo, Helena et al. 1979) at 298 K and adjusted to 323 K using the Stokes-Einstein relation. The reference for this value was not given in (Gray, Anabaraonye et al. 2018), so we are pleased to give the authors due credit here. Finally, we note that this experimentally derived value is around 6% lower than the simulated value here. This could be due the omission of electrophoretic effects (charge-cloud deformation) in the coupled diffusion model. In the reactive flow simulations described in this work, the constant diffusion model will treat all components as having the same diffusion coefficient of 1.805 x 10^{-9} m^{2}s^{-1}, equal to the combined diffusion rate of Ca^{2+} and HCO_3^-. We used the Nernst–Planck equation for fully coupled ion transport in the rest of this paper, for every grid cell and every time step. The implementation has been validated in (Gray, Anabaraonye et al. 2018) and explained in detail in Appendix 1 of this paper.

Geochemical convergence conditions were measured by the change in the average and standard deviation of chemical concentrations in the sample. For all calculations performed, fractional changes of less than 10^{-6} per time-step in both these quantities was considered steady-state. Both flow and transport models were implemented for GPUs, and used a 3-dimensional domain decomposition, which was periodically adjusted to maintain a balanced number of fluid nodes over processors as the geometry was altered during dissolution. Calculations were performed using either 8 Tesla P100 GPUs, or a heterogeneous cluster comprising 24 Tesla K40 and 24 Tesla K80 GPUs connected with FDR Infiniband.

2.1 Verification of the moving solid-liquid interface model

Here we provide a validation of our algorithm to describe the dynamics of the calcite-solution interface, which is moving as a consequence of the reactive flow process. We compare our results for a benchmark case, provided by (Molins, Soulaine et al. 2020) in Part II of their paper, directly with the results obtained from various alternative simulation methods. This concerns the simulation of flow and reactive transport in a 2D rectangular domain, with dissolution occurring on the surface of a circular calcite grain placed in the centre, due to the inflow of an HCl solution with pH=2. Only the reaction with calcite and H^+(1) is considered, neglecting fluid equilibrium reactions and saturation behaviour. Detailed information regarding the geometry and parameters used for this benchmark case are provided in Fig. 2 and Table 2 in (Molins, Soulaine et al. 2020). We conduct our simulations in a 3D domain with dimensions of 200 x 110 x 5 lattice units in X, Y and Z directions respectively, where the flow direction is in X, and the channel width in Y. Loop boundary conditions are applied in Z to both flow and transport so that the problem is equivalent to 2D. The Y direction includes solid boundaries of 5 voxels width either side of the channel, so that the flowing region of the channel is 100 lattice units wide, with a resolution of 5 micron. A fluid injection rate of $0.9\mu Lmin^{-1}$ was imposed at the inlet face, equivalent to an average injection velocity of 0.12 cms^{-1} as specified for the benchmark case. Due to the dissolution process, both the volume and area of the calcite grain are expected to diminish with time. The results of our calculations, confirm this expectation and are presented in Figure 3 a) and b). Our results were obtained up to full dissolution and show good agreement with the other simulation codes. In addition, we observe that the average dissolution rate increases with time, in good agreement with other simulation results, see Figure 3 c). This is because the area of the grain decreases more rapidly than the effluent concentration due to grain dissolution / shrinkage.

We expect that the flow field imposed leads to breaking of the fore-aft symmetry in the concentration field. Indeed this is observed in our simulations, as shown in Figure 4, in agreement with (Molins, Soulaine et al. 2020). Therefore we expect that most of the dissolution will occur on the leading (upstream) edge while the downstream point is expected to move much less. Indeed this can be observed from our simulation results, as shown in Figure 4.

In summary, we observe good agreement between our results and those obtained using alternative simulation methods. We confirm that our approach can simulate the benchmark problem accurately with our specific strategy for time stepping and process coupling.

3 Experiments

3.1 Calcite Cylinders

The calcite cylinder experiments were prepared by first drilling a 3mm hole through a solid calcite core. Matching steel inlet pieces were pushed against each end, and the arrangement placed inside a Viton sleeve. Injection was performed at 5 MPa pressure, with an applied confining pressure of 6 MPa. The core holder was heated to a temperature of 50°C. Two CO_2-saturated solutions were used, one consisting of deionised water as the solvent, and the other containing 5% by weight NaCl brine. Both solutions were equilibrated with CO_2 at 5 MPa and 50°C so that saturation was reached. Injection was performed at a number of different flow rates and resulting mass dissolution was determined by the weight change of the channels. Four sets of experiments were performed using CO_2-water, varying the length of the channel, diameter of the channel and flow rate. The experiments were also run for different times. These parameters are given in Table 2. A further two experiments were run using CO_2-saturated brine with 5% by weight NaCl, parameters for which are given in Table 3. Other parameters, such as temperature and pressure were not changed between experiments. The corresponding simulation domains were generated digitally, and included an extra inlet region 3mm in length and of the same diameter as the calcite channel, considered to be non-reactive. This was to ensure that the simulation could resolve any concentration gradients which might form before the reactive channel.

3.2 Ketton Carbonate

We consider recent micro-CT experiments by Menke *et al.* (Menke, Bijeljic et al. 2015), where a Ketton carbonate rock core was injected with CO_2-saturated brine (5% NaCl, 1% KCl by weight) at 50 °C and 10MPa, while tomographic images were taken at 15 min intervals with a 3.8 µm spatial resolution. Ketton is a >99% calcite Limestone Oolite, which has a bimodal pore structure, as witnessed by mercury intrusion experiments (Menke, Reynolds et al. 2018) . In the dissolution experiment, the reactor fluid was flowed through the core at a constant flow rate of 0.5 mL/min, corresponding to a Darcy velocity of 6.6×10^{-4} ms^{-1}. The transport properties were characterised by the Peclet number, defined as

$$Pe = \frac{U_{av}L}{D}$$

where U_{av} is the average pore velocity, defined as Darcy velocity divided by porosity. The porosity increased from 0.17 to 0.32 [-] over the course of the experiment. L is a characteristic length scale, and is chosen to be 100µm, the order of a typical pore-size. The resulting Peclet number is around $Pe \sim 50$, indicating that the transport is strongly convection dominated.

4 Results

4.1 Calcite Channels

Figure 6 shows a comparison of simulated results with experiments for two cases: C1 (CO_2-water) and C5 (CO_2-brine). Simulations in this case included the time-dependent changes of the mineral boundaries due to the surface reactions over the full experimental time-scale. Since the simulated dissolution rate shows virtually no change over time, we assume that changes in the cylindrical geometry had a negligible effect on the dissolution rate over the time-scale they were run. The mean dissolution rate was computed as the amount of dissolved solid per unit of time, in units of (mol / hr). To match the experimental conditions, the injection condition used in the simulation was a constant flow rate of 0.5 mL / min (Menke, Bijeljic et al. 2015).

Both linear ($p = 1$) and non-linear ($p = 7.76$) saturation terms are compared. Interestingly, in both cases simulations using the linear saturation model agree closely with the experiment, whereas the non-linear model gives dissolution rates approximately 40% lower. Results for all experiments are shown in Figure 7 with simulation results using both the linear and non-linear dissolution models. In almost all cases, the linear model gives much better agreement than the non-linear model derived from batch reactor experiments. This appears to be the case both for systems with CO_2-water injected and CO_2-brine injected. For example, experiments C1 and C2 (CO_2-water) correspond closely to experiments C5 and C6 (CO_2-brine) respectively, except for different run times. However in these cases, the dissolution rate is well predicted by the linear model, and in comparable disagreement with the non-linear model.

In order to better understand the effect of the saturation model exponent on the dissolution rate, a number of simulations were performed with exponents ranging from 1 (linear) to 7.76 (the experimentally derived non-linear model). These are shown in Figure 8 for the experiments C1 (CO_2-water) and C5 (CO_2-brine), with the experimental dissolution rate shown for reference. The simulated dissolution rate decreases as a function of the exponent and in both cases the resulting overall dissolution rate with the $p = 7.76$ non-linear model is approximately 2/3 the rate of the linear model. However in both cases, the linear model results in the best match for the experimental dissolution rate.

Next we consider the effects of charge-coupled diffusion, compared to using a single diffusion coefficient for all species. Simulations were performed for the experiment C5 with both coupled and constant diffusion models, and using both the linear and non-linear saturation models. These are shown in Figure 9. For both cases of saturation model, the coupled diffusion models resulted in only a slight increase in overall reaction rate compared to the case of a single, constant diffusion coefficient.

The reaction mechanisms can be understood by considering the distribution of chemical species in the system. Cutaways of the experiment C1 using the non-linear saturation model are shown in Figure 10 for the H^+, Ca^{2+} and HCO_3^- species. The H^+ concentration drops by

more than an order of magnitude from its initial solution concentration value to that on the mineral surface, the pH ranging from 3.1 to 4.6.

The surface concentrations of these chemical species, and the surface pH are shown in Figure 11a and b. These values are averaged over the cross-section of the channel, and shown as a function of position from the inlet. The pH on the mineral surface is lower than in the initial solution by 1.5 units, corresponding to more than an order of magnitude in concentration. This is because of the large amounts of HCO_3^- produced during the surface reaction affecting the equiliubrium (9). The concentration of H_2CO_3 remains close to its initial solution value. These measures can be used to determine the relative balance of the dissolution reactions (1) and (2). In Figure 11c, the ratio $k_1\langle\alpha_{H^+}\rangle/k_2\langle\alpha_{H_2CO_3}\rangle$ is shown, where $\langle\alpha_{H^+}\rangle$ is the mean activity of H^+ averaged over the channel cross-section, and correspondingly for $\langle\alpha_{H_2CO_3}\rangle$. It is clear that the mineral dissolution is overwhelmingly caused by the direct reaction of calcite with H_2CO_3, with only 1.3 – 1.8% caused by the reaction with H^+. Finally, the behaviour of the non-linear saturation term $[1 - Q/K]^p$ is shown in Figure 11d, with the saturation index Q / K. As product ions build up along the length of the system, the value of the saturation term drops from 0.4 to around 0.05. This effectively reduces the mineral dissolution reaction rates by the same factor, and explains the sensitivity of the overall dissolution rate to the saturation term exponent seen in Figure 8.

4.2 Ketton Carbonate

The initial geometry of the Ketton carbonate sample is shown in Figure 12, along with the initial velocity field computed with the lattice Boltzmann model. In the experimental work of Menke et al. (Menke, Bijeljic et al. 2015) a 3.5mm subregion, located 2mm from the inlet of the sample was imaged and analysed. To replicate this here, we took the same initial 3.5mm sample image, and mirrored the first 2mm of it backwards. The 2 mm region was added to reproduce the experiment more accurately. Although it may not exactly match the experimental sample structure, it should still be more realistic than not having it at all. We note that previous simulation papers *e.g.* (Mostaghimi, Liu et al. 2016) did not consider this missing bit of rock sample. The importance of including the 2mm region is evidenced by Fig 13, where strong changes in the concentration profiles are observed. For heterogeneous rock structures in particular, this procedure may not guarantee that the profile will be fully consistent with the experiments. Indeed, mirroring the sample may influence the results, as reported by (Guibert, Nazarova et al. 2015) and (Guibert, Horgue et al. 2016), including the possibility of changing the structure heterogeneity, removing the anisotropy of the domain and redistributing the streamlines. However, since Ketton is very homogeneous, the mirroring is likely to be a good approximation in this case. Injection of the CO_2-saturated brine solution was then simulated, and resulting mass changes quantified only in the 3.5mm subvolume and compared to experiment.

This comparison is made in Figure 13 and shows marked differences between simulated and experimental results. Both saturation models show a virtually linear dependence on the calcite mass dissolved with time, however the experimental dissolution rate decreases considerably.

The chemical system through the pore-space can be analysed in the simulation, and the concentrations of the three species H^+ (and pH), H_2CO_3 and Ca^{2+} are shown in the Ketton geometry at initial steady-state for the linear saturation model in Figure 16. This figure includes the extra 2mm inlet region in front of the 3.5mm subvolume. The H_2CO_3 distribution is almost entirely uniform throughout, owing to the low reaction rate constant of the direct H_2CO_3 – calcite reaction (2).The convective Damköhler number for this reaction $Da_C = k_2/U_{av} = 0.8 \times 10^{-3}$ while the diffusive Damköhler number $Da_D = k_2\, L/D_{H_2CO_3} = 1.5 \times 10^{-2}$. Both values are well below unity, which means we are in the reaction-limited regime. This explains the uniform concentration of H_2CO_3. The H^+ concentration on the other hand decreases sharply from the inlet equilibrium value due to buffering reaction with HCO_3^- (5) as discussed for the case of the calcite cylinders.

5 Discussion

5.1 Calcite Channels

It was interesting to note both charge-coupled and constant diffusion models give very similar results (Figure 9). This contrasts with the HCl case (Gray, Anabaraonye et al. 2018) where the coupled diffusion processes enhanced the transport of the H^+ ion as shown in Figure 2c. This resulted in a considerably higher overall dissolution rate than the case of a single diffusion coefficient. For the case of the CO_2-saturated solutions considered here, the transport of H^+ has little influence on the overall reaction rate. Instead the transport of products away from the reactive surface, affecting the local reaction rate according to the saturation term (10) is the main control on the overall dissolution rate. These slower-diffusing ions are less affected by the charge coupling, as shown in Figure 2.

In section 4.1, cutaways of the experiment C1 using the non-linear saturation model were presented in Figure 10 for the H^+, Ca^{2+} and HCO_3^- species. This figure revealed that the H^+ concentration drops by more than an order of magnitude from its initial solution concentration value to that on the mineral surface, the pH ranging from 3.1 to 4.6. Here we discuss this observation in more detail. The product species Ca^{2+} and HCO_3^- are produced on the reactive surface and diffuse into the flow-stream. These quantities are plotted along the length of the channel in Figure 11 a) and b). The behaviour of the H^+ looks similar to that of a transport-controlled reaction – an initial inlet concentration is transported along the system, and diffuses to the mineral surface where it is consumed. The flow and diffusion rates therefore control the overall dissolution rate. However, this is not the case for this particular system. Instead, the variation in H^+ distribution is determined by the local equilibrium

reactions (11) and (12). The diffusion rate of the H^+ ion itself has little effect on this boundary layer, and hence including charge-coupled diffusion effects made little difference to the simulated dissolution rates. This can be further justified by noting that the initial H^+ concentration in solution arises from the dissociation of CO_2, and is determined by the balance of H_2CO_3 and HCO_3^-, the reaction equilibrium constant, and to an extent the concentration of other chemical species through the activity coefficients. From the results of our simulations, we argue that that such a slow-down cannot be explained in terms of the reduction in surface area or change in residence time of chemical species. Note that both reduction of surface area and increase in residence time of the chemical species have been validated and correctly included in our simulation models. Our model has been extensively validated, including dissolution rates presented in (Molins, Trebotich et al. 2014).

The reactions (13) and (14) are fast enough to be considered instantaneous (Langmuir 1997) and since the concentrations of H_2CO_3 and HCO_3^- are higher than that of H^+ near the reactive surfaces by orders of magnitude, it is the former species' concentrations that are the primary controls on surface pH.

5.2 Ketton Carbonate

The main observation from the comparison with experimental results for the Ketton carbonate was the highly distinct behaviour of the overall dissolution rate with time (Figure 13). Such a decrease with time would ordinarily be explained by the surface area of the grains decreasing, with a corresponding effect on the surface reaction rate. Additionally, as the pore space increases, average fluid velocities will tend to slow down leading to longer residence times for products which would affect the reaction rate through the saturation term. However, both of these effects were captured in the simulation, but this trend was not replicated. The dissolution rate for the simulations and experimental data are shown in Figure 14. Simulated rates remain fairly constant, though the non-linear saturation model does show approximately 10% decrease in reaction rate over the course of the calculation. In this case, the simulation was continued until around 80% more mass was dissolved than in the experiment in an attempt to see if such a slow-down in disssolution rate occurred at greater reaction extents. The experimental dissolution rate on the other hand is approximately 3x lower at the end of the experiment than at the beginning. When the experimental mass dissolved is plotted against square-root time, as in Figure 15, it shows an almost ideal linear relationship, with the exception of the first point. This behaviour is usually more indicative of a diffusive process than of convection-dominated dissolution like this system where the Peclet number is around 50. In recent work, it was shown that dissolution can occur inside the grains in Ketton carbonate when CO_2-saturated brine solution is injected (Singh, Anabaraonye et al. 2018). Grain boundaries were seen to remain almost static, but the density of the grains themselves decrease from outside in due to the gradual diffusion of reactants and products through the micro-pores. In Menke et al., it was noted that solid grain densities

did not appear to have changed during the coarse of the experiment, and thus it was concluded that dissolution was not occuring inside the grain micro-pores. 3 To investigate further the possibility of diffusion inside micro-pores playing a role, the simulations may need to include transport and reactive processes inside micropores to accurately model these experimental systems.

In their simulations comparing with the same experiment, Nunes et al. (Pereira Nunes, Blunt et al. 2016) made the assumption that the pH could be considered uniform throughout the sample, and the H_2CO_3 – calcite reaction could be neglected. We observe that the pH is between 1 and 2 units lower in most of the sample than at the inlet, and that the H_2CO_3 – calcite reaction dominates. We are unable to reproduce their reported agreement with experiment. Other modelling work which assumed that H^+ - calcite dissolution pathway (1) was dominant appeared to include the reaction (2) in their dissolution rate term (namely $-A\alpha_{H_2CO_3}k_2$) in (3), however H_2CO_3 species was not included in the chemical transport model, but instead treated as constant everywhere (Gao, Xing et al. 2017). Since the distribution of this component does tend to become uniform, (Figure 16c), this probably still leads to correct results. Nonetheless, the assumption of the dissolution processes being dominated by the acid reaction (1) is not correct, according to our analysis.

Finally we note that sets of simulations were performed using both constant and coupled diffusion models, however these gave results which were almost indistinguishable. This is most likely due to the effect of coupled diffusion processes on the product ions (Ca^{2+} and HCO_3^-) being small, as well as the transport processes being convection-dominated. The influence of the more strongly-affected H^+ ion on the resulting overall dissolution rate was also comparably small, as discussed for the case of the calcite cylinders.

6 Conclusion

We explored the influence of non-linear reaction kinetics and charge-coupled diffusion on the dissolution of calcite by CO_2-saturated solution using simulation and comparing to corresponding experimental data.

We found that for the case of the simple calcite cylinder system, the experimental dissolution rates were well predicted using a linear saturation model. Interestingly, using the non-linear saturation model derived from batch-reactor experiments, the simulations significantly under-predicted the experimental dissolution rates in most cases, both for CO_2-water and CO_2-brine systems. This is particularly important for these chemical systems as the dissolution rates were shown to be strongly dependent on the state of the saturation term. One possible explanation is that the batch reactor experiments used a smoothly cut calcite surface, exposing a single crystal lattice direction whereas, for the calcite cylinder systems used here, the comparably rough surfaces expose many different crystal orientations. The charge-coupled diffusion model by contrast had little effect on the overall dissolution rate compared to using a single diffusion coefficient for all species. This too was interesting when compared

to the case of HCl-calcite dissolution in other work where it had a much greater influence. The reasons for this were understood to be because of the very limited influence of the H^+ ion on the dissolution processes in the saturated CO_2 system, contrasting with the strongly H^+-transport-controlled mechanisms for HCl. Additionally, since calcite dissolution in the saturated CO_2 system is overwhelmingly caused by the direct reaction with hydrated CO_2 (H_2CO_3) which is uncharged, and tends to spread uniformly throughout the reactive system, this component will be largely unaffected by coupled diffusion processes. It is worth noting that there is second term which can be included in the coupled diffusion model (7) which includes gradients in activity coefficients (Steefel and Maher 2009). We neglected this here mainly because in solutions with concentrated brine, gradients in activity coefficients will be very small, however it could have an effect on the transport of product ions near reactive boundaries in the CO_2-water cases. It may be of interest to quantify this in future work.

We then applied the model to dissolution in Ketton carbonate in comparison with corresponding experimental data. We found that the simulations could not match the experimental dissolution rate and trend, instead overpredicting the dissolution rate by 2 to 7x, depending on the choice of saturation model and dissolution extent. Of particular note was the correlation of dissolution rate with time. Despite continuing the dissolution to a greater extent than the experiment, our simulations did not observe a dramatic slow-down in dissolution rate seen in the experiment. The two candidate mechanisms for such a reduction in dissolution rate, namely the decrease in reactive surface area over time and increase in product residence time were both included in the simulation. The almost ideal correlation of the experimental calcite dissolution rate with square-root-time may hint at the influence of diffusive processes within the micropores. Examples of this behaviour have been seen before in Ketton carbonate (Singh, Anabaraonye et al. 2018), and suggest that modelling efforts may need to include dissolution inside microporous grains as well as the surrounding macropores to accurately predict this behaviour. Indeed, we would suggest a partial-bounceback LB method, such as developed by (Walsh, Burwinkle et al. 2009) and analysed in detail by (Ginzburg 2016), which incorporates the permeability of the micro-porous regions as a model parameter. Rather than using lattice nodes that are either solid or fluid, this approach uses a probabilistic model, where lattice node properties are varied to reflect the local permeability of the material. Such a method could account for dissolution in the micro-porosity, assuming that the degree of dissolution of the micro-porous regions is reflected by the gray scale of the micro-CT image.

Acknowledgements

We gratefully acknowledge funding from the Qatar Carbonates and Carbon Storage Research Centre (QCCSRC), provided jointly by Qatar Petroleum, Shell, and Qatar Science and Technology Park.

We thank H. Menke for providing experimental data, and M. Trusler for useful discussions. We are also grateful to M. Harvey for providing HPC support for the calculations in this study.

References

Agrawal, P., A. Raoof, O. Iliev and M. Wolthers (2020). "Evolution of pore-shape and its impact on pore conductivity during CO2 injection in calcite: Single pore simulations and microfluidic experiments." Advances in Water Resources **136**: 103480.

Anabaraonye, B. U. (2017). Experimental and Modelling Studies of Reservoir Mineral Dissolution Following Carbon Dioxide Injection. PhD, Imperial College London.

Appelo, C. A. J. and P. Wersin (2007). "Multicomponent Diffusion Modeling in Clay Systems with Application to the Diffusion of Tritium, Iodide, and Sodium in Opalinus Clay." Environmental Science & Technology **41**(14): 5002-5007.

Cadogan, S. P., G. C. Maitland and J. P. M. Trusler (2014). "Diffusion Coefficients of CO2 and N2 in Water at Temperatures between 298.15 K and 423.15 K at Pressures up to 45 MPa." Journal of Chemical & Engineering Data **59**(2): 519-525.

Fredd, C. N. and H. S. Fogler (1998). "Influence of transport and reaction on wormhole formation in porous media." AIChE journal **44**(9): 1933-1949.

Gao, J., H. Xing, Z. Tian, J. K. Pearce, M. Sedek, S. D. Golding and V. Rudolph (2017). "Reactive transport in porous media for CO2 sequestration: Pore scale modeling using the lattice Boltzmann method." Computers & Geosciences **98**: 9-20.

Giambalvo, E. R., C. I. Steefel, A. T. Fisher, N. D. Rosenberg and C. G. Wheat (2002). "Effect of fluid-sediment reaction on hydrothermal fluxes of major elements, eastern flank of the Juan de Fuca Ridge." Geochimica et Cosmochimica Acta **66**(10): 1739-1757.

Ginzburg, I. (2016). "Comment on “An improved gray Lattice Boltzmann model for simulating fluid flow in multi-scale porous media”: Intrinsic links between LBE Brinkman schemes." Advances in Water Resources **88**: 241-249.

Gray, F., B. Anabaraonye, S. Shah, E. Boek and J. Crawshaw (2018). "Chemical mechanisms of dissolution of calcite by HCl in porous media: Simulations and experiment." Advances in Water Resources **121**: 369-387.

Gray, F. and E. Boek (2016). "Enhancing Computational Precision for Lattice Boltzmann Schemes in Porous Media Flows." Computation **4**(1): 11.

Gray, F., J. Cen and E. S. Boek (2016). "Simulation of dissolution in porous media in three dimensions with lattice Boltzmann, finite-volume, and surface-rescaling methods." Physical Review E **94**(4): 043320.

Guibert, R., P. Horgue, G. Debenest and M. Quintard (2016). "A comparison of various methods for the numerical evaluation of porous media permeability tensors from pore-scale geometry." Mathematical Geosciences **48**(3): 329-347.

Guibert, R., M. Nazarova, P. Horgue, G. Hamon, P. Creux and G. Debenest (2015). "Computational permeability determination from pore-scale imaging: sample size, mesh and method sensitivities." Transport in Porous Media **107**(3): 641-656.

Langmuir, D. (1997). Aqueous Environmental Geochemistry, Prentice Hall.

Li, L., C. I. Steefel, and L. Yang (2008). "Scale dependence of mineral dissolution rates within single pores and fractures." Geochim. Cosmochim. Acta **72**: 360–377.

Lide, D. R. (1997). CRC Handbook of Chemistry and Physics.

Liu, M. and P. Mostaghimi (2017). "High-resolution pore-scale simulation of dissolution in porous media." Chemical Engineering Science **161**: 360-369.

Liu, M. and P. Mostaghimi (2018). "Numerical simulation of fluid-fluid-solid reactions in porous media." International Journal of Heat and Mass Transfer **120**: 194-201.

Lobo, V., M. Helena and S. Teixeira (1979). "Diffusion coefficients in aqueous solutions of hydrochloric acid at 298 K." Electrochimica Acta **24**(5): 565-567.

Maher, K., C. I. Steefel, D. J. DePaolo and B. E. Viani (2006). "The mineral dissolution rate conundrum: Insights from reactive transport modeling of U isotopes and pore fluid chemistry in marine sediments." Geochimica et Cosmochimica Acta **70**(2): 337-363.

McLeod, H. O. (1984). "Matrix acidizing." J. Pet. Technol. **36**(12): 2055 - 2069.
Menke, H., C. Reynolds, M. Andrew, J. P. Nunes, B. Bijeljic and M. Blunt (2018). "4D multi-scale imaging of reactive flow in carbonates: Assessing the impact of heterogeneity on dissolution regimes using streamlines at multiple length scales." Chemical Geology **481**: 27-37.
Menke, H. P., B. Bijeljic, M. G. Andrew and M. J. Blunt (2015). "Dynamic Three-Dimensional Pore-Scale Imaging of Reaction in a Carbonate at Reservoir Conditions." Environmental Science & Technology **49**(7): 4407-4414.
Molins, S., C. Soulaine, N. I. Prasianakis, A. Abbasi, P. Poncet, A. J. Ladd, V. Starchenko, S. Roman, D. Trebotich and H. A. Tchelepi (2020). "Simulation of mineral dissolution at the pore scale with evolving fluid-solid interfaces: review of approaches and benchmark problem set." Computational Geosciences: 1-34.
Molins, S., D. Trebotich, L. Yang, J. B. Ajo-Franklin, T. J. Ligocki, C. Shen and C. I. Steefel (2014). "Pore-Scale Controls on Calcite Dissolution Rates from Flow-through Laboratory and Numerical Experiments." Environmental Science & Technology **48**(13): 7453-7460.
Molins, S., Trebotich, D., Steefel, C. I., and Shen, C. (2012). "An investigation of the effect of pore scale flow on average geochemical reaction rates using direct numerical simulation." Water Resour. Res. **48**.
Mostaghimi, P., M. Liu and C. H. Arns (2016). "Numerical Simulation of Reactive Transport on Micro-CT Images." Mathematical Geosciences **48**(8): 963-983.
Muniruzzaman, M. and M. Rolle (2016). "Modeling multicomponent ionic transport in groundwater with IPhreeqc coupling: Electrostatic interactions and geochemical reactions in homogeneous and heterogeneous domains." Advances in Water Resources **98**: 1-15.
Noiriel, C., C. I. Steefel, L. Yang and J. Ajo-Franklin (2012). "Upscaling calcium carbonate precipitation rates from pore to continuum scale." Chemical Geology **318**: 60-74.
Ovaysi, S. and M. Piri (2014). "Pore-space alteration induced by brine acidification in subsurface geologic formations." Water Resources Research **50**(1): 440-452.
Peng, C., J. P. Crawshaw, G. C. Maitland and J. M. Trusler (2015). "Kinetics of calcite dissolution in CO 2-saturated water at temperatures between (323 and 373) K and pressures up to 13.8 MPa." Chemical Geology **403**: 74-85.
Pereira Nunes, J. P., M. J. Blunt and B. Bijeljic (2016). "Pore-scale simulation of carbonate dissolution in micro-CT images." Journal of Geophysical Research: Solid Earth **121**(2): 558-576.
Qajar J, A. C. (2012). "Chemical dissolution of carbonate rocks: A micro-CT study." Glob. Imaging Insights **2**.
Singh, K., B. U. Anabaraonye, M. J. Blunt and J. Crawshaw (2018). "Partial dissolution of carbonate rock grains during reactive CO2-saturated brine injection under reservoir conditions." Advances in Water Resources **122**: 27-36.
Soulaine, C., S. Roman, A. Kovscek and H. A. Tchelepi (2017). "Mineral dissolution and wormholing from a pore-scale perspective." Journal of Fluid Mechanics **827**: 457-483.
Sprocati, R., M. Masi, M. Muniruzzaman, M. Rolle (2019). "Modeling electrokinetic transport and biogeochemical reactions in porous media: A multidimensional Nernst–Planck–Poisson approach with PHREEQC coupling." Advances in Water Resources **127**: 134-147.
Steefel, C. I., C. A. J. Appelo, B. Arora, D. Jacques, T. Kalbacher, O. Kolditz, V. Lagneau, P. C. Lichtner, K. U. Mayer, J. C. L. Meeussen, S. Molins, D. Moulton, H. Shao, J. Šimůnek, N. Spycher, S. B. Yabusaki and G. T. Yeh (2015). "Reactive transport codes for subsurface environmental simulation." Computational Geosciences **19**(3): 445-478.
Steefel, C. I. and K. Maher (2009). "Fluid-Rock Interaction: A Reactive Transport Approach." Reviews in Mineralogy and Geochemistry **70**(1): 485-532.
Tian, Z. and J. Wang (2018). "Lattice Boltzmann simulation of dissolution-induced changes in permeability and porosity in 3D CO2 reactive transport." Journal of Hydrology **557**: 276-290.
Vinograd, J. R. and J. W. McBain (1941). "Diffusion of electrolytes and of the ions in their mixtures." Journal of the American Chemical Society **63**(7): 2008-2015.

Walsh, S. D., H. Burwinkle and M. O. Saar (2009). "A new partial-bounceback lattice-Boltzmann method for fluid flow through heterogeneous media." Computers & Geosciences **35**(6): 1186-1193.
Yoon, H., Q. Kang and A. Valocchi (2015). "Lattice Boltzmann-based approaches for pore-scale reactive transport." Rev Mineral Geochem **80**: 393-431.
Yoon, H., A. J. Valocchi, C. J. Werth and T. Dewers (2012). "Pore-scale simulation of mixing-induced calcium carbonate precipitation and dissolution in a microfluidic pore network." Water Resources Research **48**(2).

Tables

Table 1 – Self-diffusion coefficients for each species at T = 323 K. [a] from (Cadogan, Maitland et al. 2014), and [b] from (Lide 1997).

Species	D_i / 10^{-9} m^2s^{-1}
H_2CO_3	3.643[a]
H^+	16.53[b]
Cl^-	3.607 [b]
HCO_3^-	2.104 [b]
CO_3^{2-}	1.638 [b]
Ca^{2+}	1.406 [b]

Table 2 – Parameters for the four CO_2-water cylinder experiments.

Experiment	Diameter /mm	Length /mm	Flow Rate /mL min^{-1}	Run Time /hr
C1	3	19.5	0.168	20.50
C2	3	13.5	0.168	10.55
C3	1	18.2	0.064	25.96
C4	3	19.5	0.084	21.13

Table 3 – Parameters for the two CO_2-brine cylinder experiments.

Experiment	Diameter /mm	Length /mm	Flow Rate /mL min^{-1}	Run Time /hr
C5	3	17.2	0.168	14
C6	3	13.3	0.168	8.60

Figures

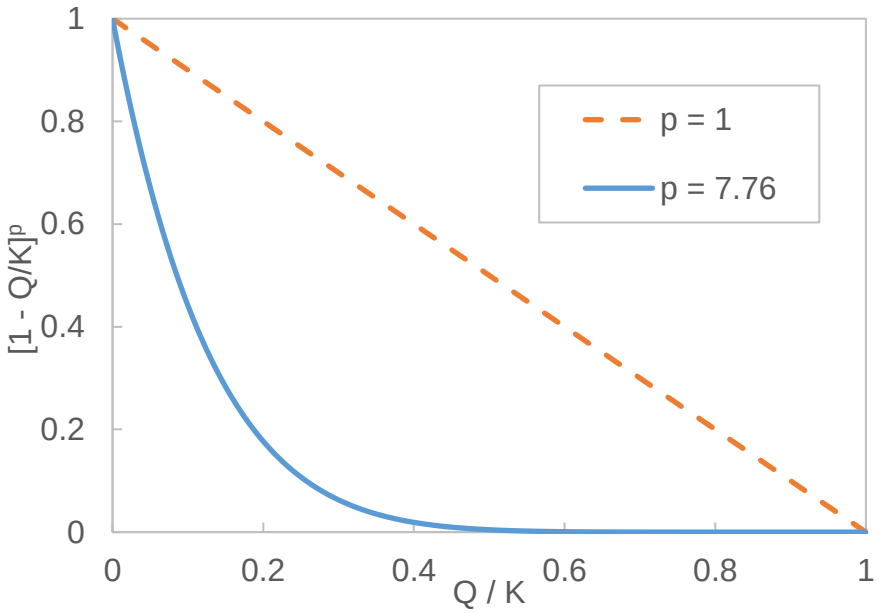

Figure 1 – The value of the saturation term $[1 - Q/K]^p$ with the saturation index Q/K for the linear model ($p = 1$) and the model of Anabaraonye et al. ($p = 7.76$).

a)

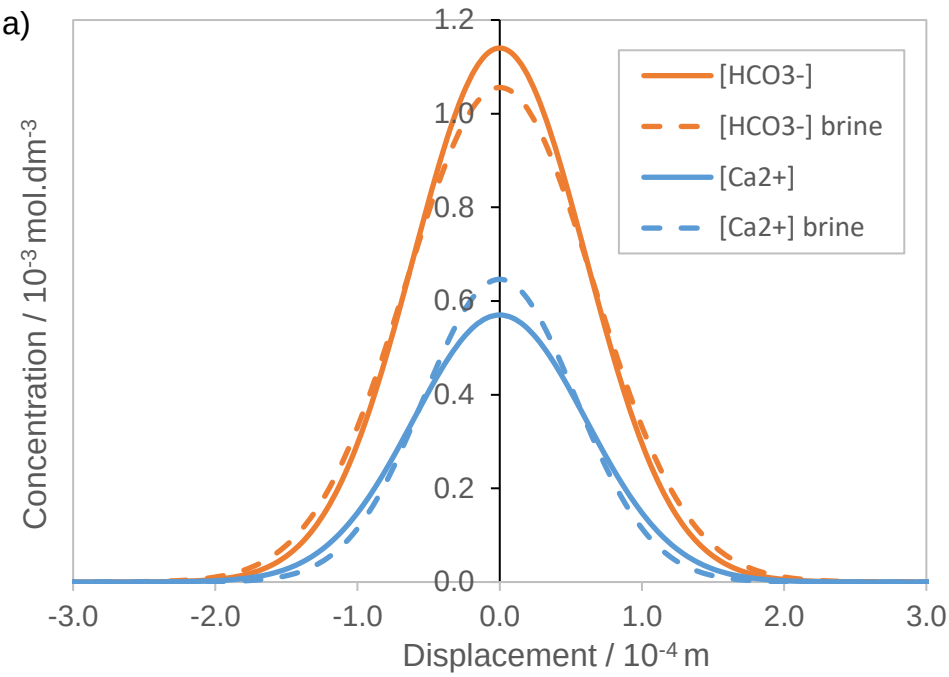
1.2
1.0
0.8
0.6
0.4
0.2
0.0
-3.0
-2.0
-1.0
0.0
1.0
2.0
3.0
Concentration / 10-3 mol.dm-3
Displacement / 10-4 m
[HCO3-]
[HCO3-] brine
[Ca2+]
[Ca2+] brine

b)

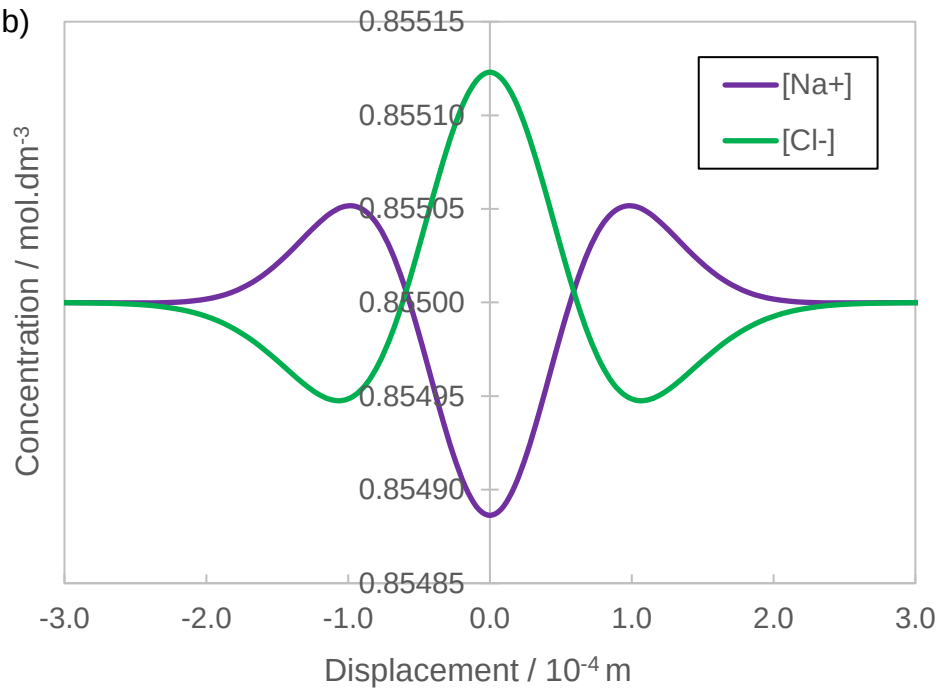
0.85515
0.85510
0.85505
0.85500
0.85495
0.85490
0.85485
-3.0
-2.0
-1.0
0.0
1.0
2.0
3.0
Concentration / mol.dm-3
Displacement / 10-4 m
[Na+]
[Cl-]

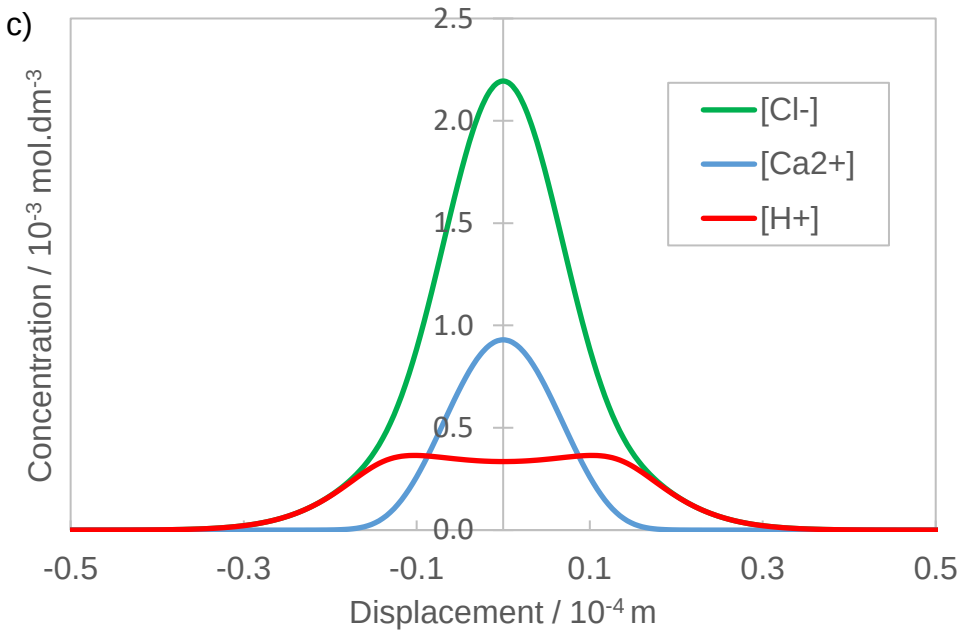

Figure 2 – a) concentration distributions of Ca^{2+} and HCO_3^- ions after diffusing from a point source after 1.03 s. Solid lines are Ca^{2+} and HCO_3^- ions in water, and dashed lines are in a background solution of 0.855 M NaCl brine. The effective diffusion coefficient of both ions is 1.805 x 10^{-9} m^2s^{-1} in water, however in the presence of brine Ca^{2+} and HCO_3^- diffuse with their self-diffusion coefficients. b) the distribution of ions of the background brine solution of 0.855 M NaCl after 1.03 s of diffusion. c) the concentration distributions of H^+, Cl^- and Ca^{2+} ions after diffusion from a point source after 1.03 s.

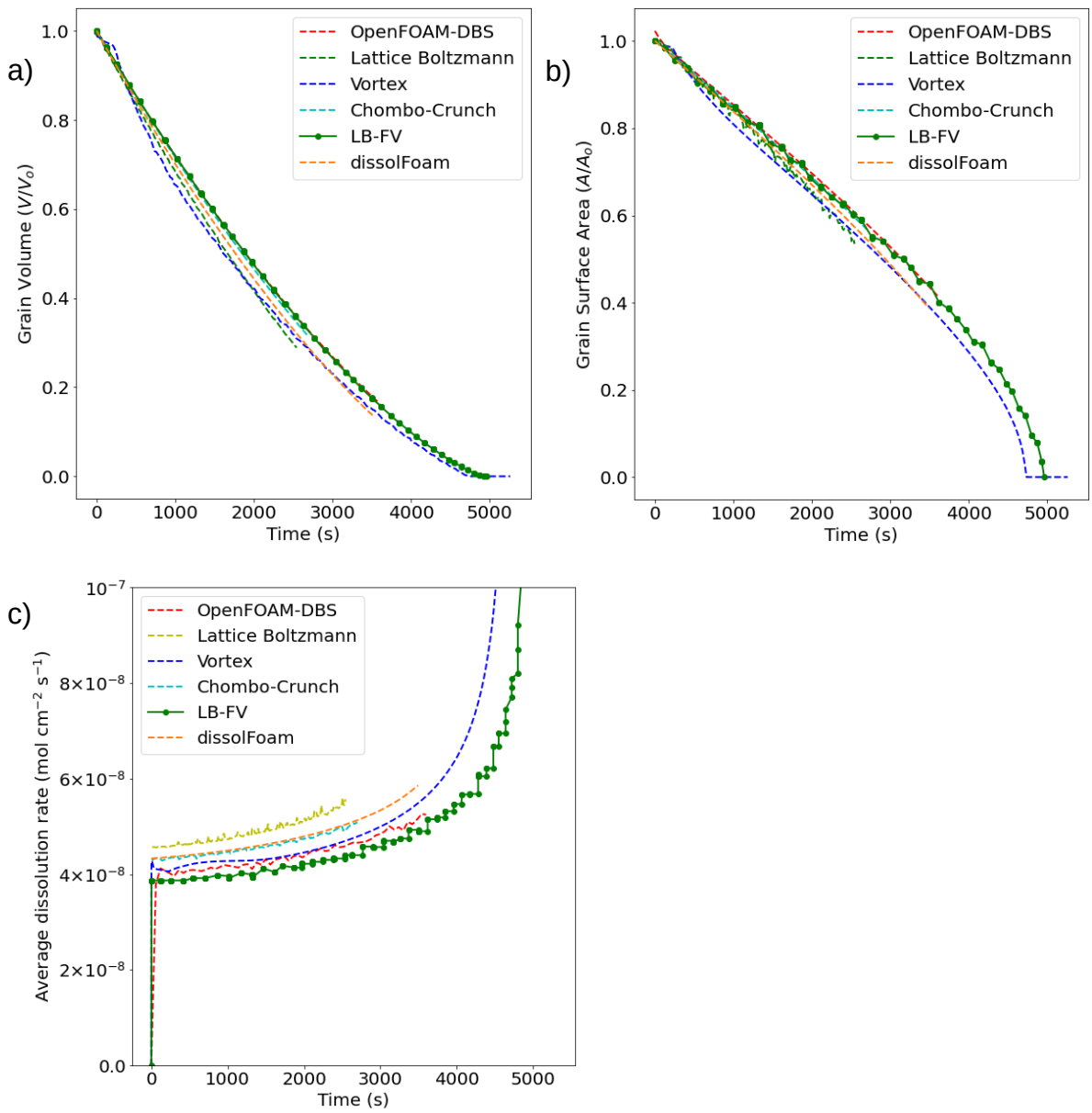

Figure 3: Evolution of a) volume (area in two dimensions), b) surface area (perimeter in two dimensions), and c) average dissolution rate, as a function of time during the dissolution of a two-dimensional calcite disk as described in part II of (Molins, Soulaine et al. 2020). Our calculations are shown as "LB-FV" using green markers and solid interpolation curve, in comparison with other simulation results (dashed lines) detailed in (Molins, Soulaine et al. 2020).

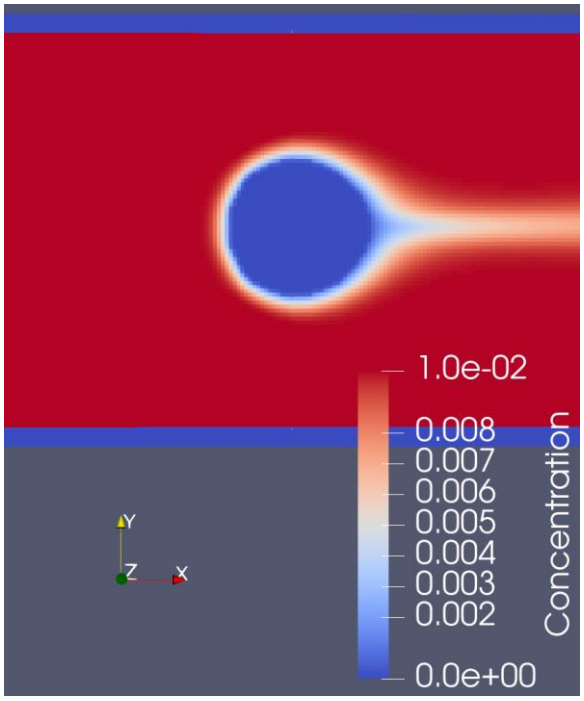

Figure 4: H^+ ion concentration contours for the 2D dissolution of a cylindrical calcite grain in a solution of HCl at pH=2, obtained from our LB-FV calculations at t =1000 s.

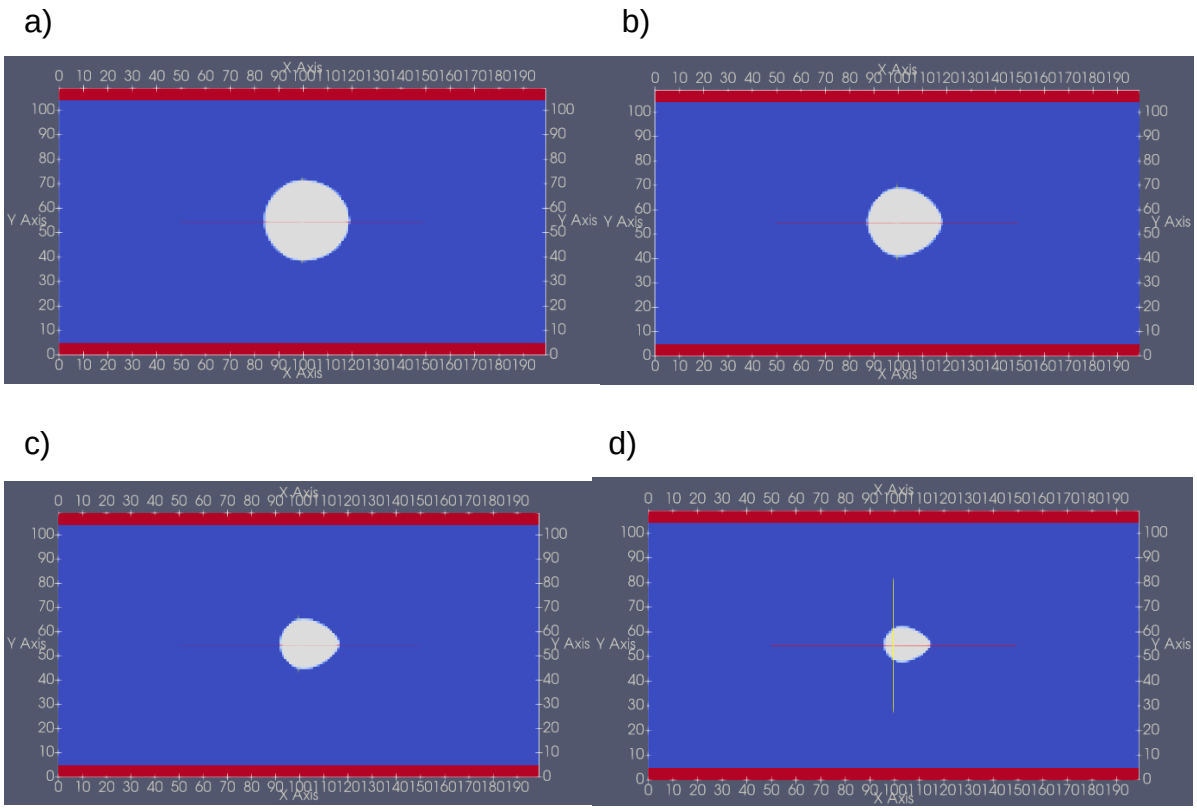

Figure 5: Evolution of calcite grain shape due to dissolution under flowing conditions after a) 15 min., b) 30 min., c) 45 min. and d) 60 min., observed from our LB-FV simulations.

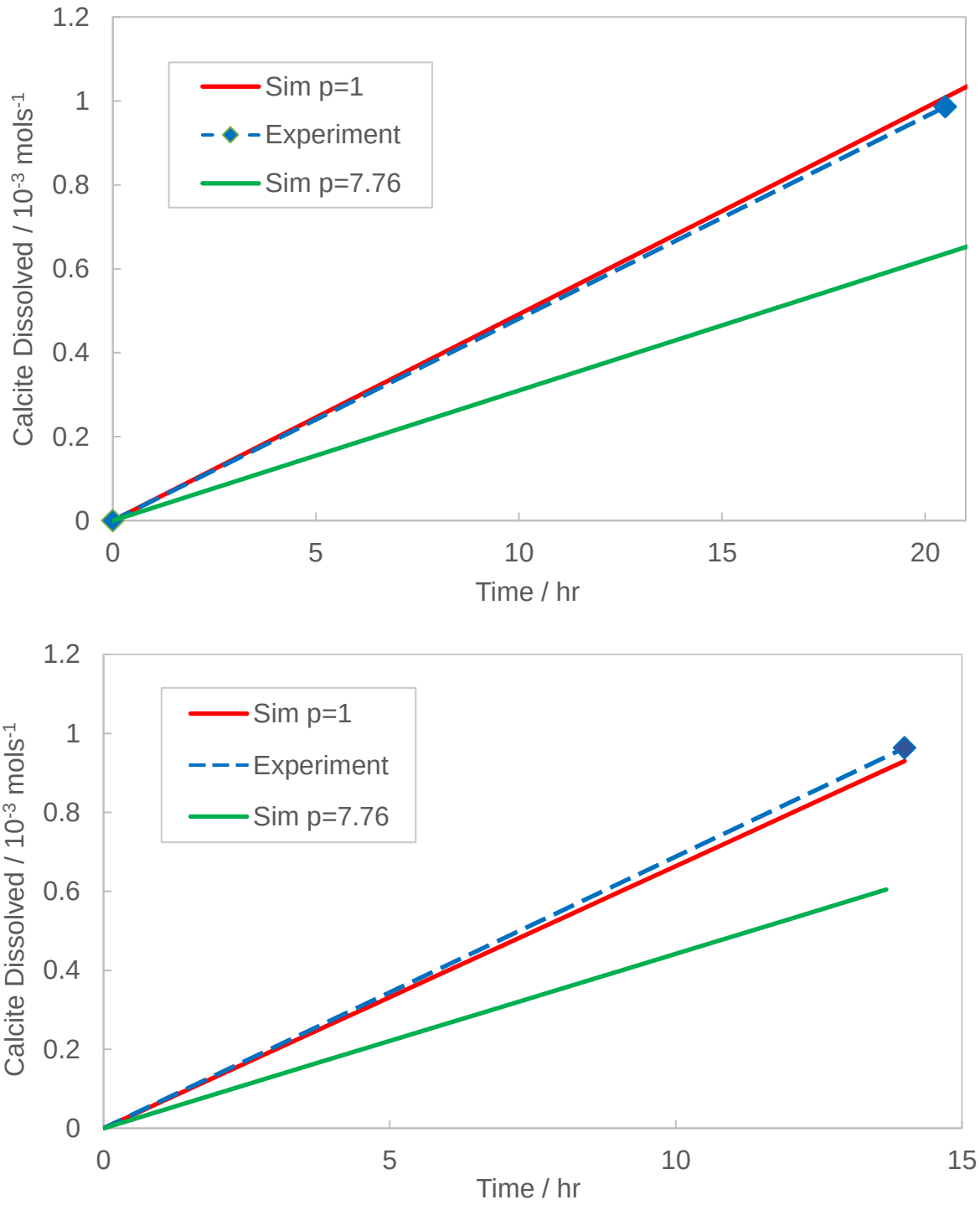

Figure 6 – Moles of calcite dissolved over time for the channels for top: C1 (CO_2-water) and bottom: C5 (CO_2-brine) dissolution experiments. Experimental lines (dashed) were obtained by measuring the weight change after a given time. Solid lines are simulated using the linear saturation model and the non-linear model with exponent $p = 7.76$.

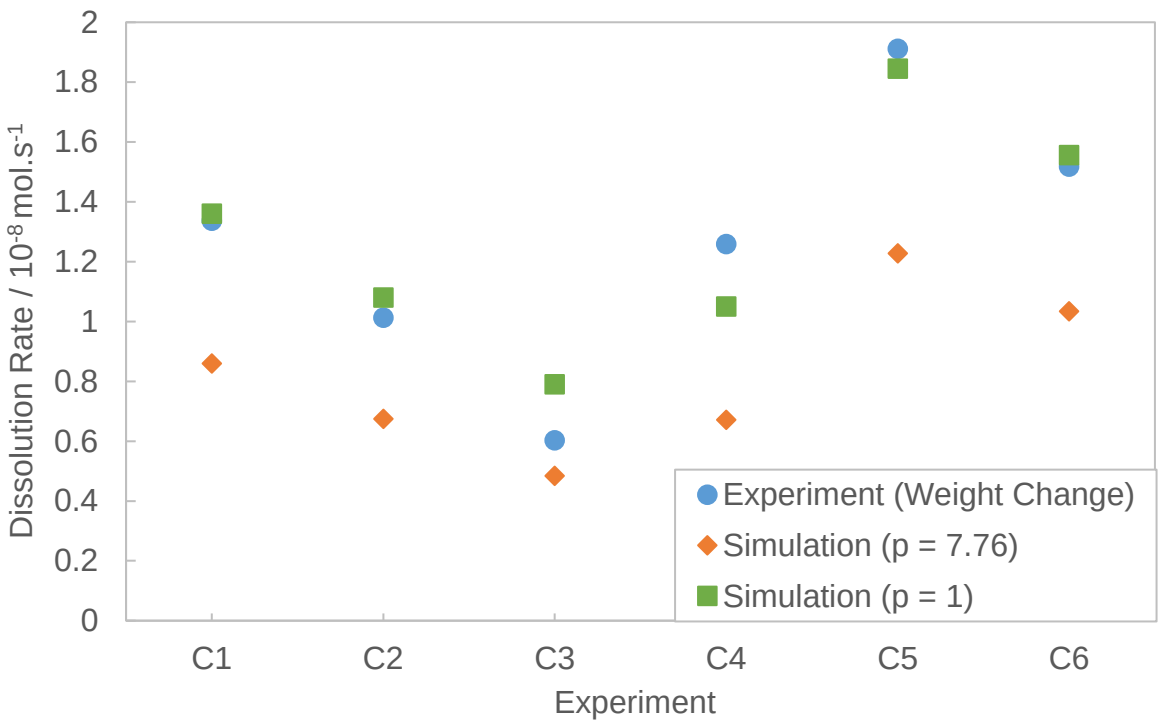

Figure 7 – The dissolution rate for the cylindrical channels injected with CO_2-water solution. Experimental results were obtained from effluent analysis and are compared with simulations performed using saturation exponents of p = 7.76 and p = 1.

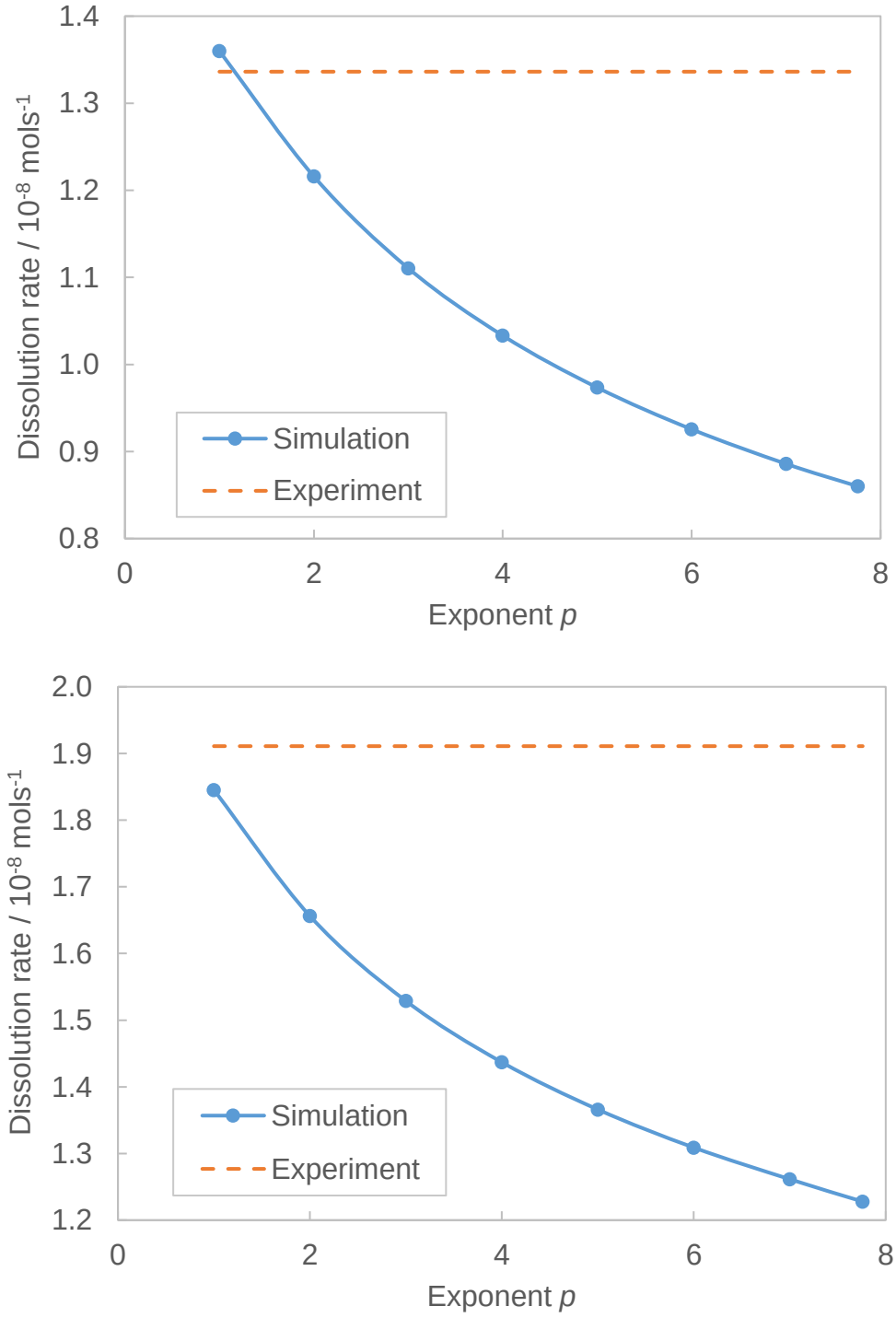

Figure 8 – Calcite dissolution rates simulated using different values of the non-linear saturation exponent p for CO_2-water experiment C1 (top) and CO_2-brine experiment C5 (bottom). The dashed lines are the experimental dissolution rates. Best fit values of the exponent are linear in both cases.

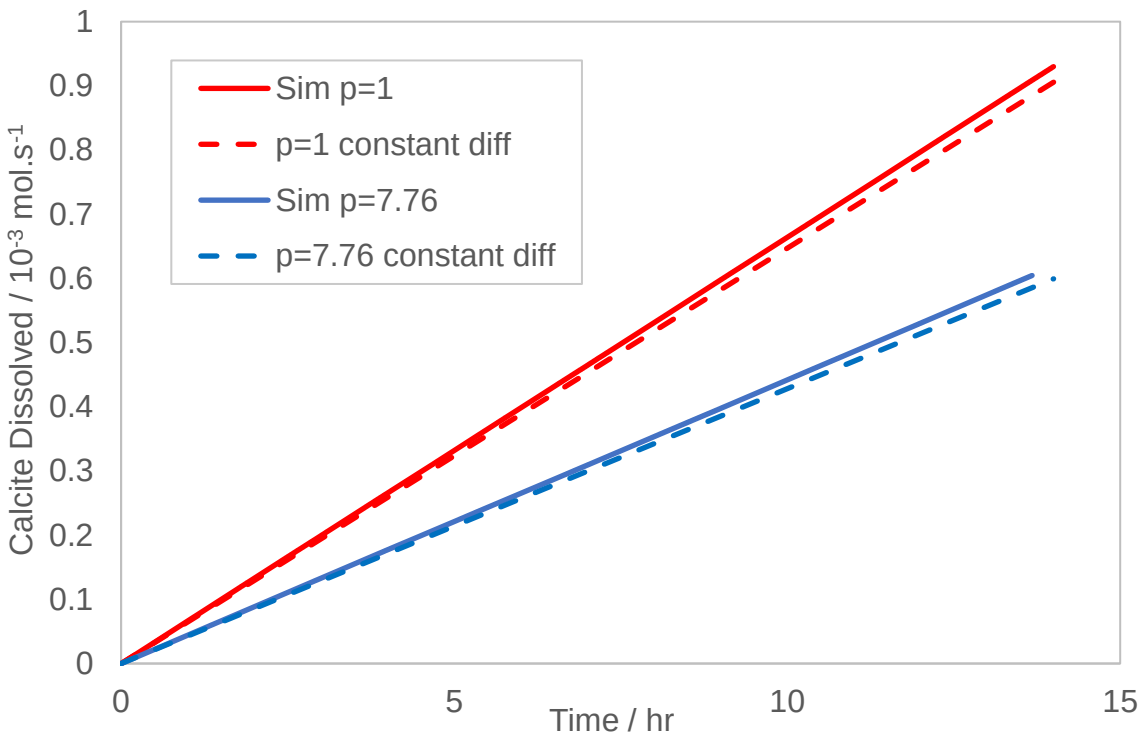

Figure 9 – Dissolved mols of calcite over time simulated for the parameters of experiment C5 using: (solid lines) the coupled ion diffusion model and (dashed lines) a constant diffusion rate of 1.805 x 10^{-9} m^2s^{-1}, and performed for both the linear and non-linear saturation models.

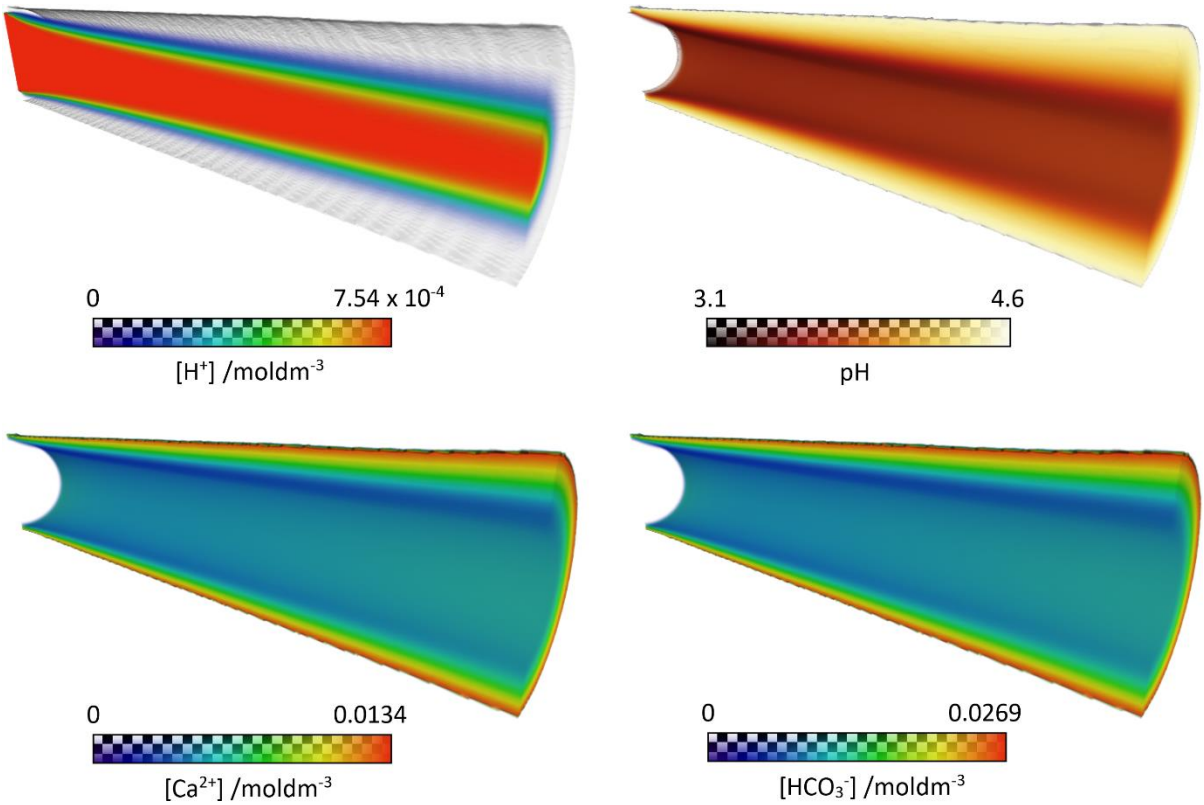

Figure 10 – Cutaways of concentration fields of H^+, Ca^{2+}, HCO_3^- and the pH along the channel for the CO_2-water calculation, using a saturation exponent of $p = 7.76$. Injection was from left.

a)

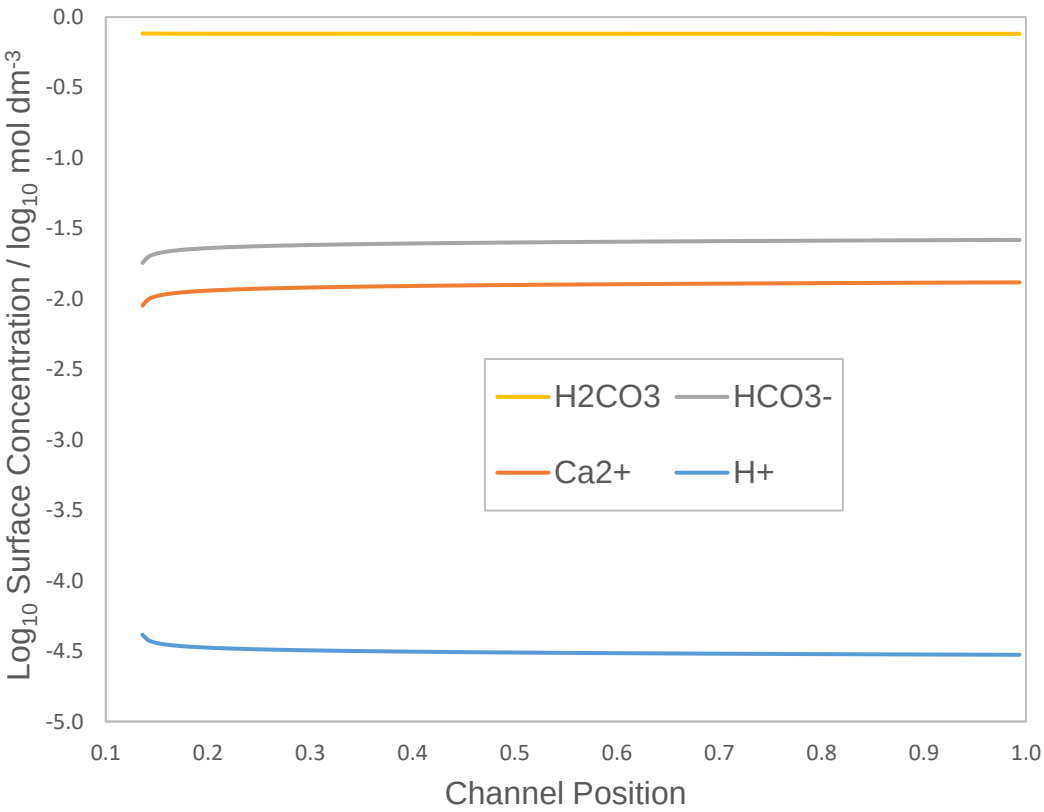

b)

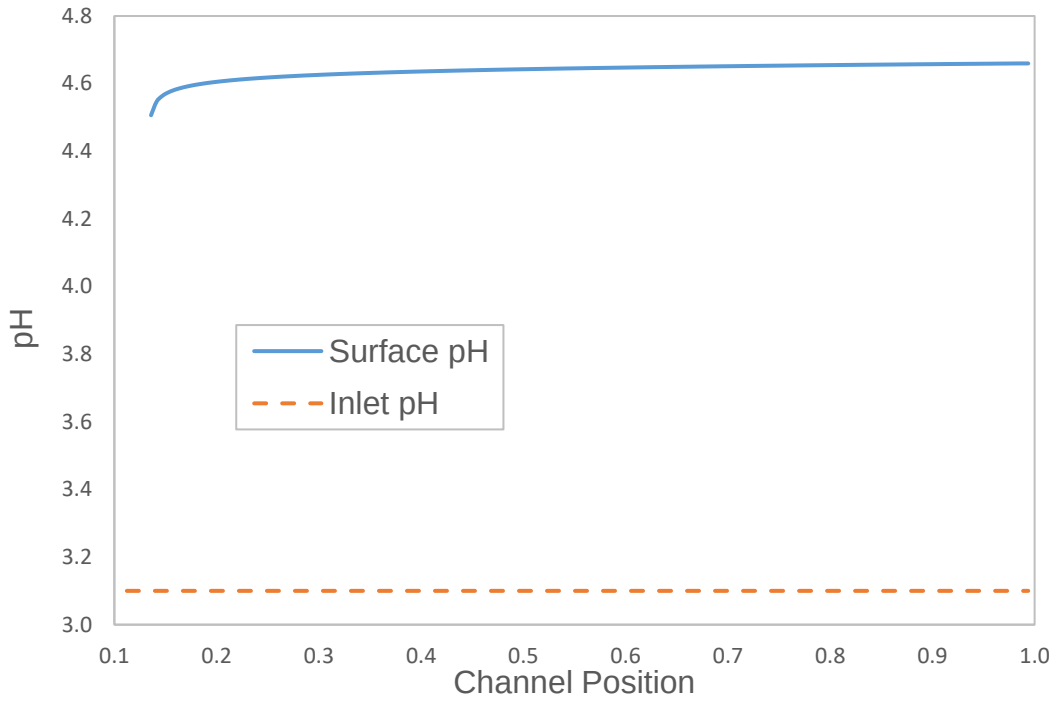
4.8
4.6
4.4
4.2
4.0
3.8
3.6
3.4
3.2
3.0
pH
Surface pH
Inlet pH
0.1
0.2
0.3
0.4
0.5
0.6
0.7
0.8
0.9
1.0
Channel Position

c)

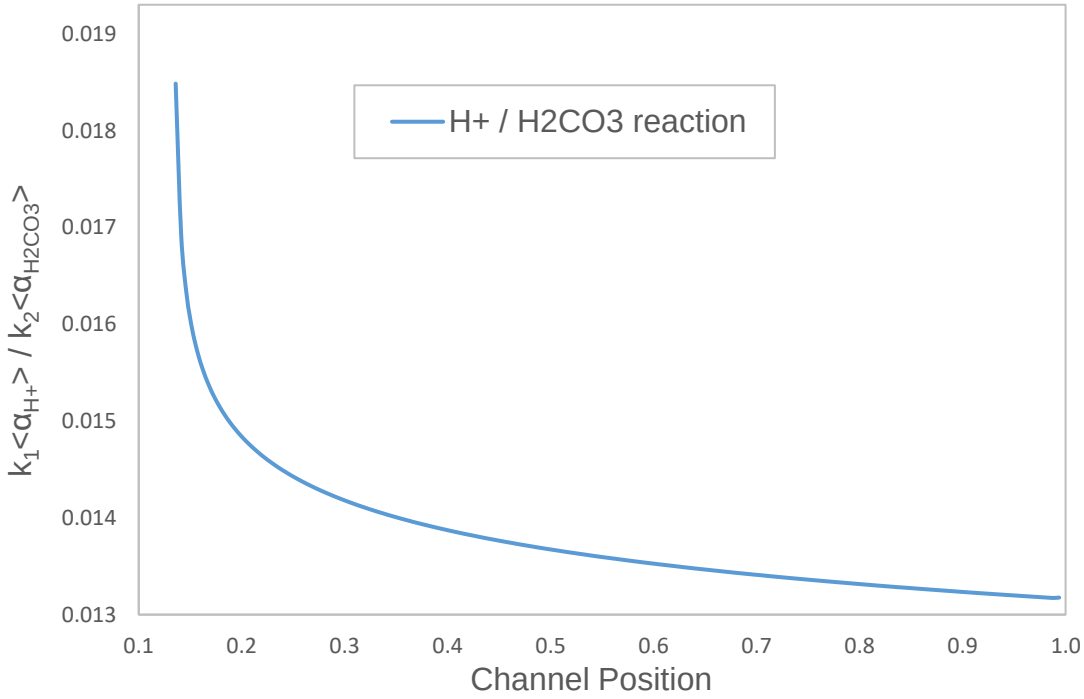
0.019
0.018
0.017
0.016
0.015
0.014
0.013
k1<αH+> / k2<αH2CO3>
H+ / H2CO3 reaction
0.1
0.2
0.3
0.4
0.5
0.6
0.7
0.8
0.9
1.0
Channel Position

d)

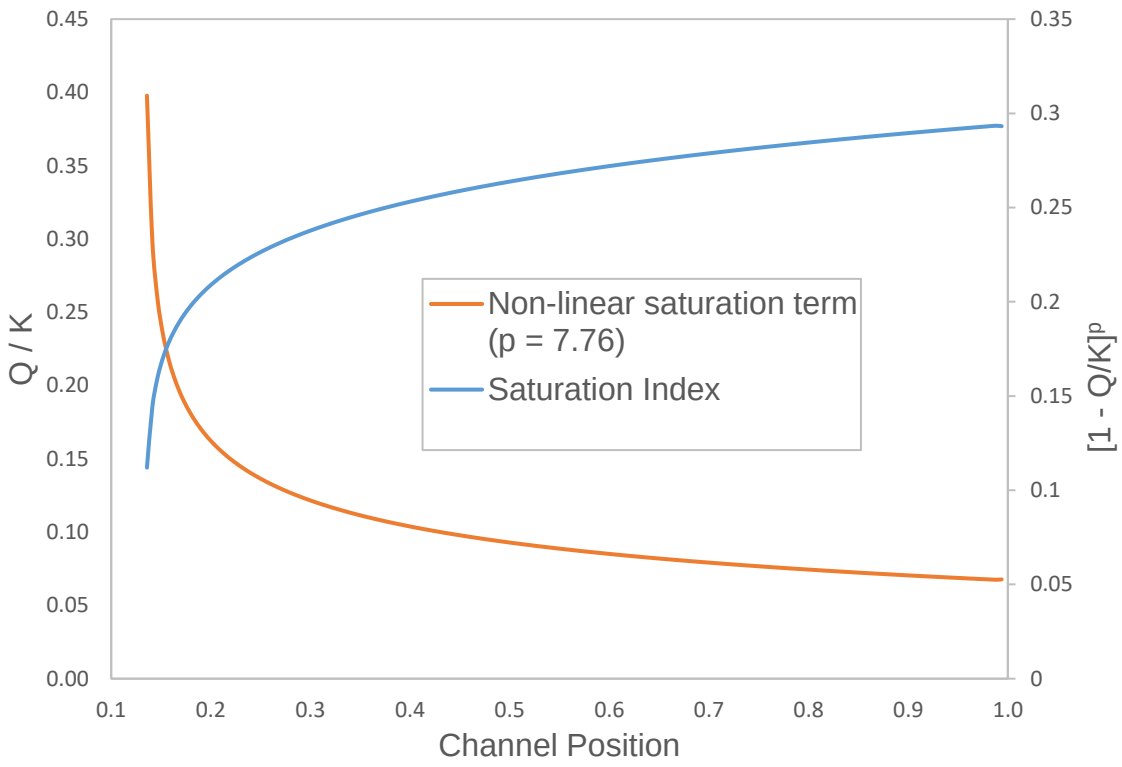

Figure 11 – Quantities sampled over the length of the channel from simulation of CO_2-water using the exponent $p = 7.76$. a) concentrations of chemical components on the channel surface. b) surface pH compared to inlet solution pH. c) the relative contribution of the H^+ and H_2CO_3 dissolution pathways computed using mean surface activities of the respective species. d) the saturation index Q / K and the value of the non-linear saturation term on the channel surface. Data is only shown for the calcite part of the channel (i.e. excluding the inlet region).

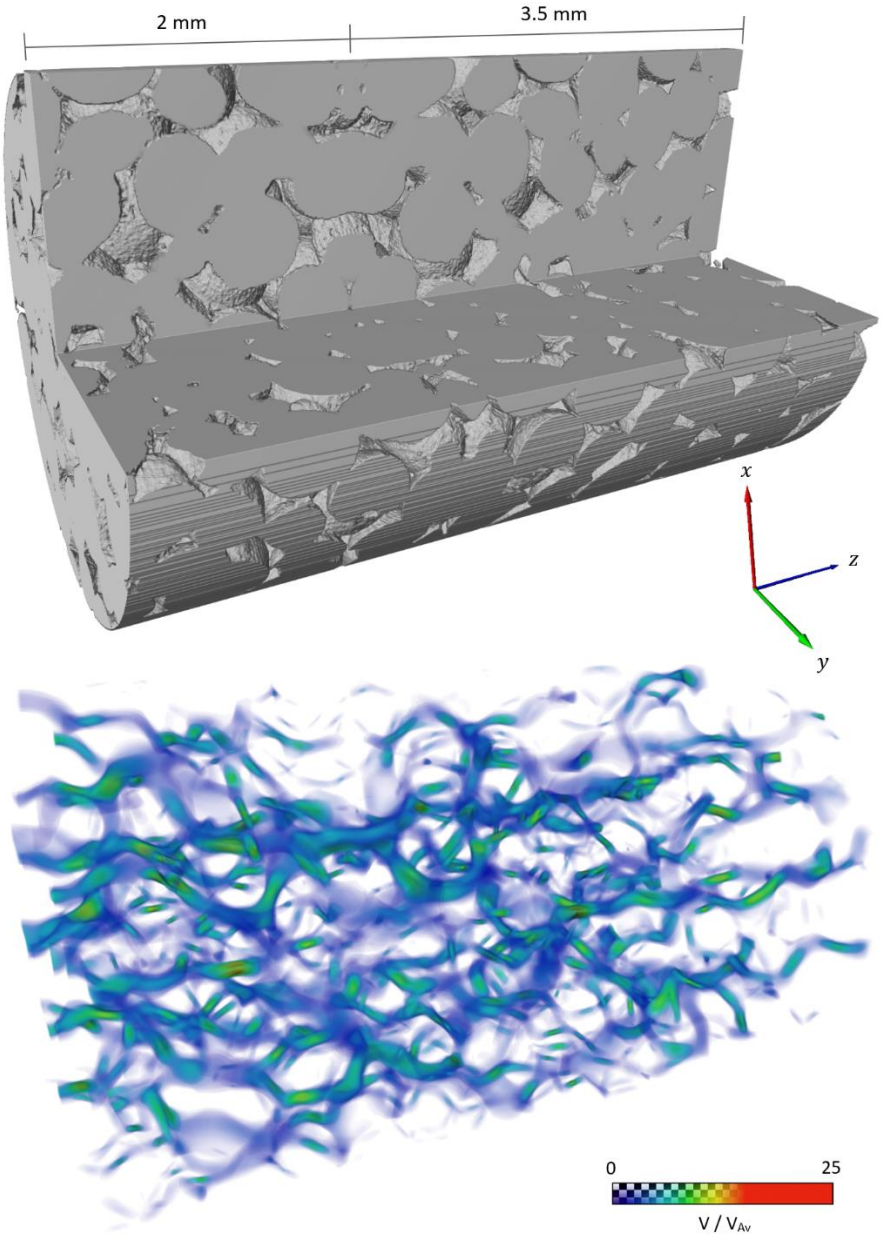

Figure 12 – The Ketton carbonate sample from Menke et al. (Menke, Bijeljic et al. 2015) with an extra 2 mm region added by mirroring part of the sample backwards. The geometry is shown, indicating both the 3.5 mm sample region from Menke et al. and the extra 2 mm inlet region (top) with the initial velocity field computed using lattice Boltzmann (bottom). The size of the domain is 922 x 902 x 1436 lattice units, at a resolution of 3.81 µm.

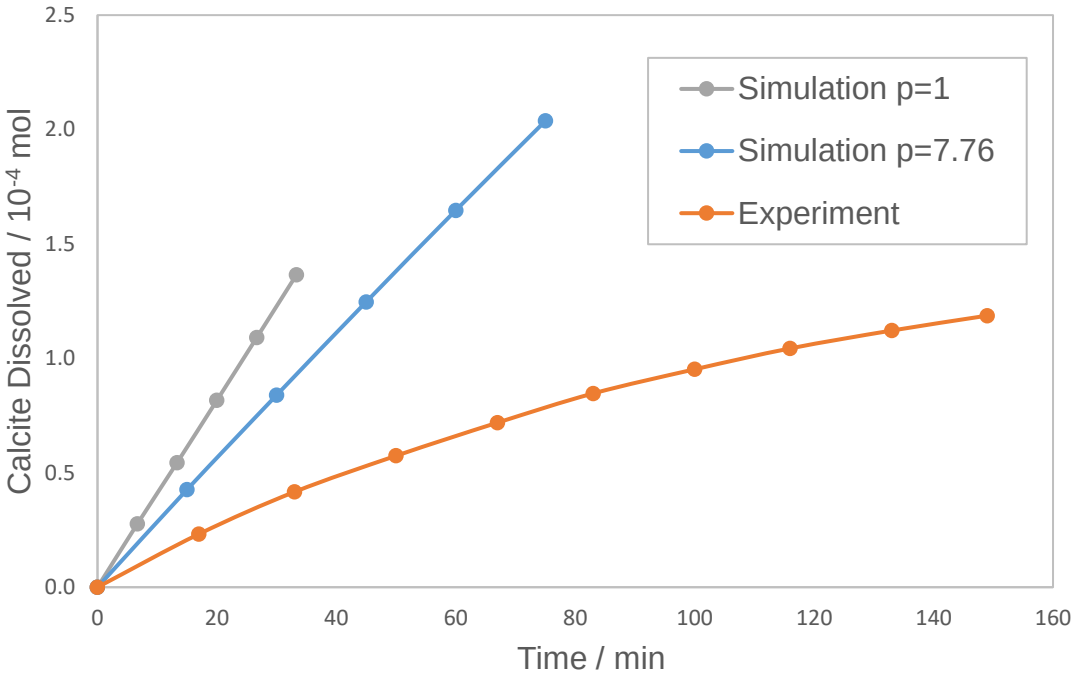

Figure 13 – Dissolved moles of calcite over time within the 3.5 mm subvolume in simulations using both linear (p = 1) and non-linear (p = 7.76) saturation laws, compared with experiment. Constant diffusion and coupled diffusion models gave almost indistinguishable results.

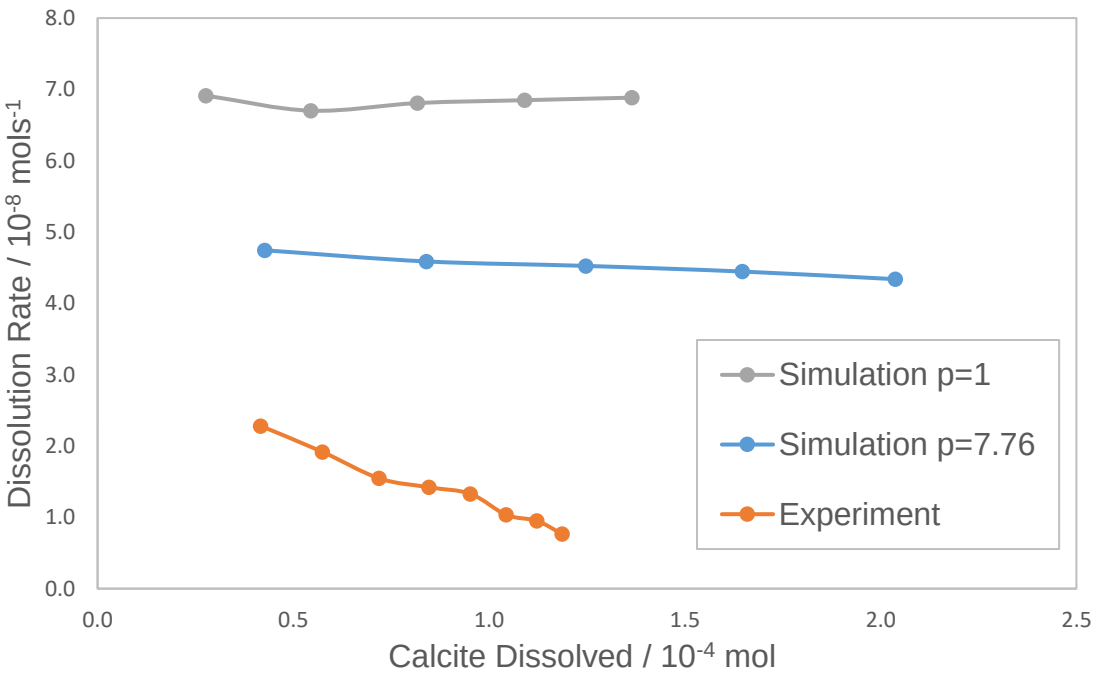

Figure 14 – The dissolution rate with amount of calcite dissolved in the 3.5 mm subvolume in simulations using both linear (p = 1) and non-linear (p = 7.76) saturation laws, and experiment.

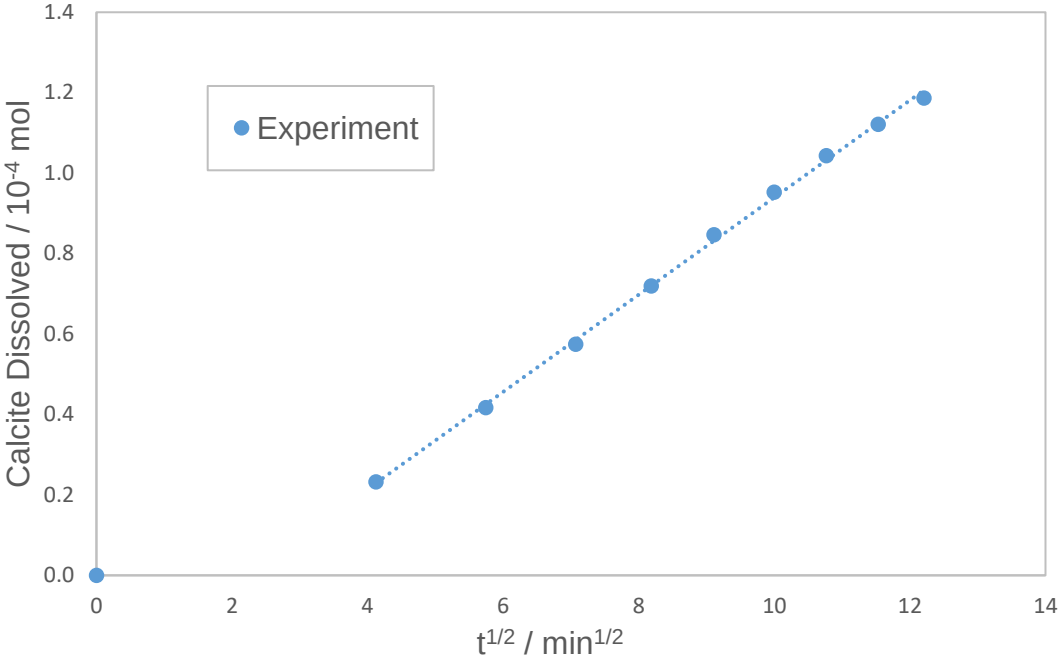

Figure 15 – Dissolved moles of calcite over square-root time in the experiment of Menke et al. (2015). A linear fit for all except the first point is included. Aside from the first point, the data follows almost ideally a square-root dependence on time.

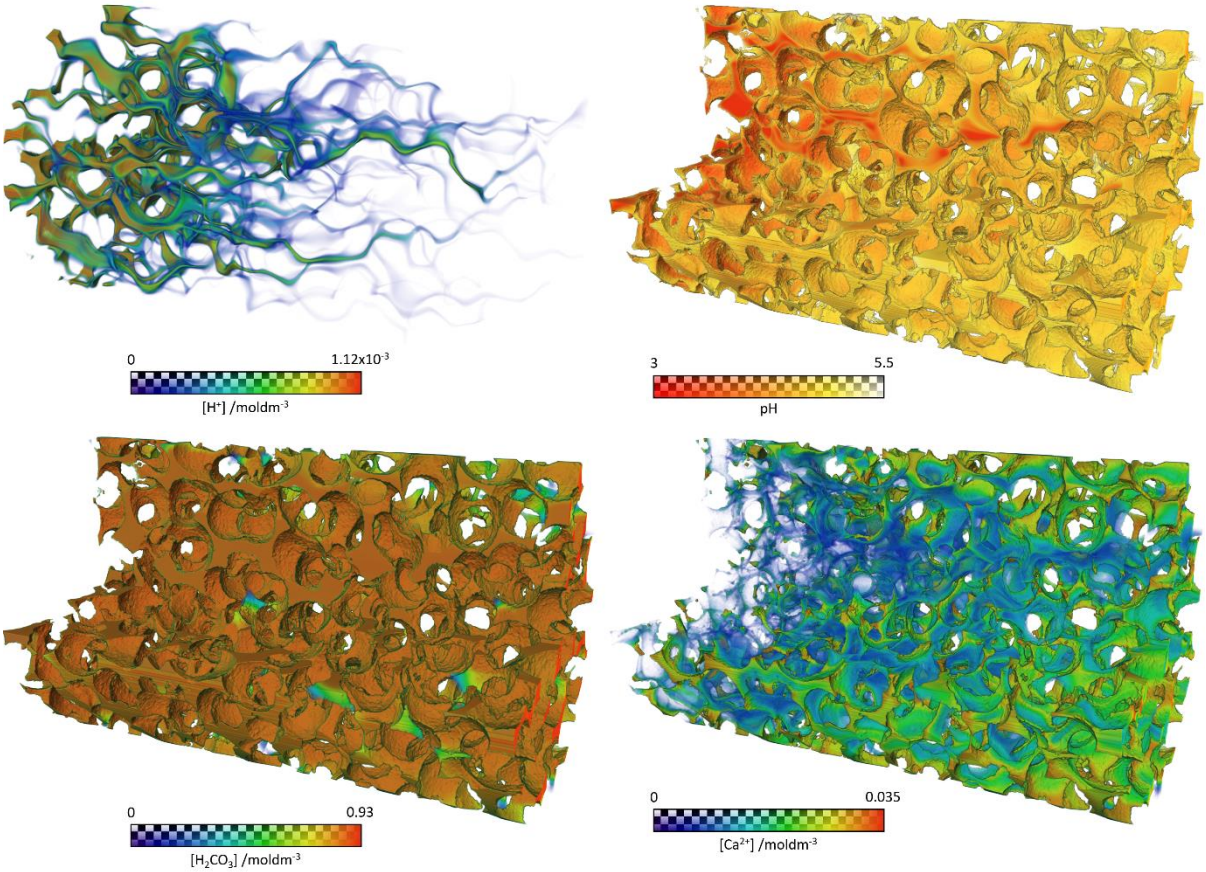

Figure 16 – Concentration fields of a) H+, and cutaways of b) pH, c) H_2CO_3 and d) Ca^{2+} in the Ketton carbonate core at initial steady-state, including the extra 2mm inlet region. The exponent p = 1 and injection was from left.

Pore-Scale Dissolution Mechanisms in Calcite-CO_2-brine Systems: The Impact of Non-Linear Reaction Kinetics and Coupled Ion Transport

F. Gray[1]*, B. U. Anabaraonye[1], J. P. Crawshaw[1] and E. S. Boek[2+]

[1]Qatar Carbonates and Carbon Storage Research Centre (QCCSRC), Department of Chemical Engineering, South Kensington Campus, Imperial College London, London SW7 2AZ, United Kingdom.

[2]Division of Chemical Engineering, School of Engineering and Materials Science, Queen Mary University of London, Mile End Road, London E1 4NS, U.K.

*farrel.gray@imperial.ac.uk [+]e.boek@qmul.ac.uk

Abstract

We simulate two sets of dissolution experiments in which CO_2-saturated solutions are injected into calcite formations. We explore the impact of non-linear reaction kinetics and charge-coupled ion transport in systems representing different levels of flow and mineralogical complexity. First, we flow CO_2-saturated water and brine through cylindrical channels drilled through solid calcite cores and compare directly with experimental dissolution rates. We find that simulations using a linear saturation model match experimental results much better than the batch-reactor-derived non-linear saturation model. The use of a coupled diffusion model causes only a very small increase in the overall dissolution rate compared to a single diffusion coefficient, due to the increase in transport rates of reaction products, particularly the highly charged Ca^{2+} ion. We also determine the relative importance of the two calcite dissolution pathways, with H^+ and H_2CO_3, and conclude that the H_2CO_3 – calcite reaction is by far the more dominant, in contrast with common assumptions in the literature. Then, we compare to the experiments of Menke et al. (2015) in which CO_2-saturated brine was injected into a microporous Ketton carbonate, and compare dissolution rates over time. We find that including non-linear saturation behaviour markedly changes the simulated dissolution rate, by up to a factor of 0.7 in the case of the experimentally derived saturation model of Anabaraonye et al. (2018), however neither case matches the experimental result which is several times slower than the simulation. Including the effects of coupled ion transport lead to virtually no change in overall dissolution rate due to the convection dominated behaviour. The model also shows differences in the trend of the dissolution rate over time observed in Menke et al, with an approximately linear relationship with time compared to the experimental square-root dependence on time. We conclude that the geochemical model may need to include other effects such as dissolution inside microporous regions.

1 Introduction

A better understanding of the detailed dissolution mechanisms in carbonate rock by CO_2 – brine systems is of great fundamental and applied interest. Applications include field scale operations in carbonate reservoirs such as CO_2 sequestration (Molins 2012), where the acid is formed by dissolution of the injected CO_2 in the brine present in the reservoir; and matrix acidizing for hydrocarbon recovery (McLeod 1984, Fredd and Fogler 1998), where the acid is injected directly into the formation to increase permeability and reservoir productivity.

Recently, a number of detailed pore scale investigations have been reported on the dissolution of carbonate rocks by acidic solutions. These include micro-CT imaging studies by Qajar and Arns (Qajar J 2012) and image based modelling studies by Nunes *et al*. (Pereira Nunes, Blunt et al. 2016). In particular, we mention the micro-CT imaging paper by Menke *et al*. (Menke, Bijeljic et al. 2015) in which CO_2-saturated brine was injected into a microporous Ketton carbonate, and full time-dependent dissolution was resolved. Dissolution of carbonate minerals is a complex process encompassing the interaction between transport and chemical reaction processes in porous media.

Indeed, accurate modelling of calcite dissolution at the pore scale, including the complex feedback between flow and surface chemistry, requires detailed verification of the modelling framework used. Before considering complex diffusion and chemical reaction mechanisms in complex 3D porous media, it is recommended to carry out detailed verifications that the code is working properly, in particular regarding moving fluid and solid boundaries. Molins *et al.* (Molins, Soulaine et al. 2020) reviewed and proposed a benchmark problem set of test cases for the simulation of mineral dissolution at the pore scale with evolving fluid-solid interfaces. In a previous paper (Gray, Cen et al. 2016), we carried out a detailed verification study of our modelling framework, including diffusion, mesh convergence and concentration fields in flow past a single sphere in a channel. In addition, we introduced and verified the surface rescaling method used in our current manuscript. These verifications are similar to some of the test cases proposed by (Molins, Soulaine et al. 2020). We include a comparison with one of their benchmark cases in the present work. As further validation, we simulated the geochemical system of (Molins, Trebotich et al. 2014) using their micro-CT data set. Our model gave close agreement to their simulated dissolution rates. Results will be discussed in more detail in future work.

Furthermore, the experimental framework has to be verified before considering the full complexity of diffusion and chemical reaction mechanisms in complex 3D porous media. As an example verification we note the microfluidic experiments of a calcite crystal dissolving in a microchannel (Soulaine, Roman et al. 2017). Inspired by this study, in a previous paper we carried out a validation study to examine dissolution in a 1 mm diameter cylindrical channel drilled through a solid calcite crystal, using a combination of micro-fluidic experiments and simulations (Gray, Anabaraonye et al. 2018). In addition, very recently calcite cylinder

dissolution experiments similar to our current work (see section 4.1) were reported by (Agrawal, Raoof et al. 2020). Regarding reaction kinetics, (Noiriel, Steefel et al. 2012) studied calcite precipitation rates in porous media and found nearly linear dependence of the rates on supersaturation, which could not be attributed to a diffusion control..

In our previous paper (Gray, Anabaraonye et al. 2018), we also discussed the chemical mechanisms of dissolution of calcite by HCl in porous media, using a combination of computer simulations and experiments. Here we extend these studies to CO_2-brine systems.

The main aims of this paper are to examine the influence of the following effects on the dissolution process: a) charge coupled diffusion, b) non-linear reaction kinetics and c) the controlling dissolution reaction pathway. We will discuss each of these aims in the following sections.

As discussed in our earlier paper (Gray, Anabaraonye et al. 2018), the diffusion of charged species in electrolytes is controlled by the Nernst-Planck-Arrhenius equations (Vinograd and McBain 1941). This has led to the development of multi-component diffusion models, including charge-coupling effects on ion diffusion rates (Steefel and Maher 2009), which have been used to interpret multi-component diffusion effects in bulk solutions (Maher, Steefel et al. 2006) and porous media (Giambalvo, Steefel et al. 2002) (Appelo and Wersin 2007). To the best of our knowledge, only a few papers in the literature have extended this effect to reactive flow models. In the majority of research papers on this topic, a single diffusion coefficient is used for all species (Yoon, Valocchi et al. 2012, Yoon, Kang et al. 2015, Gao, Xing et al. 2017, Liu and Mostaghimi 2017, Liu and Mostaghimi 2018). This maintains electro-neutrality, but does not capture electrochemical migration effects. In a few cases, however, multicomponent diffusion effects have been included alongside chemical reactions. In particular, Muniruzzaman and Rolle (Muniruzzaman and Rolle 2016) used a multicomponent ionic transport model coupled to a geochemical reaction network to investigate dispersion in 2D systems at the core-scale. Recently, Sprocati et al. (Sprocati 2019) extended this to core-scale modelling of electrokinetic reactive transport processes in saturated porous media. They emphasized the importance of Coulombic interactions in electrokinetic applications using a variety of benchmark tests. Their reactive transport model was compared with PHREEQC (Steefel, Appelo et al. 2015) simulation data, including surface complexation reactions, but not directly with reactive transport experiments. In the case of pore-scale simulation studies in the literature, Ovaysi and Piri (Ovaysi and Piri 2014) included a multicomponent diffusion term in their particle-based reaction model, as did Li *et al*. (Li 2008) in their study of flow past a dissolving calcite surface. In our earlier paper (Gray, Anabaraonye et al. 2018) we observed that, for dissolution of calcite by HCl, it was important to include the effect of charge coupled diffusion. Here we will investigate if the same is true for dissolution of calcite by CO_2-water/brine solution, using a direct comparison of new experimental data and our reactive transport model including charge-coupling effects.

Regarding the effect of reaction kinetics on dissolution mechanisms, the majority of papers in the literature use simple linear saturation models. For example, Ovaysi and Piri (Ovaysi and Piri 2014) simulated a reactive flow experiment in a microfluidic channel performed by Li *et al*. (Li 2008) and found good agreement for the Ca^{2+} concentration as a function of flow rate.

Recent batch reactor studies, however, suggest that reaction kinetics close to equilibrium may become non-linear due to a switch in dissolution mechanism related to the surface properties of the underlying crystal. In particular, Anabaraonye *et al*. (Anabaraonye 2017) found dissolution kinetics of calcite to be highly non-linear in batch reactor studies, where a single calcite crystal surface was exposed to dissolution. As shown in Figure 1, they observed a substantially faster reduction in reaction rate with increasing saturation state for the non-linear model compared to the linear model. In our previous paper on dissolution of calcite by HCl (Gray, Anabaraonye et al. 2018), the saturation term was unimportant as the reactions were far from equilibrium. In the current work on CO_2 -saturated solutions however, the chemical conditions are closer to equilibrium and therefore we expect the saturation term to have a strong influence on the overall dissolution rate.

Finally, we explore the details of the controlling reaction pathway for dissolution. The dissolution of calcite by carbonic acidic solutions is usually described in terms of two main reaction pathways:

$$CaCO_3 + H^+ \leftrightarrows Ca^{2+} + HCO_3^- \quad (1)$$

$$CaCO_3 + H_2CO_3 \leftrightarrows Ca^{2+} + 2HCO_3^- \quad (2)$$

Many papers in the literature on this topic assume reaction (1) to be dominant, and state that the overall dissolution can be expressed solely by this pathway (Pereira Nunes, Blunt et al. 2016, Gao, Xing et al. 2017, Tian and Wang 2018). Here we examine this assumption and hypothesize that the H^+ concentration near the reactive surface may well be substantially lower than in the inlet solution, causing reaction (2) to make an important contribution. In the below, we directly compute the relative influence of the two pathways using the concentration fields of the relevant chemical species. This allows us to establish which of the two reaction pathways (1) and (2) is most important. To the best of our knowledge, this has not yet been reported in the literature.

Then we consider recent micro-CT imaging experiments, in which CO_2-saturated brine was injected into a micro-porous Ketton carbonate (Menke, Bijeljic et al. 2015), as an example of a more complex porous medium. We use these imaging data to calculate the experimental amount of calcite dissolved as a function of time. This is compared directly, using the same time lapse image series, with our dissolution simulations. The model used here only considers dissolution at the grain surfaces. In a recent experimental study of micro-porous carbonate limestone dissolution by Singh *et al.*(Singh, Anabaraonye et al. 2018), evidence is presented that dissolution reactions are mainly occurring in the micro-pores, not at the surface of the carbonate rock samples. Such dissolution processes involving micro-porosity are not yet fully

understood, and modelling efforts may need to take into account these micro-pore effects too.

1.1 Geochemical Model

We consider the dissolution of calcite by carbonic acidic solutions as described by the two main reaction pathways, defined in reactions (1) and (2) above. The total dissolution rate is generally described by a linear reaction model in far-from-equilibrium conditions given by: $R = -A\alpha_{H^+}k_1 - A\alpha_{H_2CO_3}k_2$, where R is the dissolution rate in mol s^{-1}, A is the surface area in m^2, α_x is the activity of given species x, and $k_1 = 2.5 \times 10^{-4}\mathrm{ms}^{-1}$ and $k_2 = 5.5 \times 10^{-7}\mathrm{ms}^{-1}$ are the reaction rate constants of the reactions (1) and (2) respectively at 50C (Peng, Crawshaw et al. 2015).

The dissolution kinetics of calcite has been found to be highly non-linear in batch reactor studies, where a single calcite crystal surface was exposed to dissolution (Molins 2012, Peng, Crawshaw et al. 2015). According to the model of Anabaraonye et al. (Anabaraonye 2017), the non-linear behaviour can be described by a single fitted exponent of the form

$$R = -(A\alpha_{H^+}k_1 + A\alpha_{H_2CO_3}k_2)\left[1 - \frac{Q}{K}\right]^p \tag{3}$$

Here, Q is the solubility product, defined in terms of the ratio of products to reactants

$$Q = \frac{\alpha_{Ca^{2+}} \cdot \alpha_{HCO_3^-}}{\alpha_{H^+}} \tag{4}$$

$K = 27.07$ is the equilibrium constant and the exponent $p = 7.76$ (Anabaraonye 2017). Q/K is the saturation index and $[1 - Q/K]^p$ is the saturation term. The behaviour of this non-linear saturation model is shown in Figure 1, and shows a substantially greater reduction in the saturation term, and therefore in reaction rate, with increasing saturation state compared to the linear model.

During the formation of carbonic acid, CO_2 quickly dissolves into solution to produce aqueous H_2CO_3. This then produces the acid species H^+ through the equilibrium reactions:

$$H_2CO_3 \leftrightarrows H^+ + HCO_3^- \tag{5}$$

$$HCO_3^- \leftrightarrows H^+ + CO_3^{2-} \tag{6}$$

The additional contribution through the dissociation of water $H_2O \leftrightarrows H^+ + OH^-$ can be ignored at low enough pH, such as are considered here.

2 Simulation Model

The systems considered are investigated using a high resolution pore-scale reactive flow model (Gray, Anabaraonye et al. 2018). The flow-field inside the domain is computed using the multi-relaxation-time lattice Boltzmann model (Gray and Boek 2016) and chemical

transport is performed using an explicit second order flux-limiter scheme (Gray, Cen et al. 2016). Fluid chemical equilibrium reactions were computed to steady-state at each time-step using a Newton-Raphson solver, and heterogeneous reactions at mineral surfaces were performed using a 4th order accurate numerical integration step (Gray, Anabaraonye et al. 2018). Surface area was determined for heterogeneous reactions from the Cartesian grid surface by locally interpolating parabolic surface elements. The projection of the grid block surface onto the smooth element is then used to estimate the true area represented by the exposed grid surface (Gray, Cen et al. 2016).

The effects of charge coupling on ion diffusion rates was included by incorporating an extra electrochemical term into the diffusive flux (Steefel and Maher 2009).

$$J_j = -D_j \frac{\partial C_j}{\partial x} + \frac{z_j D_j C_j}{\sum_k z_k^2 D_k C_k} \sum_k z_k D_k \frac{\partial C_k}{\partial x} \tag{7}$$

where J_j is the diffusive flux for each species j, C_j is the species concentration, z_j the ionic charge and D_j are the self-diffusion coefficients.

To demonstrate the effect of this term, a system of Ca^{2+} and HCO_3^- ions in a 1 : 2 ratio was simulated. The mixture was initialised as a point source at the origin with initial concentrations of 1 x 10^{-4} [mol L^{-1}] and 2 x 10^{-4} [mol L^{-1}] respectively, and allowed to diffuse for 1.03 s. The resulting distributions are shown in Figure 2a (solid lines). The literature values for the self-diffusion coefficients of these ions were found to be 1.406 x 10^{-9} m^2s^{-1} [6] and 2.104 x 10^{-9} m^2s^{-1} [7] respectively. However, due to the charge coupling effect, we observe that both ions actually diffuse at the same rate, as is required to conserve electroneutrality in the solution. In this case, the distributions of both ions are Gaussian and their effective diffusion coefficient is 1.805 x 10^{-9} m^2s^{-1}. This was computed as half the rate of change of the variance σ_i^2 in the concentration distributions for each species i, namely

$$D_i^{Eff} = \frac{1}{2}\frac{d\sigma_i^2}{dt} \tag{8}$$

A second calculation is also shown in Figure 2a (dashed lines) in which the same point source of ions was allowed to diffuse in a background mixture of 0.855 M NaCl brine. In this case, electrochemical migration effects are observed. The ions now diffuse at different rates, which are in fact equal to (or indistinguishable from at the resolution of simulation) their self-diffusion coefficients. The reason for this is that the Na^+ and Cl^- ions in the background brine can also migrate, as shown in Figure 2b where small perturbations from the initial 0.855 mol. dm^{-3} solution concentration are apparent. Li *et al.* (Li 2008) performed similar experiments but found rates that were considerably lower for water without NaCl. They noted that an explanation might have been a slower rate of diffusion from the pore wall to the center of the pore caused by smaller gradient in chemical potential in pure water compared to a 10 mM NaCl solution. In the saturated CO_2-brine systems used in this work, the activity coefficients for the chemical species will be almost entirely determined by the background

NaCl concentration, and therefore gradients in chemical activities are unlikely to be significant.

With more complex mixtures of ions, individual species can diffuse at different rates, whilst still maintaining electroneutrality, and their behaviour is not necessarily Gaussian. An example of this is shown in Figure 2c, which consists of an initial mixture of H^+ (0.0167 mol.dm^{-3}), Cl^-(0.05 mol.dm^{-3}) and Ca^{2+} (0.0167 mol.dm^{-3}) ions. Such a system is applicable to the case of 0.05 mol.dm^{-3} HCl being injected into a calcite ($CaCO_3$) system, for example the calcite cylinder validation example in Gray et al. (Gray, Anabaraonye et al. 2018). Here we assume that 1/3 of the initial H^+ has reacted with calcite to produce corresponding amounts of Ca^{2+} and HCO_3^- ions. Then, due to the equilibrium reaction (5), almost all of the HCO_3^- has then reacted with remaining H^+ to produce H_2CO_3. Since HCO_3^- now exists only in trace amounts, and H_2CO_3 is uncharged and thus unaffected by (7), these components are neglected. Once again, the mixture was initialised as a point source and allowed to diffuse for 1.03 s. The ions in this case once again diffuse at different rates, whilst maintaining electroneutrality, however it is clear from Figure 2c that the distribution of H^+ is highly non-Gaussian. The effective dispersivity was again computed using (8), and gave $D_{H^+}^{Eff}$ = 8.415 x 10^{-9} m^{2}s^{-1}, $D_{Ca^{2+}}^{Eff}$ = 1.705 x 10^{-9} m^{2}s^{-1} and $D_{Cl^-}^{Eff}$ = 3.942 x 10^{-9} m^{2}s^{-1}. By comparison, if equal amounts of H^+ and Cl^- diffuse together without any Ca^{2+} ions, they maintain a Gaussian distribution with an effective diffusion coefficient of 5.922 x 10^{-9} m^{2}s^{-1}. It is therefore interesting to note how the addition of product ions from the surface reactions allows the H^+ ion to diffuse much faster than in the initial HCl solution. This would explain why using a constant diffusion coefficient in the cylinder example in Gray et al. (Gray, Anabaraonye et al. 2018) lead to a considerably slower overall dissolution rate than when the coupled diffusion model was used. With the coupled model, the transport rate of H^+ ions to the reactive surface was increased further down the system as product ions built up from surface reactions. We would like to point out that the value of the HCl diffusion coefficient used in Gray et al. (Gray, Anabaraonye et al. 2018) of 5.6 x 10^{-9} m^{2}s^{-1} was obtained using the value from Lobo et al. (Lobo, Helena et al. 1979) at 298 K and adjusted to 323 K using the Stokes-Einstein relation. The reference for this value was not given in (Gray, Anabaraonye et al. 2018), so we are pleased to give the authors due credit here. Finally, we note that this experimentally derived value is around 6% lower than the simulated value here. This could be due the omission of electrophoretic effects (charge-cloud deformation) in the coupled diffusion model. In the reactive flow simulations described in this work, the constant diffusion model will treat all components as having the same diffusion coefficient of 1.805 x 10^{-9} m^{2}s^{-1}, equal to the combined diffusion rate of Ca^{2+} and HCO_3^-. We used the Nernst–Planck equation for fully coupled ion transport in the rest of this paper, for every grid cell and every time step. The implementation has been validated in (Gray, Anabaraonye et al. 2018) and explained in detail in Appendix 1 of this paper.

Geochemical convergence conditions were measured by the change in the average and standard deviation of chemical concentrations in the sample. For all calculations performed, fractional changes of less than 10^{-6} per time-step in both these quantities was considered steady-state. Both flow and transport models were implemented for GPUs, and used a 3-dimensional domain decomposition, which was periodically adjusted to maintain a balanced number of fluid nodes over processors as the geometry was altered during dissolution. Calculations were performed using either 8 Tesla P100 GPUs, or a heterogeneous cluster comprising 24 Tesla K40 and 24 Tesla K80 GPUs connected with FDR Infiniband.

2.1 Verification of the moving solid-liquid interface model

Here we provide a validation of our algorithm to describe the dynamics of the calcite-solution interface, which is moving as a consequence of the reactive flow process. We compare our results for a benchmark case, provided by (Molins, Soulaine et al. 2020) in Part II of their paper, directly with the results obtained from various alternative simulation methods. This concerns the simulation of flow and reactive transport in a 2D rectangular domain, with dissolution occurring on the surface of a circular calcite grain placed in the centre, due to the inflow of an HCl solution with pH=2. Only the reaction with calcite and H^+(1) is considered, neglecting fluid equilibrium reactions and saturation behaviour. Detailed information regarding the geometry and parameters used for this benchmark case are provided in Fig. 2 and Table 2 in (Molins, Soulaine et al. 2020). We conduct our simulations in a 3D domain with dimensions of 200 x 110 x 5 lattice units in X, Y and Z directions respectively, where the flow direction is in X, and the channel width in Y. Loop boundary conditions are applied in Z to both flow and transport so that the problem is equivalent to 2D. The Y direction includes solid boundaries of 5 voxels width either side of the channel, so that the flowing region of the channel is 100 lattice units wide, with a resolution of 5 micron. A fluid injection rate of 0.9μLmin^{-1} was imposed at the inlet face, equivalent to an average injection velocity of 0.12 cms^{-1} as specified for the benchmark case. Due to the dissolution process, both the volume and area of the calcite grain are expected to diminish with time. The results of our calculations, confirm this expectation and are presented in Figure 3~~Figure 3~~ a) and b). Our results were obtained up to full dissolution and show good agreement with the other simulation codes. In addition, we observe that the average dissolution rate increases with time, in good agreement with other simulation results, see Figure 3~~Figure 3~~ c). This is because the area of the grain decreases more rapidly than the effluent concentration due to grain dissolution / shrinkage.

We expect that the flow field imposed leads to breaking of the fore-aft symmetry in the concentration field. Indeed this is observed in our simulations, as shown in Figure 4~~Figure 4~~, in agreement with (Molins, Soulaine et al. 2020). Therefore we expect that most of the dissolution will occur on the leading (upstream) edge while the downstream point is expected to move much less. Indeed this can be observed from our simulation results, as shown in Figure 4~~Figure 4~~.

In summary, we observe good agreement between our results and those obtained using alternative simulation methods. We confirm that our approach can simulate the benchmark problem accurately with our specific strategy for time stepping and process coupling.

3 Experiments

3.1 Calcite Cylinders

The calcite cylinder experiments were prepared by first drilling a 3mm hole through a solid calcite core. Matching steel inlet pieces were pushed against each end, and the arrangement placed inside a Viton sleeve. Injection was performed at 5 MPa pressure, with an applied confining pressure of 6 MPa. The core holder was heated to a temperature of 50°C. Two CO_2-saturated solutions were used, one consisting of deionised water as the solvent, and the other containing 5% by weight NaCl brine. Both solutions were equilibrated with CO_2 at 5 MPa and 50°C so that saturation was reached. Injection was performed at a number of different flow rates and resulting mass dissolution was determined by the weight change of the channels. Four sets of experiments were performed using CO_2-water, varying the length of the channel, diameter of the channel and flow rate. The experiments were also run for different times. These parameters are given in Table 2. A further two experiments were run using CO_2-saturated brine with 5% by weight NaCl, parameters for which are given in Table 3. Other parameters, such as temperature and pressure were not changed between experiments. The corresponding simulation domains were generated digitally, and included an extra inlet region 3mm in length and of the same diameter as the calcite channel, considered to be non-reactive. This was to ensure that the simulation could resolve any concentration gradients which might form before the reactive channel.

3.2 Ketton Carbonate

We consider recent micro-CT experiments by Menke *et al.* (Menke, Bijeljic et al. 2015), where a Ketton carbonate rock core was injected with CO_2-saturated brine (5% NaCl, 1% KCl by weight) at 50 °C and 10MPa, while tomographic images were taken at 15 min intervals with a 3.8 µm spatial resolution. Ketton is a >99% calcite Limestone Oolite, which has a bimodal pore structure, as witnessed by mercury intrusion experiments (Menke, Reynolds et al. 2018) . In the dissolution experiment, the reactor fluid was flowed through the core at a constant flow rate of 0.5 mL/min, corresponding to a Darcy velocity of 6.6×10^{-4} ms^{-1}. The transport properties were characterised by the Peclet number, defined as

$$Pe = \frac{U_{av} L}{D}$$

where U_{av} is the average pore velocity, defined as Darcy velocity divided by porosity. The porosity increased from 0.17 to 0.32 [-] over the course of the experiment. L is a characteristic length scale, and is chosen to be 100µm, the order of a typical pore-size. The resulting Peclet number is around $Pe \sim 50$, indicating that the transport is strongly convection dominated.

4 Results

4.1 Calcite Channels

Figure 6~~Figure 6~~ shows a comparison of simulated results with experiments for two cases: C1 (CO_2-water) and C5 (CO_2-brine). Simulations in this case included the time-dependent changes of the mineral boundaries due to the surface reactions over the full experimental time-scale. Since the simulated dissolution rate shows virtually no change over time, we assume that changes in the cylindrical geometry had a negligible effect on the dissolution rate over the time-scale they were run. The mean dissolution rate was computed as the amount of dissolved solid per unit of time, in units of (mol / hr). To match the experimental conditions, the injection condition used in the simulation was a constant flow rate of 0.5 mL / min (Menke, Bijeljic et al. 2015).

Both linear ($p = 1$) and non-linear ($p = 7.76$) saturation terms are compared. Interestingly, in both cases simulations using the linear saturation model agree closely with the experiment, whereas the non-linear model gives dissolution rates approximately 40% lower. Results for all experiments are shown in Figure 7 with simulation results using both the linear and non-linear dissolution models. In almost all cases, the linear model gives much better agreement than the non-linear model derived from batch reactor experiments. This appears to be the case both for systems with CO_2-water injected and CO_2-brine injected. For example, experiments C1 and C2 (CO_2-water) correspond closely to experiments C5 and C6 (CO_2-brine) respectively, except for different run times. However in these cases, the dissolution rate is well predicted by the linear model, and in comparable disagreement with the non-linear model.

In order to better understand the effect of the saturation model exponent on the dissolution rate, a number of simulations were performed with exponents ranging from 1 (linear) to 7.76 (the experimentally derived non-linear model). These are shown in Figure 8 for the experiments C1 (CO_2-water) and C5 (CO_2-brine), with the experimental dissolution rate shown for reference. The simulated dissolution rate decreases as a function of the exponent and in both cases the resulting overall dissolution rate with the $p = 7.76$ non-linear model is approximately 2/3 the rate of the linear model. However in both cases, the linear model results in the best match for the experimental dissolution rate.

Next we consider the effects of charge-coupled diffusion, compared to using a single diffusion coefficient for all species. Simulations were performed for the experiment C5 with both coupled and constant diffusion models, and using both the linear and non-linear saturation models. These are shown in Figure 9. For both cases of saturation model, the coupled diffusion models resulted in only a slight increase in overall reaction rate compared to the case of a single, constant diffusion coefficient.

The reaction mechanisms can be understood by considering the distribution of chemical species in the system. Cutaways of the experiment C1 using the non-linear saturation model are shown in Figure 10 for the H^+, Ca^{2+} and HCO_3^- species. The H^+ concentration drops by

more than an order of magnitude from its initial solution concentration value to that on the mineral surface, the pH ranging from 3.1 to 4.6.

The surface concentrations of these chemical species, and the surface pH are shown in Figure 11a and b. These values are averaged over the cross-section of the channel, and shown as a function of position from the inlet. The pH on the mineral surface is lower than in the initial solution by 1.5 units, corresponding to more than an order of magnitude in concentration. This is because of the large amounts of HCO_3^- produced during the surface reaction affecting the equiliubrium (9). The concentration of H_2CO_3 remains close to its initial solution value. These measures can be used to determine the relative balance of the dissolution reactions (1) and (2). In Figure 11c, the ratio $k_1\langle\alpha_{H^+}\rangle/k_2\langle\alpha_{H_2CO_3}\rangle$ is shown, where $\langle\alpha_{H^+}\rangle$ is the mean activity of H^+ averaged over the channel cross-section, and correspondingly for $\langle\alpha_{H_2CO_3}\rangle$. It is clear that the mineral dissolution is overwhelmingly caused by the direct reaction of calcite with H_2CO_3, with only 1.3 – 1.8% caused by the reaction with H^+. Finally, the behaviour of the non-linear saturation term $[1 - Q/K]^p$ is shown in Figure 11d, with the saturation index Q / K. As product ions build up along the length of the system, the value of the saturation term drops from 0.4 to around 0.05. This effectively reduces the mineral dissolution reaction rates by the same factor, and explains the sensitivity of the overall dissolution rate to the saturation term exponent seen in Figure 8.

4.2 Ketton Carbonate

The initial geometry of the Ketton carbonate sample is shown in Figure 12, along with the initial velocity field computed with the lattice Boltzmann model. In the experimental work of Menke et al. (Menke, Bijeljic et al. 2015) a 3.5mm subregion, located 2mm from the inlet of the sample was imaged and analysed. To replicate this here, we took the same initial 3.5mm sample image, and mirrored the first 2mm of it backwards. The 2 mm region was added to reproduce the experiment more accurately. Although it may not exactly match the experimental sample structure, it should still be more realistic than not having it at all. We note that previous simulation papers *e.g.* (Mostaghimi, Liu et al. 2016) did not consider this missing bit of rock sample. The importance of including the 2mm region is evidenced by Fig 13, where strong changes in the concentration profiles are observed. For heterogeneous rock structures in particular, this procedure may not guarantee that the profile will be fully consistent with the experiments. Indeed, mirroring the sample may influence the results, as reported by (Guibert, Nazarova et al. 2015) and (Guibert, Horgue et al. 2016), including the possibility of changing the structure heterogeneity, removing the anisotropy of the domain and redistributing the streamlines. However, since Ketton is very homogeneous, the mirroring is likely to be a good approximation in this case. Injection of the CO_2-saturated brine solution was then simulated, and resulting mass changes quantified only in the 3.5mm subvolume and compared to experiment.

This comparison is made in Figure 13 and shows marked differences between simulated and experimental results. Both saturation models show a virtually linear dependence on the calcite mass dissolved with time, however the experimental dissolution rate decreases considerably.

The chemical system through the pore-space can be analysed in the simulation, and the concentrations of the three species H^+ (and pH), H_2CO_3 and Ca^{2+} are shown in the Ketton geometry at initial steady-state for the linear saturation model in Figure 16. This figure includes the extra 2mm inlet region in front of the 3.5mm subvolume. The H_2CO_3 distribution is almost entirely uniform throughout, owing to the low reaction rate constant of the direct H_2CO_3 – calcite reaction (2).The convective Damköhler number for this reaction $Da_C = k_2/U_{av} = 0.8 \times 10^{-3}$ while the diffusive Damköhler number $Da_D = k_2\, L/D_{H_2CO_3} = 1.5 \times 10^{-2}$. Both values are well below unity, which means we are in the reaction-limited regime. This explains the uniform concentration of H_2CO_3. The H^+ concentration on the other hand decreases sharply from the inlet equilibrium value due to buffering reaction with HCO_3^- (5) as discussed for the case of the calcite cylinders.

5 Discussion

5.1 Calcite Channels

It was interesting to note both charge-coupled and constant diffusion models give very similar results (Figure 9). This contrasts with the HCl case (Gray, Anabaraonye et al. 2018) where the coupled diffusion processes enhanced the transport of the H^+ ion as shown in Figure 2c. This resulted in a considerably higher overall dissolution rate than the case of a single diffusion coefficient. For the case of the CO_2-saturated solutions considered here, the transport of H^+ has little influence on the overall reaction rate. Instead the transport of products away from the reactive surface, affecting the local reaction rate according to the saturation term (10) is the main control on the overall dissolution rate. These slower-diffusing ions are less affected by the charge coupling, as shown in Figure 2.

In section 4.1, cutaways of the experiment C1 using the non-linear saturation model were presented in Figure 10 for the H^+, Ca^{2+} and HCO_3^- species. This figure revealed that the H^+ concentration drops by more than an order of magnitude from its initial solution concentration value to that on the mineral surface, the pH ranging from 3.1 to 4.6. Here we discuss this observation in more detail. The product species Ca^{2+} and HCO_3^- are produced on the reactive surface and diffuse into the flow-stream. These quantities are plotted along the length of the channel in Figure 11 a) and b). The behaviour of the H^+ looks similar to that of a transport-controlled reaction – an initial inlet concentration is transported along the system, and diffuses to the mineral surface where it is consumed. The flow and diffusion rates therefore control the overall dissolution rate. However, this is not the case for this particular system. Instead, the variation in H^+ distribution is determined by the local equilibrium

reactions (11) and (12). The diffusion rate of the H^+ ion itself has little effect on this boundary layer, and hence including charge-coupled diffusion effects made little difference to the simulated dissolution rates. This can be further justified by noting that the initial H^+ concentration in solution arises from the dissociation of CO_2, and is determined by the balance of H_2CO_3 and HCO_3^-, the reaction equilibrium constant, and to an extent the concentration of other chemical species through the activity coefficients. From the results of our simulations, we argue that that such a slow-down cannot be explained in terms of the reduction in surface area or change in residence time of chemical species. Note that both reduction of surface area and increase in residence time of the chemical species have been validated and correctly included in our simulation models. Our model has been extensively validated, including dissolution rates presented in (Molins, Trebotich et al. 2014).

The reactions (13) and (14) are fast enough to be considered instantaneous (Langmuir 1997) and since the concentrations of H_2CO_3 and HCO_3^- are higher than that of H^+ near the reactive surfaces by orders of magnitude, it is the former species' concentrations that are the primary controls on surface pH.

5.2 Ketton Carbonate

The main observation from the comparison with experimental results for the Ketton carbonate was the highly distinct behaviour of the overall dissolution rate with time (Figure 13). Such a decrease with time would ordinarily be explained by the surface area of the grains decreasing, with a corresponding effect on the surface reaction rate. Additionally, as the pore space increases, average fluid velocities will tend to slow down leading to longer residence times for products which would affect the reaction rate through the saturation term. However, both of these effects were captured in the simulation, but this trend was not replicated. The dissolution rate for the simulations and experimental data are shown in Figure 14. Simulated rates remain fairly constant, though the non-linear saturation model does show approximately 10% decrease in reaction rate over the course of the calculation. In this case, the simulation was continued until around 80% more mass was dissolved than in the experiment in an attempt to see if such a slow-down in disssolution rate occurred at greater reaction extents. The experimental dissolution rate on the other hand is approximately 3x lower at the end of the experiment than at the beginning. When the experimental mass dissolved is plotted against square-root time, as in Figure 15, it shows an almost ideal linear relationship, with the exception of the first point. This behaviour is usually more indicative of a diffusive process than of convection-dominated dissolution like this system where the Peclet number is around 50. In recent work, it was shown that dissolution can occur inside the grains in Ketton carbonate when CO_2-saturated brine solution is injected (Singh, Anabaraonye et al. 2018). Grain boundaries were seen to remain almost static, but the density of the grains themselves decrease from outside in due to the gradual diffusion of reactants and products through the micro-pores. In Menke et al., it was noted that solid grain densities

did not appear to have changed during the coarse of the experiment, and thus it was concluded that dissolution was not occuring inside the grain micro-pores. 3 To investigate further the possibility of diffusion inside micro-pores playing a role, the simulations may need to include transport and reactive processes inside micropores to accurately model these experimental systems.

In their simulations comparing with the same experiment, Nunes et al. (Pereira Nunes, Blunt et al. 2016) made the assumption that the pH could be considered uniform throughout the sample, and the H_2CO_3 – calcite reaction could be neglected. We observe that the pH is between 1 and 2 units lower in most of the sample than at the inlet, and that the H_2CO_3 – calcite reaction dominates. We are unable to reproduce their reported agreement with experiment. Other modelling work which assumed that H^+ - calcite dissolution pathway (1) was dominant appeared to include the reaction (2) in their dissolution rate term (namely $-A\alpha_{H_2CO_3}k_2$) in (3), however H_2CO_3 species was not included in the chemical transport model, but instead treated as constant everywhere (Gao, Xing et al. 2017). Since the distribution of this component does tend to become uniform, (Figure 16c), this probably still leads to correct results. Nonetheless, the assumption of the dissolution processes being dominated by the acid reaction (1) is not correct, according to our analysis.

Finally we note that sets of simulations were performed using both constant and coupled diffusion models, however these gave results which were almost indistinguishable. This is most likely due to the effect of coupled diffusion processes on the product ions (Ca^{2+} and HCO_3^-) being small, as well as the transport processes being convection-dominated. The influence of the more strongly-affected H^+ ion on the resulting overall dissolution rate was also comparably small, as discussed for the case of the calcite cylinders.

6 Conclusion

We explored the influence of non-linear reaction kinetics and charge-coupled diffusion on the dissolution of calcite by CO_2-saturated solution using simulation and comparing to corresponding experimental data.

We found that for the case of the simple calcite cylinder system, the experimental dissolution rates were well predicted using a linear saturation model. Interestingly, using the non-linear saturation model derived from batch-reactor experiments, the simulations significantly under-predicted the experimental dissolution rates in most cases, both for CO_2-water and CO_2-brine systems. This is particularly important for these chemical systems as the dissolution rates were shown to be strongly dependent on the state of the saturation term. One possible explanation is that the batch reactor experiments used a smoothly cut calcite surface, exposing a single crystal lattice direction whereas, for the calcite cylinder systems used here, the comparably rough surfaces expose many different crystal orientations. The charge-coupled diffusion model by contrast had little effect on the overall dissolution rate compared to using a single diffusion coefficient for all species. This too was interesting when compared

to the case of HCl-calcite dissolution in other work where it had a much greater influence. The reasons for this were understood to be because of the very limited influence of the H^+ ion on the dissolution processes in the saturated CO_2 system, contrasting with the strongly H^+-transport-controlled mechanisms for HCl. Additionally, since calcite dissolution in the saturated CO_2 system is overwhelmingly caused by the direct reaction with hydrated CO_2 (H_2CO_3) which is uncharged, and tends to spread uniformly throughout the reactive system, this component will be largely unaffected by coupled diffusion processes. It is worth noting that there is second term which can be included in the coupled diffusion model (7) which includes gradients in activity coefficients (Steefel and Maher 2009). We neglected this here mainly because in solutions with concentrated brine, gradients in activity coefficients will be very small, however it could have an effect on the transport of product ions near reactive boundaries in the CO_2-water cases. It may be of interest to quantify this in future work.

We then applied the model to dissolution in Ketton carbonate in comparison with corresponding experimental data. We found that the simulations could not match the experimental dissolution rate and trend, instead overpredicting the dissolution rate by 2 to 7x, depending on the choice of saturation model and dissolution extent. Of particular note was the correlation of dissolution rate with time. Despite continuing the dissolution to a greater extent than the experiment, our simulations did not observe a dramatic slow-down in dissolution rate seen in the experiment. The two candidate mechanisms for such a reduction in dissolution rate, namely the decrease in reactive surface area over time and increase in product residence time were both included in the simulation. The almost ideal correlation of the experimental calcite dissolution rate with square-root-time may hint at the influence of diffusive processes within the micropores. Examples of this behaviour have been seen before in Ketton carbonate (Singh, Anabaraonye et al. 2018), and suggest that modelling efforts may need to include dissolution inside microporous grains as well as the surrounding macropores to accurately predict this behaviour. Indeed, we would suggest a partial-bounceback LB method, such as developed by (Walsh, Burwinkle et al. 2009) and analysed in detail by (Ginzburg 2016), which incorporates the permeability of the micro-porous regions as a model parameter. Rather than using lattice nodes that are either solid or fluid, this approach uses a probabilistic model, where lattice node properties are varied to reflect the local permeability of the material. Such a method could account for dissolution in the micro-porosity, assuming that the degree of dissolution of the micro-porous regions is reflected by the gray scale of the micro-CT image.

Acknowledgements

We gratefully acknowledge funding from the Qatar Carbonates and Carbon Storage Research Centre (QCCSRC), provided jointly by Qatar Petroleum, Shell, and Qatar Science and Technology Park.

We thank H. Menke for providing experimental data, and M. Trusler for useful discussions. We are also grateful to M. Harvey for providing HPC support for the calculations in this study.

References

Agrawal, P., A. Raoof, O. Iliev and M. Wolthers (2020). "Evolution of pore-shape and its impact on pore conductivity during CO2 injection in calcite: Single pore simulations and microfluidic experiments." Advances in Water Resources **136**: 103480.

Anabaraonye, B. U. (2017). Experimental and Modelling Studies of Reservoir Mineral Dissolution Following Carbon Dioxide Injection. PhD, Imperial College London.

Appelo, C. A. J. and P. Wersin (2007). "Multicomponent Diffusion Modeling in Clay Systems with Application to the Diffusion of Tritium, Iodide, and Sodium in Opalinus Clay." Environmental Science & Technology **41**(14): 5002-5007.

Cadogan, S. P., G. C. Maitland and J. P. M. Trusler (2014). "Diffusion Coefficients of CO2 and N2 in Water at Temperatures between 298.15 K and 423.15 K at Pressures up to 45 MPa." Journal of Chemical & Engineering Data **59**(2): 519-525.

Fredd, C. N. and H. S. Fogler (1998). "Influence of transport and reaction on wormhole formation in porous media." AIChE journal **44**(9): 1933-1949.

Gao, J., H. Xing, Z. Tian, J. K. Pearce, M. Sedek, S. D. Golding and V. Rudolph (2017). "Reactive transport in porous media for CO2 sequestration: Pore scale modeling using the lattice Boltzmann method." Computers & Geosciences **98**: 9-20.

Giambalvo, E. R., C. I. Steefel, A. T. Fisher, N. D. Rosenberg and C. G. Wheat (2002). "Effect of fluid-sediment reaction on hydrothermal fluxes of major elements, eastern flank of the Juan de Fuca Ridge." Geochimica et Cosmochimica Acta **66**(10): 1739-1757.

Ginzburg, I. (2016). "Comment on “An improved gray Lattice Boltzmann model for simulating fluid flow in multi-scale porous media”: Intrinsic links between LBE Brinkman schemes." Advances in Water Resources **88**: 241-249.

Gray, F., B. Anabaraonye, S. Shah, E. Boek and J. Crawshaw (2018). "Chemical mechanisms of dissolution of calcite by HCl in porous media: Simulations and experiment." Advances in Water Resources **121**: 369-387.

Gray, F. and E. Boek (2016). "Enhancing Computational Precision for Lattice Boltzmann Schemes in Porous Media Flows." Computation **4**(1): 11.

Gray, F., J. Cen and E. S. Boek (2016). "Simulation of dissolution in porous media in three dimensions with lattice Boltzmann, finite-volume, and surface-rescaling methods." Physical Review E **94**(4): 043320.

Guibert, R., P. Horgue, G. Debenest and M. Quintard (2016). "A comparison of various methods for the numerical evaluation of porous media permeability tensors from pore-scale geometry." Mathematical Geosciences **48**(3): 329-347.

Guibert, R., M. Nazarova, P. Horgue, G. Hamon, P. Creux and G. Debenest (2015). "Computational permeability determination from pore-scale imaging: sample size, mesh and method sensitivities." Transport in Porous Media **107**(3): 641-656.

Langmuir, D. (1997). Aqueous Environmental Geochemistry, Prentice Hall.

Li, L., C. I. Steefel, and L. Yang (2008). "Scale dependence of mineral dissolution rates within single pores and fractures." Geochim. Cosmochim. Acta **72**: 360–377.

Lide, D. R. (1997). CRC Handbook of Chemistry and Physics.

Liu, M. and P. Mostaghimi (2017). "High-resolution pore-scale simulation of dissolution in porous media." Chemical Engineering Science **161**: 360-369.

Liu, M. and P. Mostaghimi (2018). "Numerical simulation of fluid-fluid-solid reactions in porous media." International Journal of Heat and Mass Transfer **120**: 194-201.

Lobo, V., M. Helena and S. Teixeira (1979). "Diffusion coefficients in aqueous solutions of hydrochloric acid at 298 K." Electrochimica Acta **24**(5): 565-567.

Maher, K., C. I. Steefel, D. J. DePaolo and B. E. Viani (2006). "The mineral dissolution rate conundrum: Insights from reactive transport modeling of U isotopes and pore fluid chemistry in marine sediments." Geochimica et Cosmochimica Acta **70**(2): 337-363.

McLeod, H. O. (1984). "Matrix acidizing." J. Pet. Technol. **36**(12): 2055 - 2069.
Menke, H., C. Reynolds, M. Andrew, J. P. Nunes, B. Bijeljic and M. Blunt (2018). "4D multi-scale imaging of reactive flow in carbonates: Assessing the impact of heterogeneity on dissolution regimes using streamlines at multiple length scales." Chemical Geology **481**: 27-37.
Menke, H. P., B. Bijeljic, M. G. Andrew and M. J. Blunt (2015). "Dynamic Three-Dimensional Pore-Scale Imaging of Reaction in a Carbonate at Reservoir Conditions." Environmental Science & Technology **49**(7): 4407-4414.
Molins, S., C. Soulaine, N. I. Prasianakis, A. Abbasi, P. Poncet, A. J. Ladd, V. Starchenko, S. Roman, D. Trebotich and H. A. Tchelepi (2020). "Simulation of mineral dissolution at the pore scale with evolving fluid-solid interfaces: review of approaches and benchmark problem set." Computational Geosciences: 1-34.
Molins, S., D. Trebotich, L. Yang, J. B. Ajo-Franklin, T. J. Ligocki, C. Shen and C. I. Steefel (2014). "Pore-Scale Controls on Calcite Dissolution Rates from Flow-through Laboratory and Numerical Experiments." Environmental Science & Technology **48**(13): 7453-7460.
Molins, S., Trebotich, D., Steefel, C. I., and Shen, C. (2012). "An investigation of the effect of pore scale flow on average geochemical reaction rates using direct numerical simulation." Water Resour. Res. **48**.
Mostaghimi, P., M. Liu and C. H. Arns (2016). "Numerical Simulation of Reactive Transport on Micro-CT Images." Mathematical Geosciences **48**(8): 963-983.
Muniruzzaman, M. and M. Rolle (2016). "Modeling multicomponent ionic transport in groundwater with IPhreeqc coupling: Electrostatic interactions and geochemical reactions in homogeneous and heterogeneous domains." Advances in Water Resources **98**: 1-15.
Noiriel, C., C. I. Steefel, L. Yang and J. Ajo-Franklin (2012). "Upscaling calcium carbonate precipitation rates from pore to continuum scale." Chemical Geology **318**: 60-74.
Ovaysi, S. and M. Piri (2014). "Pore-space alteration induced by brine acidification in subsurface geologic formations." Water Resources Research **50**(1): 440-452.
Peng, C., J. P. Crawshaw, G. C. Maitland and J. M. Trusler (2015). "Kinetics of calcite dissolution in CO 2-saturated water at temperatures between (323 and 373) K and pressures up to 13.8 MPa." Chemical Geology **403**: 74-85.
Pereira Nunes, J. P., M. J. Blunt and B. Bijeljic (2016). "Pore-scale simulation of carbonate dissolution in micro-CT images." Journal of Geophysical Research: Solid Earth **121**(2): 558-576.
Qajar J, A. C. (2012). "Chemical dissolution of carbonate rocks: A micro-CT study." Glob. Imaging Insights **2**.
Singh, K., B. U. Anabaraonye, M. J. Blunt and J. Crawshaw (2018). "Partial dissolution of carbonate rock grains during reactive CO2-saturated brine injection under reservoir conditions." Advances in Water Resources **122**: 27-36.
Soulaine, C., S. Roman, A. Kovscek and H. A. Tchelepi (2017). "Mineral dissolution and wormholing from a pore-scale perspective." Journal of Fluid Mechanics **827**: 457-483.
Sprocati, R., M. Masi, M. Muniruzzaman, M. Rolle (2019). "Modeling electrokinetic transport and biogeochemical reactions in porous media: A multidimensional Nernst–Planck–Poisson approach with PHREEQC coupling." Advances in Water Resources **127**: 134-147.
Steefel, C. I., C. A. J. Appelo, B. Arora, D. Jacques, T. Kalbacher, O. Kolditz, V. Lagneau, P. C. Lichtner, K. U. Mayer, J. C. L. Meeussen, S. Molins, D. Moulton, H. Shao, J. Šimůnek, N. Spycher, S. B. Yabusaki and G. T. Yeh (2015). "Reactive transport codes for subsurface environmental simulation." Computational Geosciences **19**(3): 445-478.
Steefel, C. I. and K. Maher (2009). "Fluid-Rock Interaction: A Reactive Transport Approach." Reviews in Mineralogy and Geochemistry **70**(1): 485-532.
Tian, Z. and J. Wang (2018). "Lattice Boltzmann simulation of dissolution-induced changes in permeability and porosity in 3D CO2 reactive transport." Journal of Hydrology **557**: 276-290.
Vinograd, J. R. and J. W. McBain (1941). "Diffusion of electrolytes and of the ions in their mixtures." Journal of the American Chemical Society **63**(7): 2008-2015.

Walsh, S. D., H. Burwinkle and M. O. Saar (2009). "A new partial-bounceback lattice-Boltzmann method for fluid flow through heterogeneous media." Computers & Geosciences **35**(6): 1186-1193.

Yoon, H., Q. Kang and A. Valocchi (2015). "Lattice Boltzmann-based approaches for pore-scale reactive transport." Rev Mineral Geochem **80**: 393-431.

Yoon, H., A. J. Valocchi, C. J. Werth and T. Dewers (2012). "Pore-scale simulation of mixing-induced calcium carbonate precipitation and dissolution in a microfluidic pore network." Water Resources Research **48**(2).

Tables

Table 1 – Self-diffusion coefficients for each species at T = 323 K. [a] from (Cadogan, Maitland et al. 2014), and [b] from (Lide 1997).

Species	D_i / 10^{-9} m^2s^{-1}
H_2CO_3	3.643[a]
H^+	16.53[b]
Cl^-	3.607 [b]
HCO_3^-	2.104 [b]
CO_3^{2-}	1.638 [b]
Ca^{2+}	1.406 [b]

Table 2 – Parameters for the four CO_2-water cylinder experiments.

Experiment	Diameter /mm	Length /mm	Flow Rate /mL min^{-1}	Run Time /hr
C1	3	19.5	0.168	20.50
C2	3	13.5	0.168	10.55
C3	1	18.2	0.064	25.96
C4	3	19.5	0.084	21.13

Table 3 – Parameters for the two CO_2-brine cylinder experiments.

Experiment	Diameter /mm	Length /mm	Flow Rate /mL min^{-1}	Run Time /hr
C5	3	17.2	0.168	14
C6	3	13.3	0.168	8.60

Figures

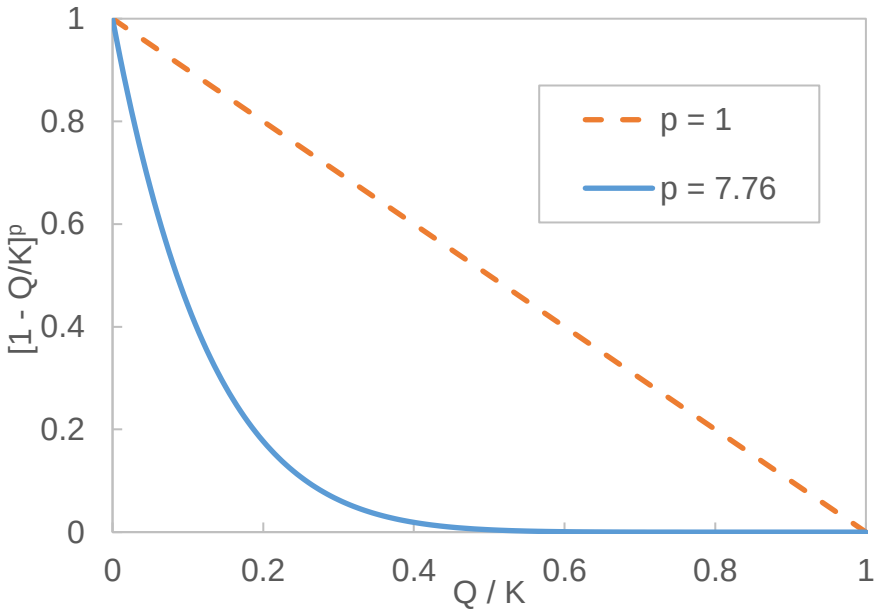

Figure 1 – The value of the saturation term $[1 - Q/K]^p$ with the saturation index Q/K for the linear model ($p = 1$) and the model of Anabaraonye et al. ($p = 7.76$).

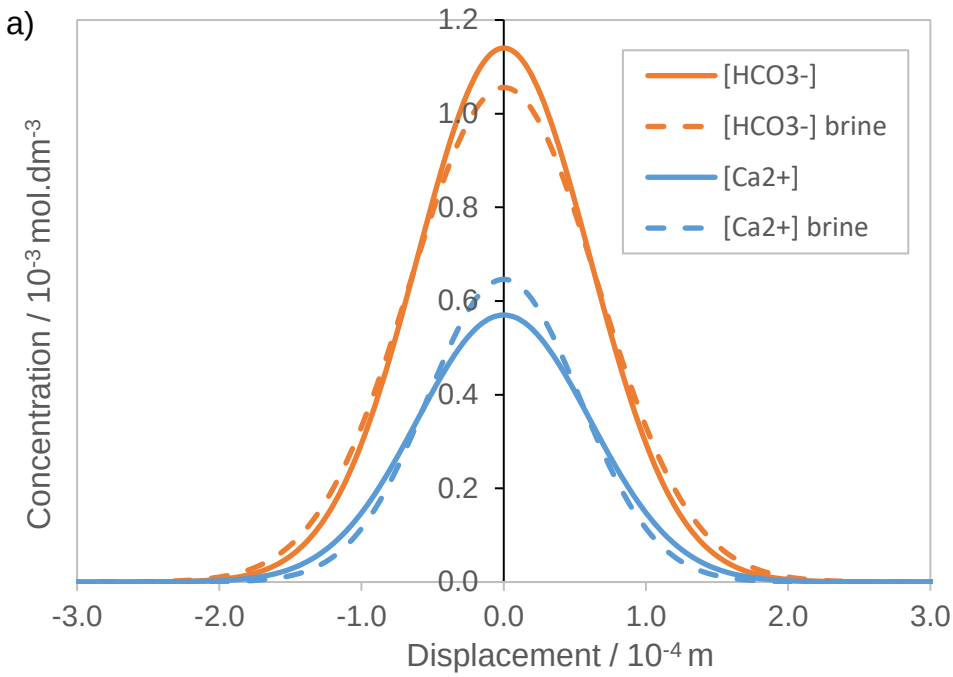
a)
1.2
1.0
0.8
0.6
0.4
0.2
0.0
-3.0
-2.0
-1.0
0.0
1.0
2.0
3.0
Concentration / 10-3 mol.dm-3
Displacement / 10-4 m
[HCO3-]
[HCO3-] brine
[Ca2+]
[Ca2+] brine

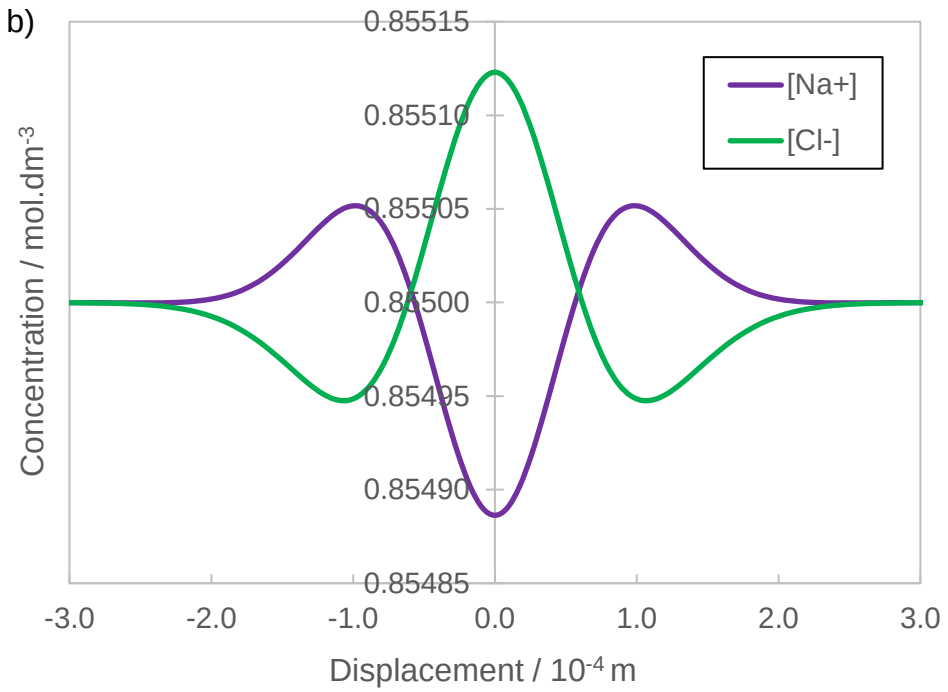
b)
0.85515
0.85510
0.85505
0.85500
0.85495
0.85490
0.85485
-3.0
-2.0
-1.0
0.0
1.0
2.0
3.0
Concentration / mol.dm-3
Displacement / 10-4 m
[Na+]
[Cl-]

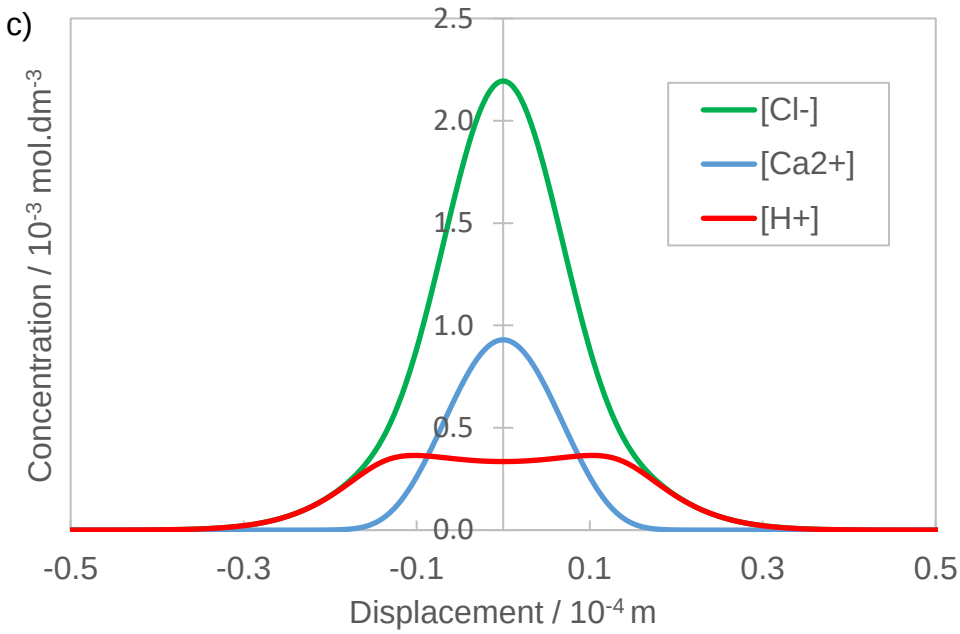

Figure 2 – a) concentration distributions of Ca^{2+} and HCO_3^- ions after diffusing from a point source after 1.03 s. Solid lines are Ca^{2+} and HCO_3^- ions in water, and dashed lines are in a background solution of 0.855 M NaCl brine. The effective diffusion coefficient of both ions is 1.805 x 10^{-9} m^2s^{-1} in water, however in the presence of brine Ca^{2+} and HCO_3^- diffuse with their self-diffusion coefficients. b) the distribution of ions of the background brine solution of 0.855 M NaCl after 1.03 s of diffusion. c) the concentration distributions of H^+, Cl^- and Ca^{2+} ions after diffusion from a point source after 1.03 s.

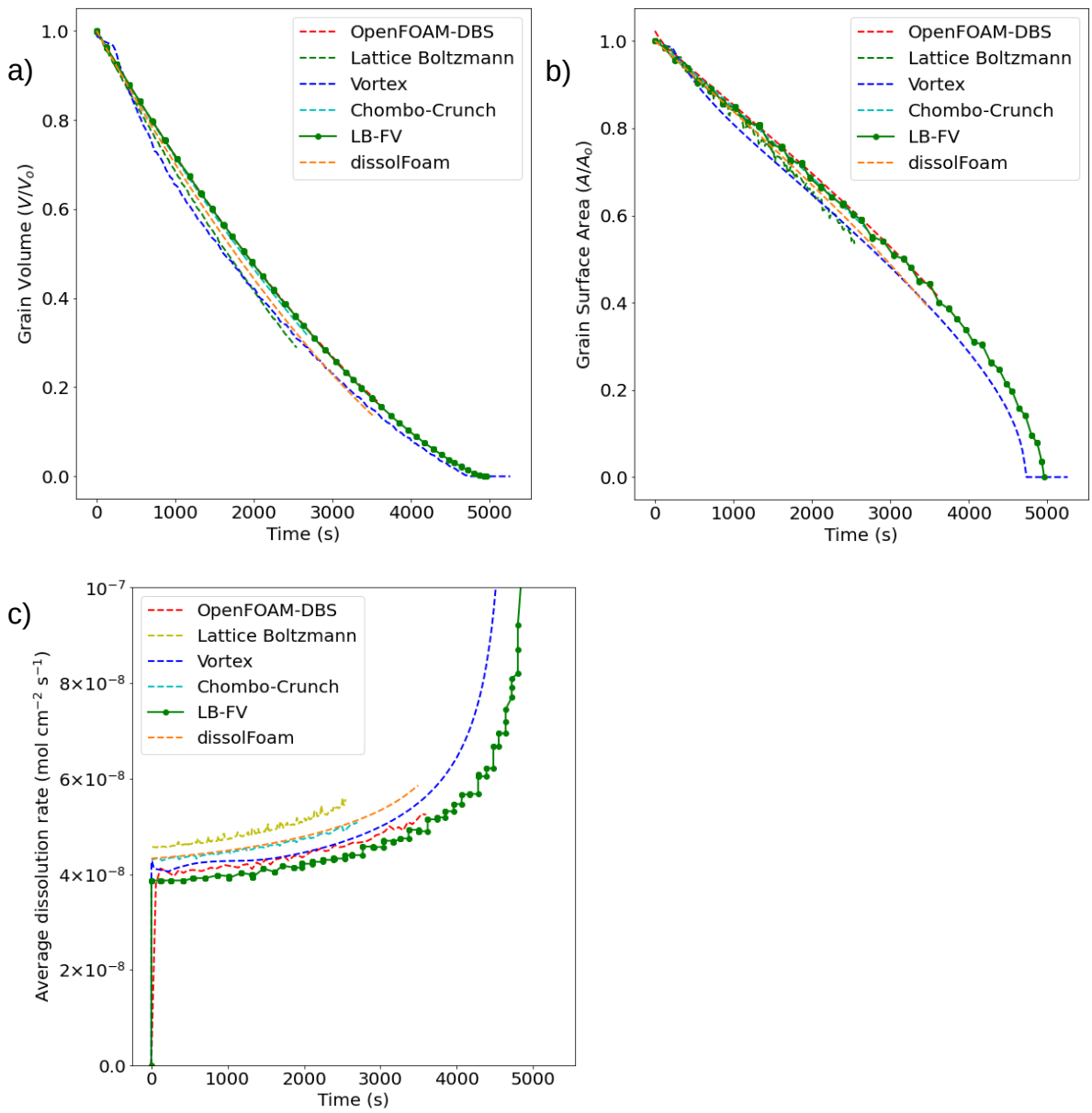

Figure 3: Evolution of a) volume (area in two dimensions), b) surface area (perimeter in two dimensions), and c) average dissolution rate, as a function of time during the dissolution of a two-dimensional calcite disk as described in part II of (Molins, Soulaine et al. 2020). Our calculations are shown as "LB-FV" using green markers and solid interpolation curve, in comparison with other simulation results (dashed lines) detailed in (Molins, Soulaine et al. 2020).

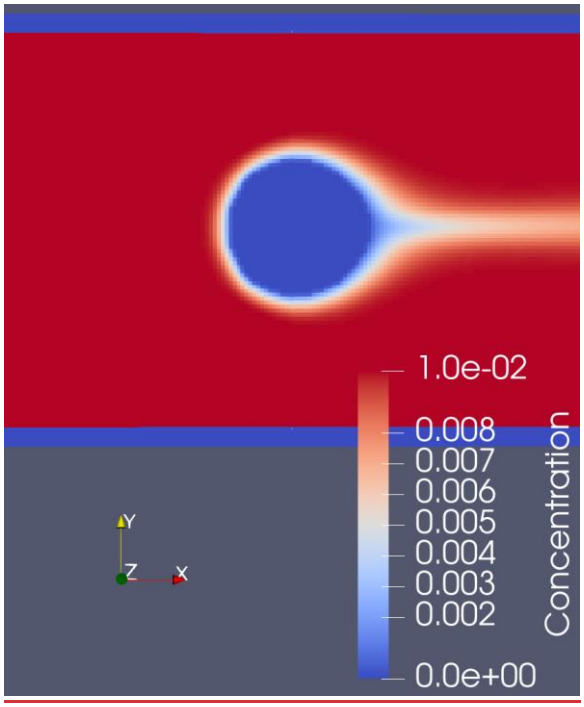

Figure 4: H^+ ion concentration contours for the 2D dissolution of a cylindrical calcite grain in a solution of HCl at pH=2, obtained from our LB-FV calculations at t =1000 s.

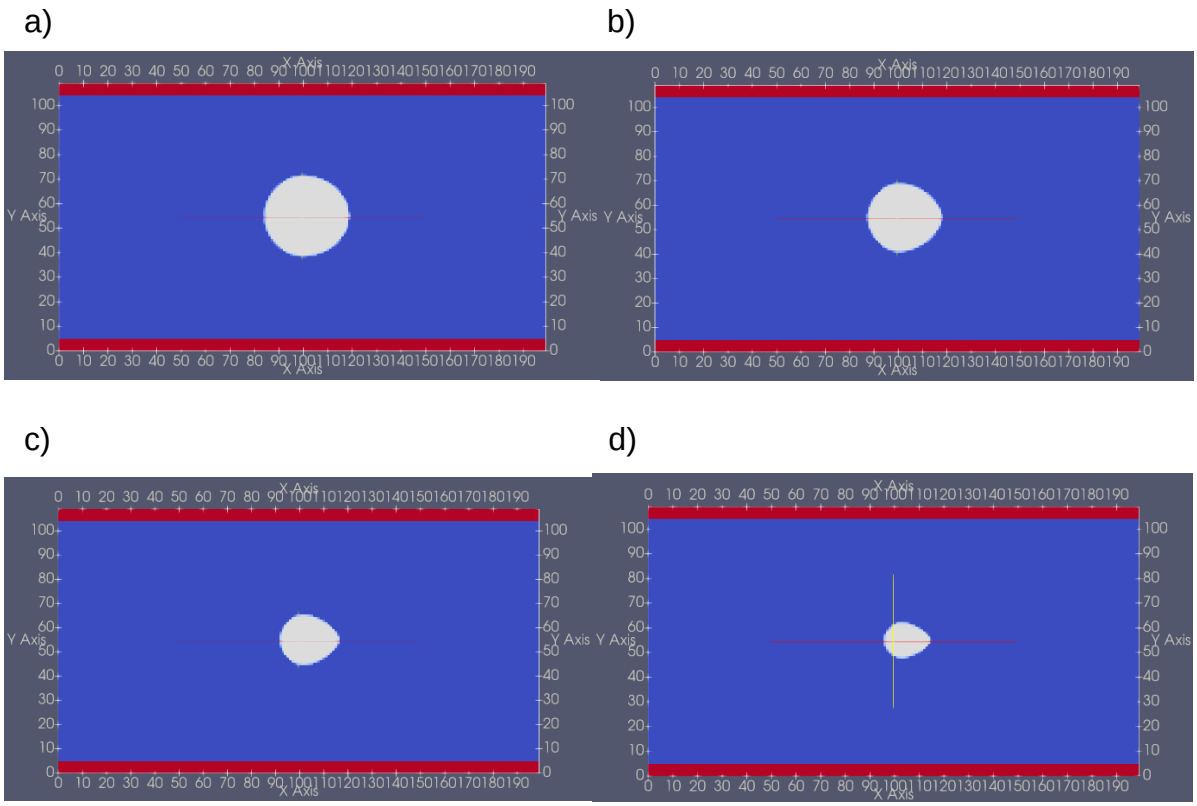

Figure 5: Evolution of calcite grain shape due to dissolution under flowing conditions after a) 15 min., b) 30 min., c) 45 min. and d) 60 min., observed from our LB-FV simulations.

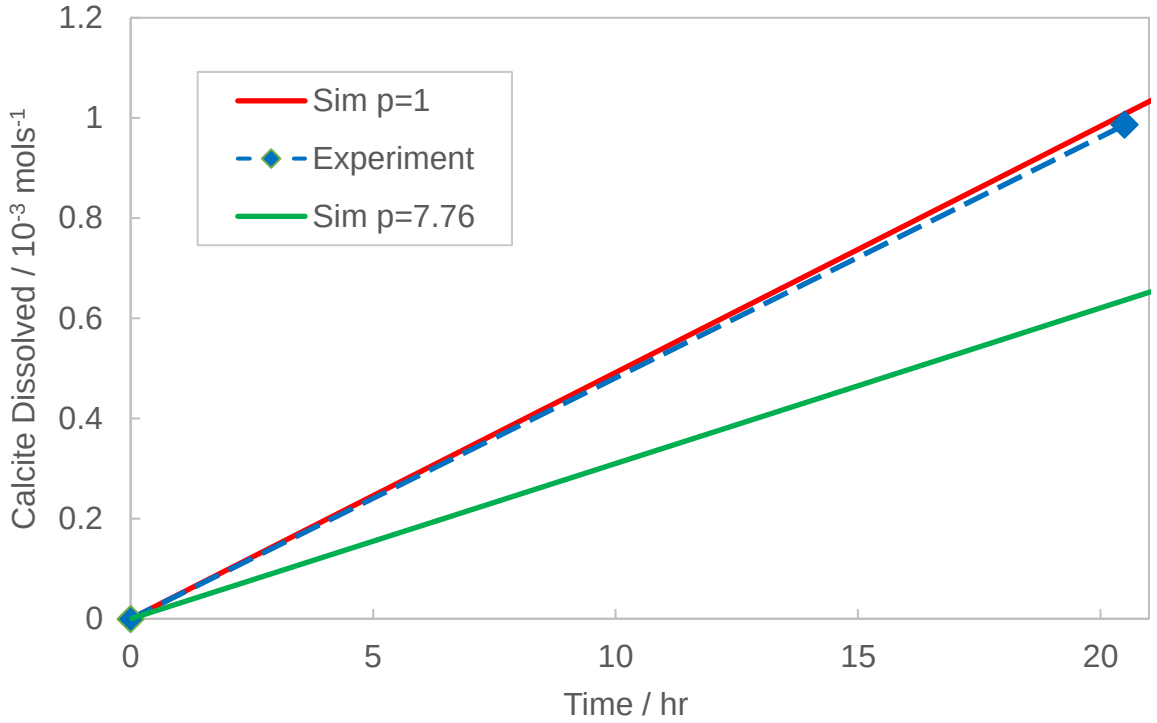

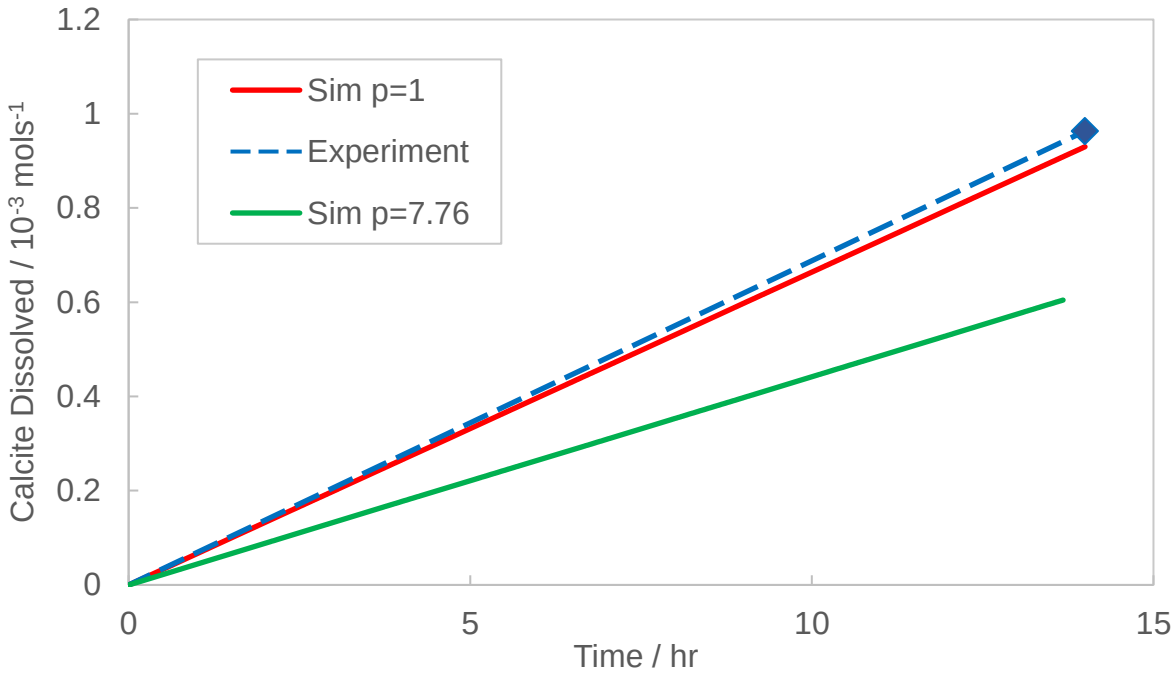

Figure 6 – Moles of calcite dissolved over time for the channels for top: C1 (CO_2-water) and bottom: C5 (CO_2-brine) dissolution experiments. Experimental lines (dashed) were obtained by measuring the weight change after a given time. Solid lines are simulated using the linear saturation model and the non-linear model with exponent $p = 7.76$.

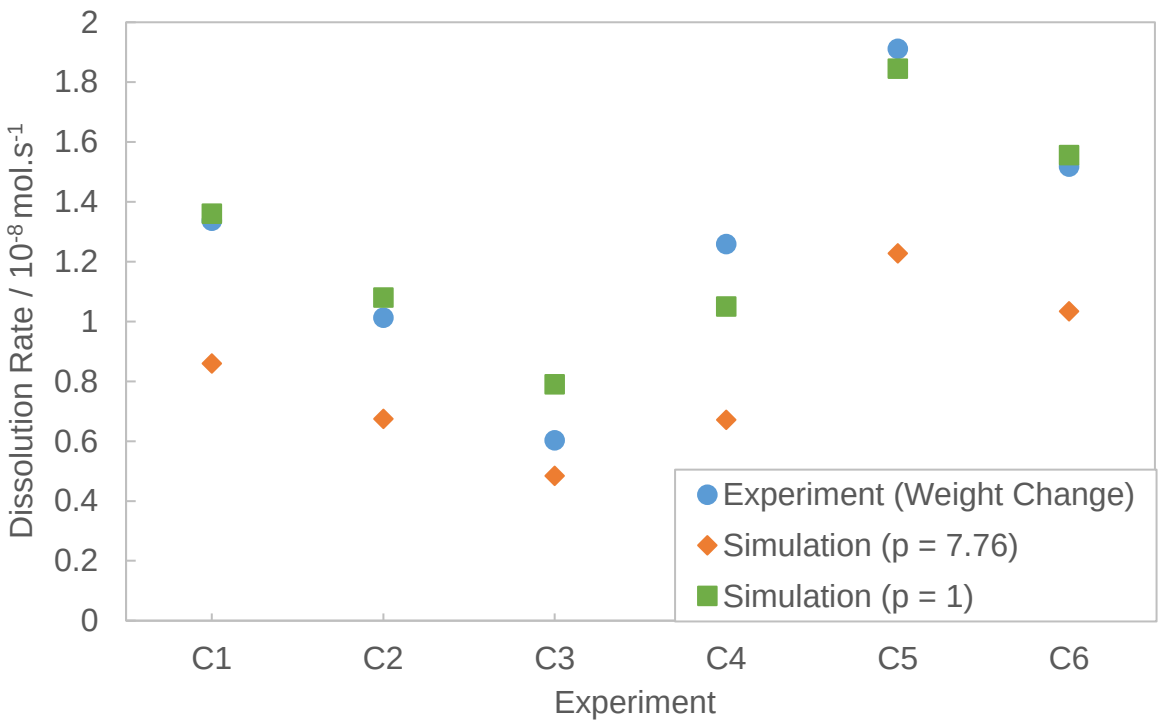

Figure 7 – The dissolution rate for the cylindrical channels injected with CO_2-water solution. Experimental results were obtained from effluent analysis and are compared with simulations performed using saturation exponents of p = 7.76 and p = 1.

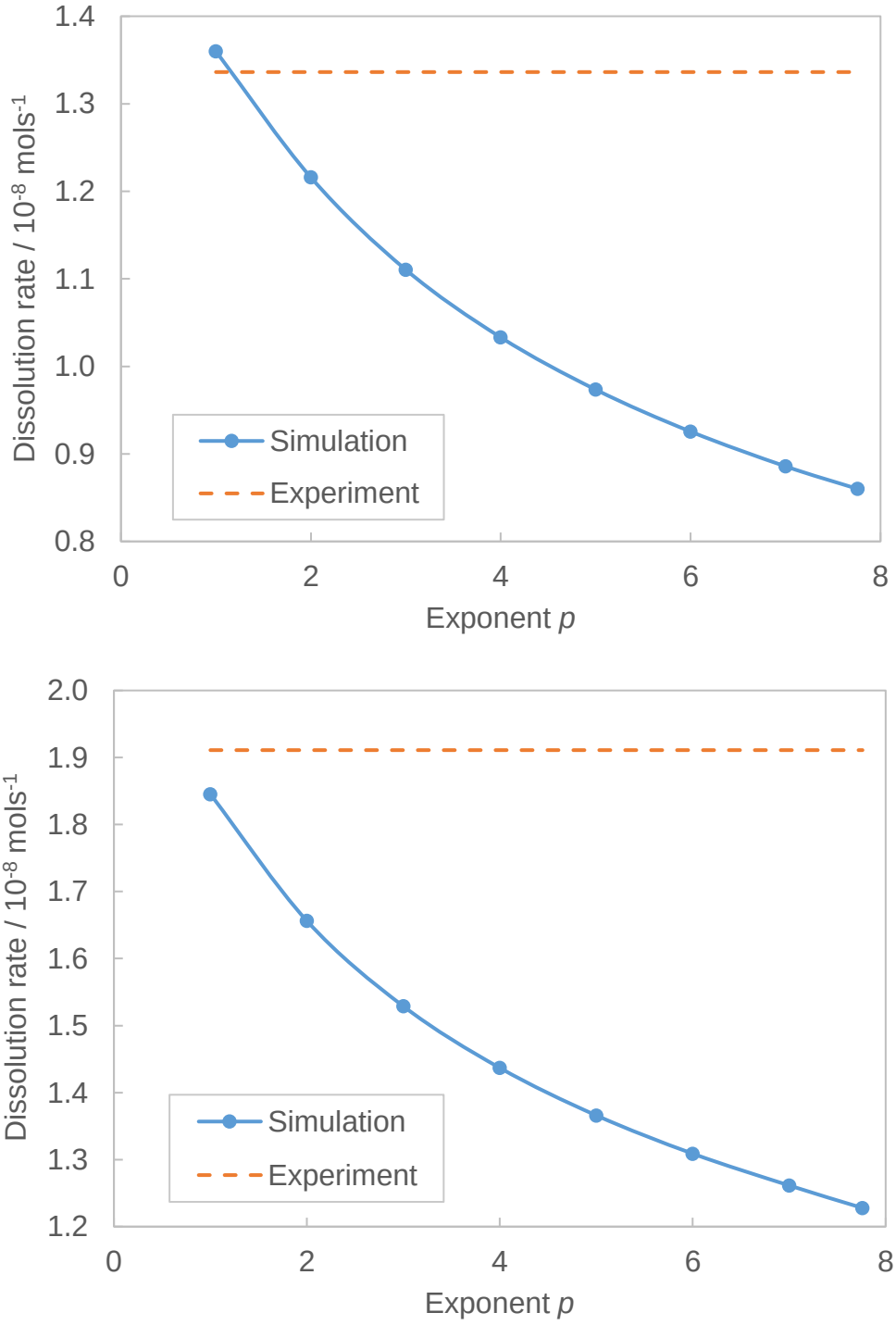

Figure 8 – Calcite dissolution rates simulated using different values of the non-linear saturation exponent p for CO_2-water experiment C1 (top) and CO_2-brine experiment C5 (bottom). The dashed lines are the experimental dissolution rates. Best fit values of the exponent are linear in both cases.

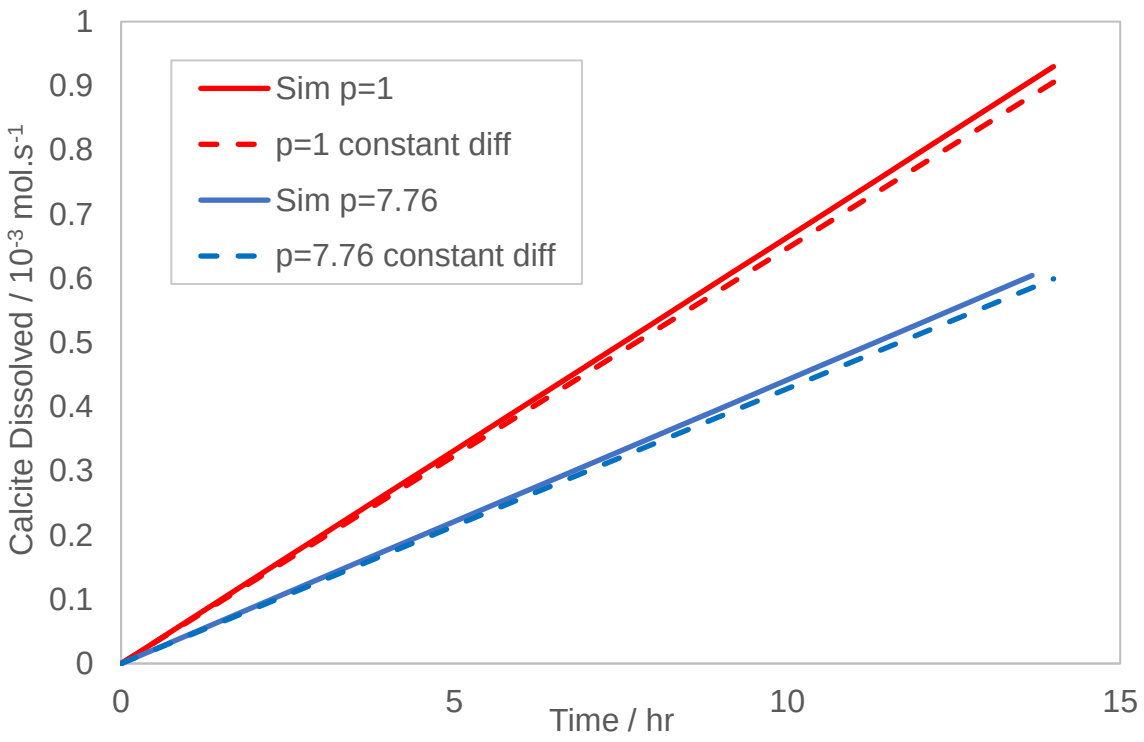

Figure 9 – Dissolved mols of calcite over time simulated for the parameters of experiment C5 using: (solid lines) the coupled ion diffusion model and (dashed lines) a constant diffusion rate of 1.805 x 10^{-9} m^2s^{-1}, and performed for both the linear and non-linear saturation models.

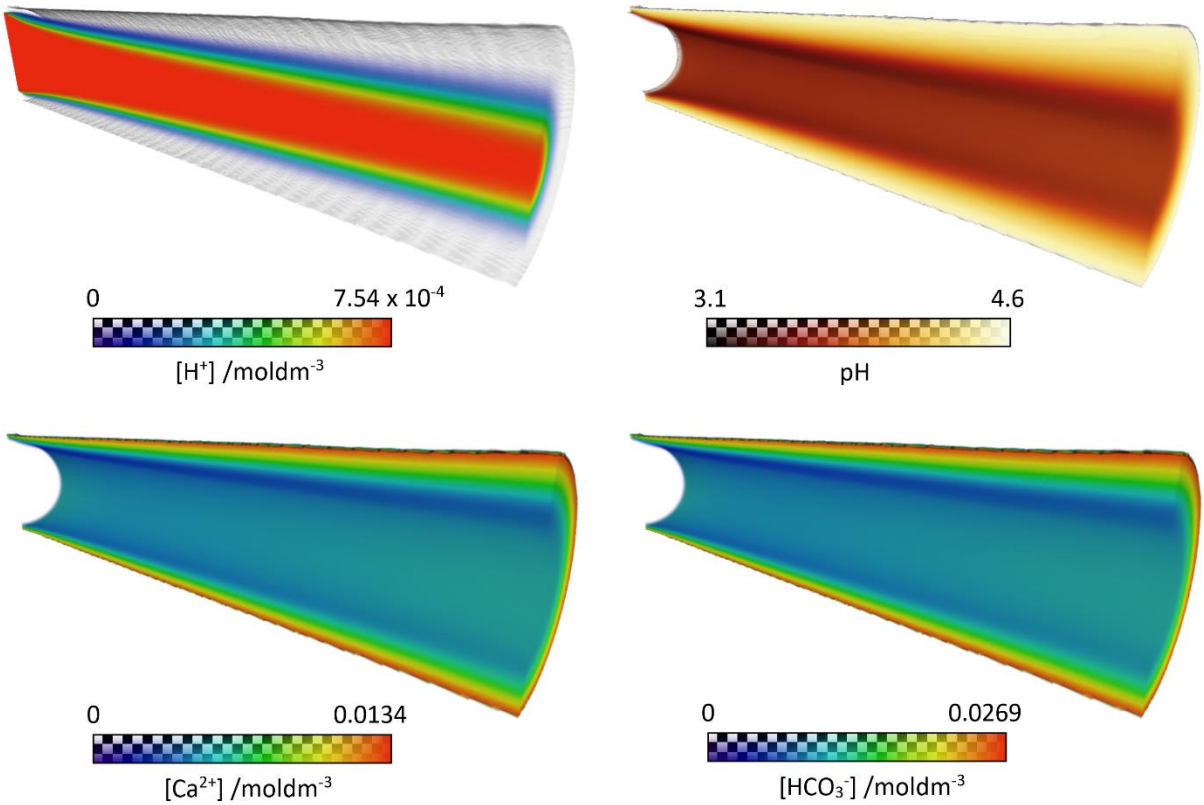

Figure 10 – Cutaways of concentration fields of H^+, Ca^{2+}, HCO_3^- and the pH along the channel for the CO_2-water calculation, using a saturation exponent of $p = 7.76$. Injection was from left.

a)

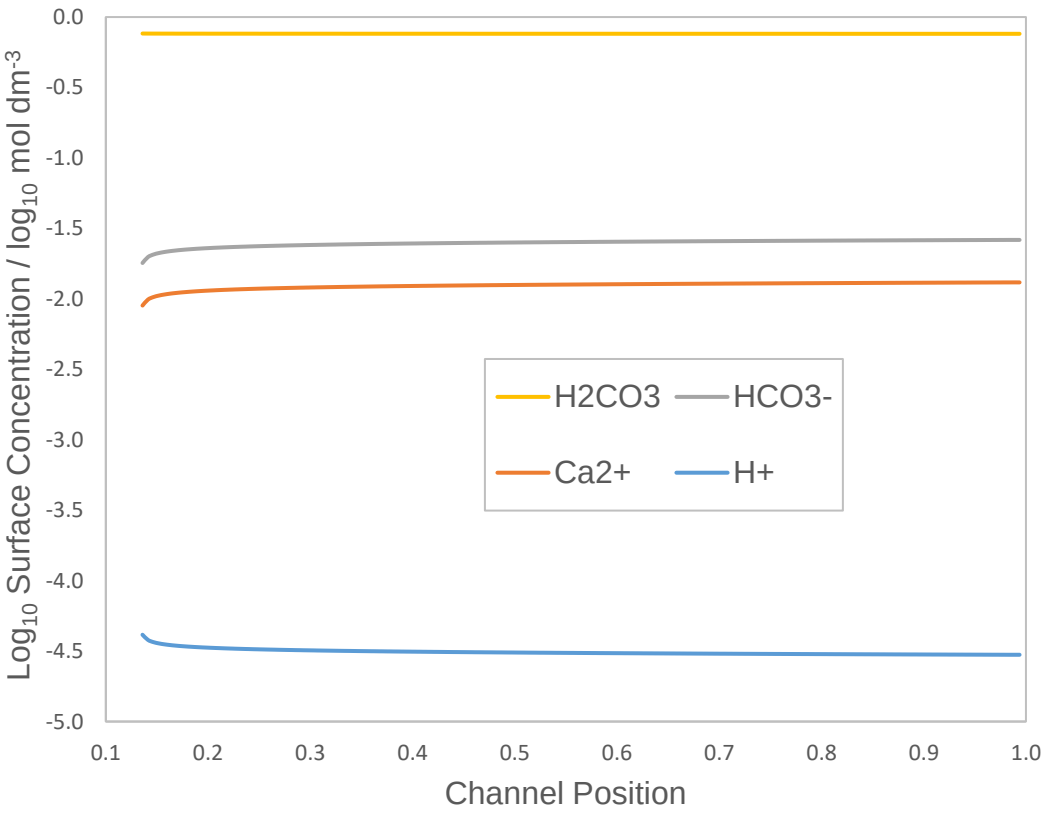

b)

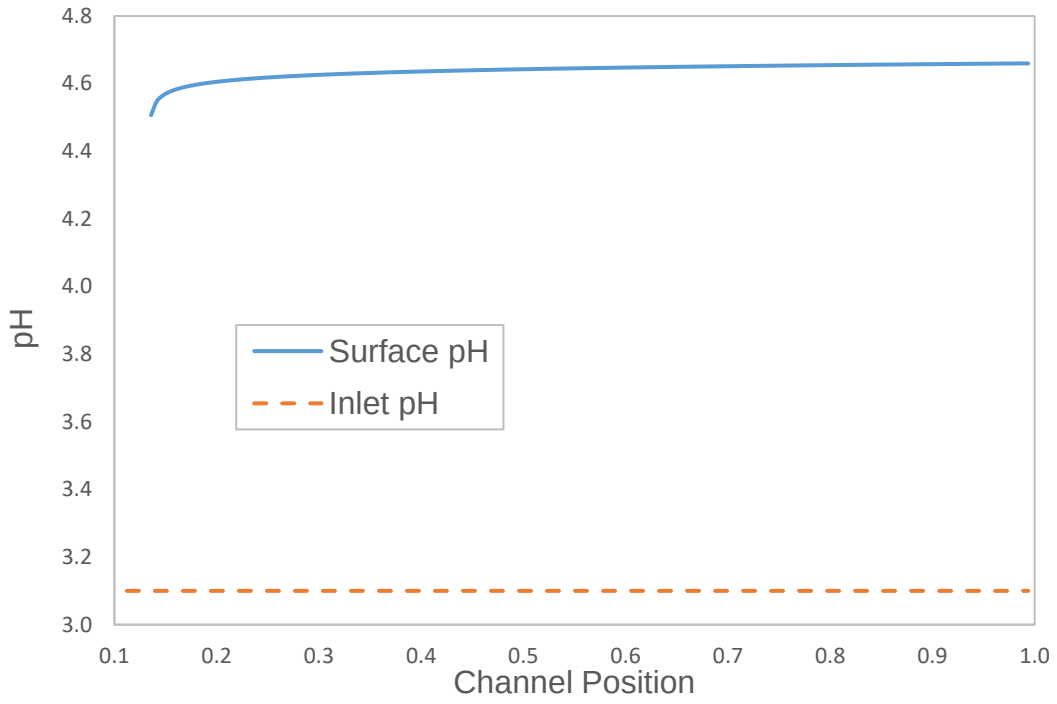
4.8
4.6
4.4
4.2
4.0
3.8
3.6
3.4
3.2
3.0
pH
Surface pH
Inlet pH
0.1
0.2
0.3
0.4
0.5
0.6
0.7
0.8
0.9
1.0
Channel Position

c)

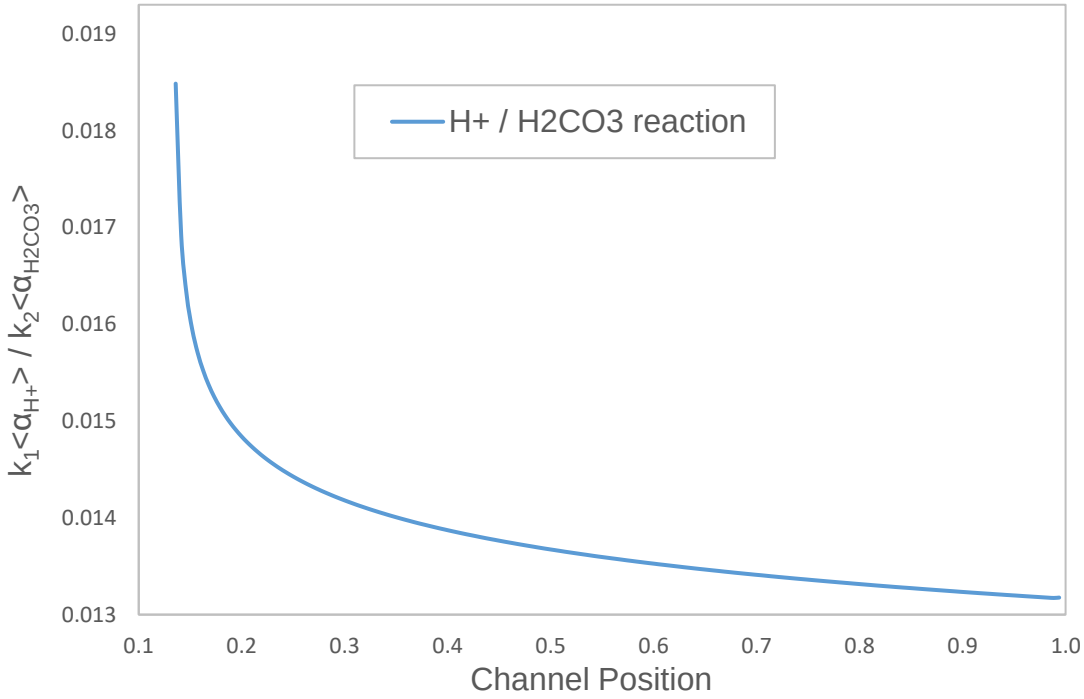
0.019
0.018
0.017
0.016
0.015
0.014
0.013
k1<αH+> / k2<αH2CO3>
H+ / H2CO3 reaction
0.1
0.2
0.3
0.4
0.5
0.6
0.7
0.8
0.9
1.0
Channel Position

d)

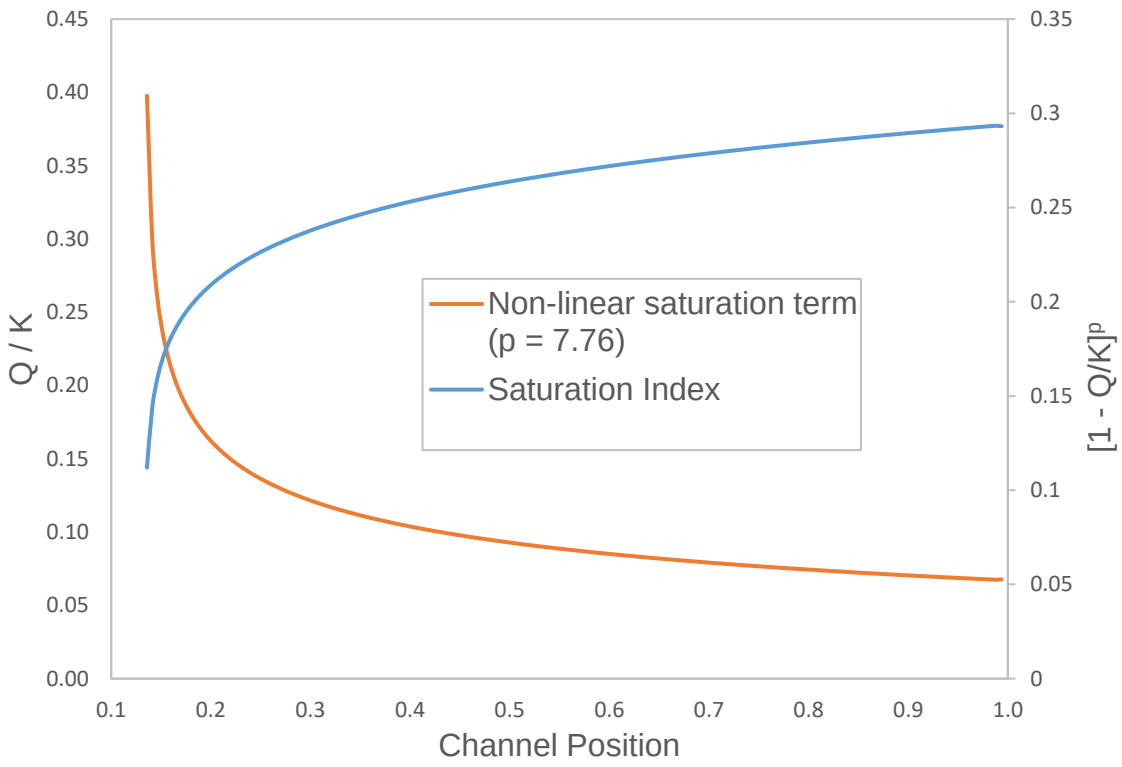

Figure 11 – Quantities sampled over the length of the channel from simulation of CO_2-water using the exponent $p = 7.76$. a) concentrations of chemical components on the channel surface. b) surface pH compared to inlet solution pH. c) the relative contribution of the H^+ and H_2CO_3 dissolution pathways computed using mean surface activities of the respective species. d) the saturation index Q / K and the value of the non-linear saturation term on the channel surface. Data is only shown for the calcite part of the channel (i.e. excluding the inlet region).

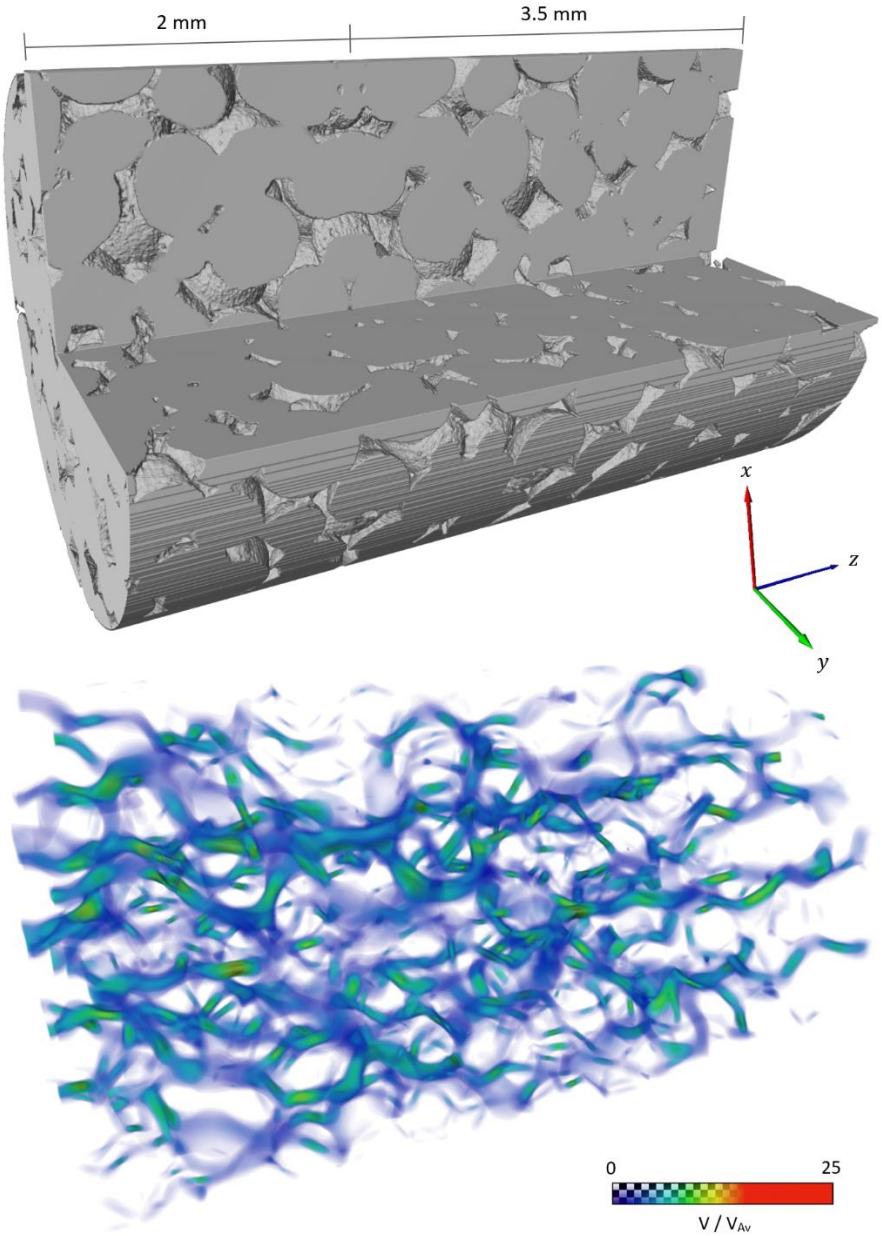

Figure 12 – The Ketton carbonate sample from Menke et al. (Menke, Bijeljic et al. 2015) with an extra 2 mm region added by mirroring part of the sample backwards. The geometry is shown, indicating both the 3.5 mm sample region from Menke et al. and the extra 2 mm inlet region (top) with the initial velocity field computed using lattice Boltzmann (bottom). The size of the domain is 922 x 902 x 1436 lattice units, at a resolution of 3.81 µm.

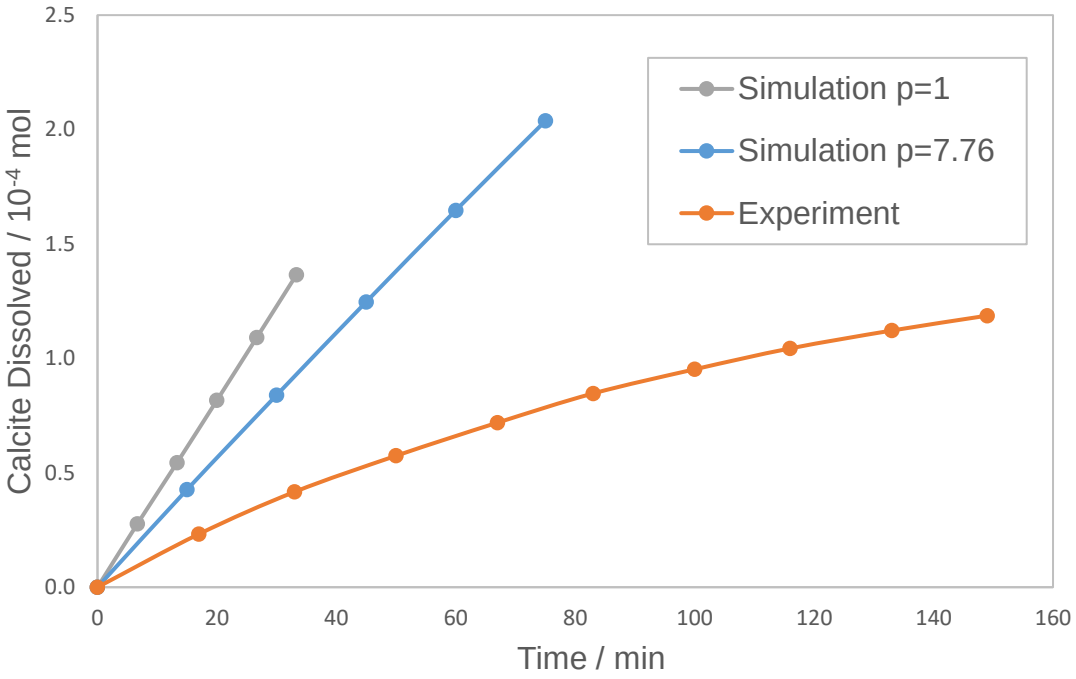

Figure 13 – Dissolved moles of calcite over time within the 3.5 mm subvolume in simulations using both linear (p = 1) and non-linear (p = 7.76) saturation laws, compared with experiment. Constant diffusion and coupled diffusion models gave almost indistinguishable results.

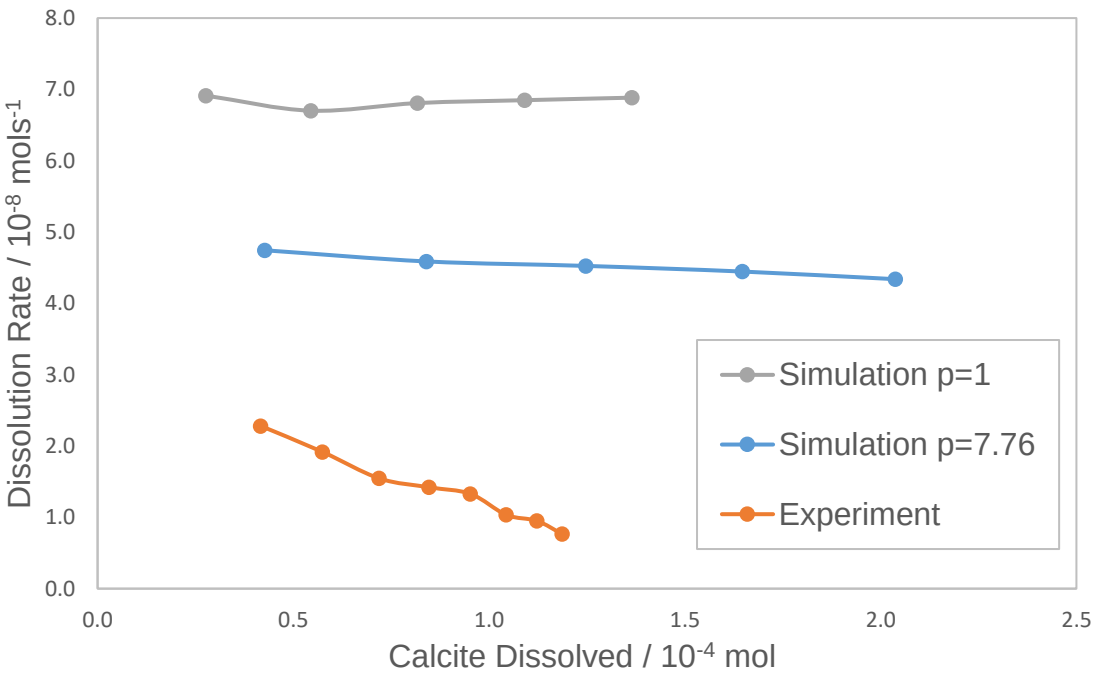

Figure 14 – The dissolution rate with amount of calcite dissolved in the 3.5 mm subvolume in simulations using both linear (p = 1) and non-linear (p = 7.76) saturation laws, and experiment.

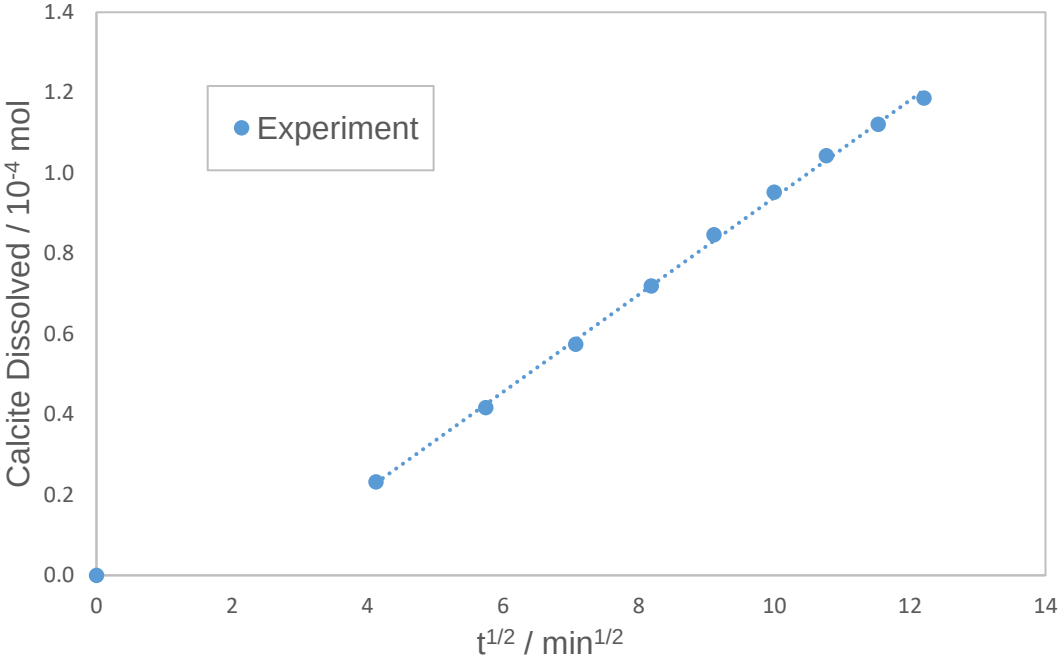

Figure 15 – Dissolved moles of calcite over square-root time in the experiment of Menke et al. (2015). A linear fit for all except the first point is included. Aside from the first point, the data follows almost ideally a square-root dependence on time.

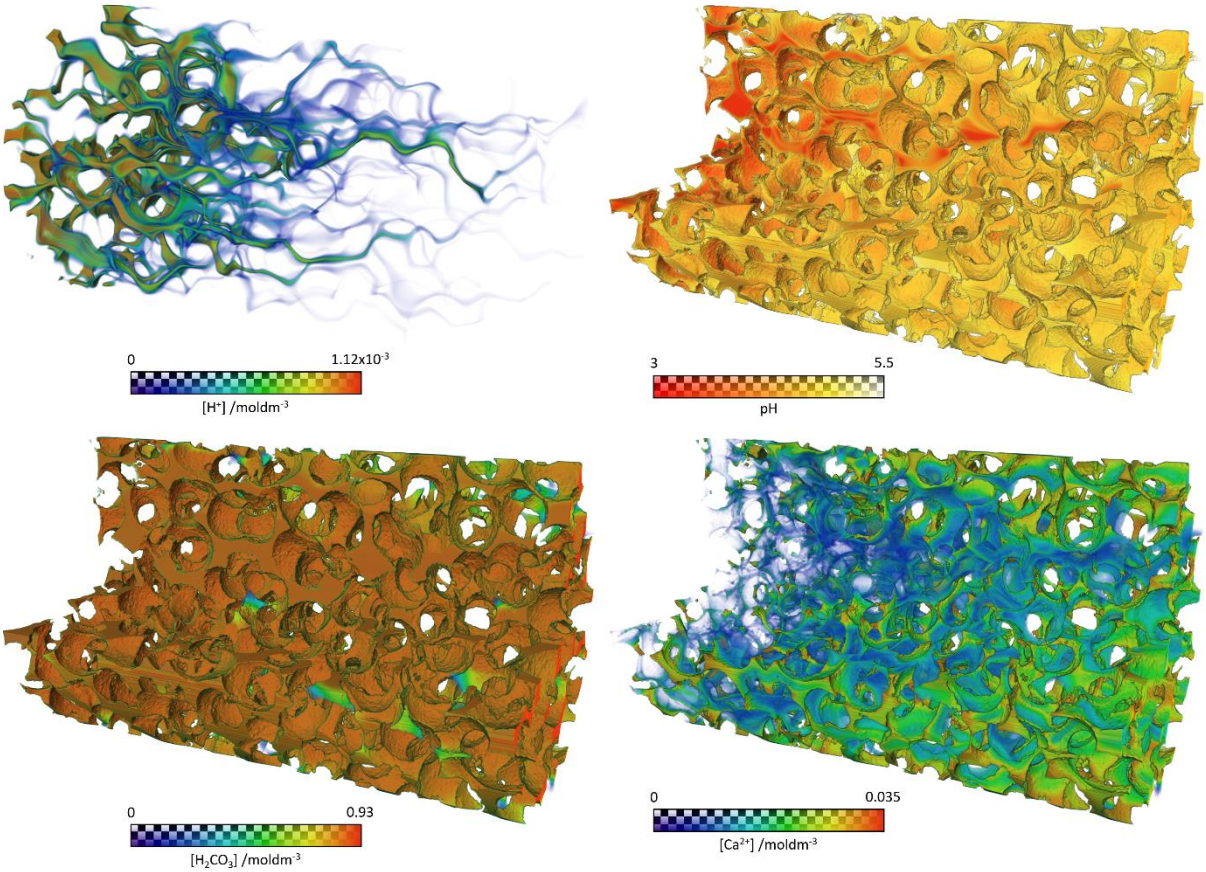

Figure 16 – Concentration fields of a) H+, and cutaways of b) pH, c) H_2CO_3 and d) Ca^{2+} in the Ketton carbonate core at initial steady-state, including the extra 2mm inlet region. The exponent p = 1 and injection was from left.

Click here to access/download
Electronic Annex
Comparisons.xlsx

Click here to access/download
Manuscript Source Files
Dissolution in CO2-brine systems
v2.23_AcceptChanges.docx

*Declaration of Interest Statement

Declaration of interests

☒ The authors declare that they have no known competing financial interests or personal relationships that could have appeared to influence the work reported in this paper.

☐The authors declare the following financial interests/personal relationships which may be considered as potential competing interests: